UNIVERSITY OF CALIFORNIA
RIVERSIDE

Density Functional Theory for Confined Electrolytes: Phase Behavior, Interfacial Phenomena and Application to Capacitive Energy Storage

A Dissertation submitted in partial satisfaction
of the requirements for the degree of

Doctor of Philosophy

in

Chemical and Environment Engineering

by

Kun Liu

March 2019

Dissertation Committee:
Dr. Jianzhong Wu, Chairperson
Dr. Bryan M. Wong
Dr. De-en Jiang

The Dissertation of Kun Liu is approved:

_____

_____

_____

Committee Chairperson

University of California, Riverside

Acknowledgements

I would like to express my deep gratitude to Professor Jianzhong Wu, my supervisor, for his mentorship, advice and nuggets of wisdom. Over the last five years, he has motivated me to work on the exciting research topic about energy storage, taught me how to think and work as a researcher, and encouraged me to build up the confidence. His depth of knowledge and insights impressed me from the very beginning of my research. He not only helps me solve specific problems in my thesis, but also gives me a lot of priceless suggestions for my future career. Without his help, I would not have been here.

Deep thanks to Prof. De-en Jiang and Prof. Bryan M. Wong for their time serving on my thesis committee. I also would like to thank Prof. David Kisailus and Prof. Phillip Christopher for serving on my oral preliminary exam committee. Without the tremendous support from my collaborators, I could not have finished this thesis work. Dr. Pengfei Zhang taught me a lot about physics. Dr. Cheng Lian helped me tremendously at the early stage of my research and he is always willing to share with me his experience and ideas. Discussion with them gives me great inspirations. I also gratefully appreciate numerous discussion with Professor Douglas Henderson and with several current and former members in Wu Group: Alejandro Gallegos, Musen Zhou, Xiaoyu Hu, Yun Tian, and Jipeng Li. I enjoyed the time in office with their help and friendship.

On a personal note, deep thanks to all my friends for their support and companion over the years. You made my life enjoyable.

I gratefully acknowledge the financial support from the Fluid Interface Reactions, Structures and Transport (FIRST) Center, an Energy Frontier Research Center funded by the US Department of Energy, Office of Science, Office of Basic Energy Sciences. This work utilizes supercomputer from the National Energy Research Scientific Computing Center (NERSC).

Last but certainly not the least, I thank my parents and grandparents for their unending love. They gave me the best education in my life about how to be a person with integrity, courage and kindness.

Published materials are used as the following:

Chapter 3: K. Liu and J. Wu, "Boosting the Performance of Ionic-Liquid-Based Supercapacitors with Polar Additives", The Journal of Physical Chemistry C, vol. 120, no. 42, pp. 24041-24047, 2016.

Chapter 4: K. Liu, C. Lian, D. Henderson, and J. Wu, "Impurity Effects on Ionic-liquid-Based Supercapacitors", Molecular Physics, vol. 115, no. 4, pp. 454-464, 2016.

Chapter 5: C. Lian, K. Liu, H. Liu, and J. Wu, "Impurity Effects on Charging Mechanism and Energy Storage of Nanoporous Supercapacitors", The Journal of Physical Chemistry C, vol. 121, no. 26, pp. 14066-14072, 2017.

Chapter 6: K. Liu, P. Zhang, and J. Wu, "Does Capillary Evaporation Limit the Accessibility of Nonaqueous Electrolytes to the Ultrasmall Pores of Carbon Electrodes?", The Journal of Chemical Physics, vol. 149, no. 23, p. 234708, 2018.

ABSTRACT OF THE DISSERTATION

Density Functional Theory for Confined Electrolytes: Phase Behavior, Interfacial Phenomena and Application to Capacitive Energy Storage

by

Kun Liu

Doctor of Philosophy
Graduate Program in Chemical and Environmental Engineering
University of California, Riverside, March 2019
Dr. Jianzhong Wu, Chairperson

Electric Double Layer Capacitor (EDLC) is a promising candidate for the next generation energy storage device. Recent experimental breakthroughs in developing novel electrode and/or electrolyte material have greatly improved the energy density and charging kinetics of EDLC, which usually limit the widespread application of EDLC. Meanwhile, theory, modeling and simulation can effectively complement experimental efforts by providing insight into mechanisms, predicting trends, identifying new material and thus guiding experiments. Among different theoretical methodologies, Classical Density Functional Theory (CDFT) is a versatile and efficient tool to study interfacial phenomena and phase behavior in confined fluids, which are of critical importance for the fundamental understanding of EDLCs. In this thesis, CDFT will be applied to study several important topics in capacitive energy storage, including electrolyte composition,

charge storage mechanisms, and the wettability of non-aqueous electrolytes on porous electrode materials.

We first explored how a small amount of impurity influences the capacitive energy storage. The impurity can be considered either as an 'additive' or as a 'contaminant', depending on whether it is purposefully introduced into the EDLC. Our theoretical calculations are based on a coarse-grained model for the electrolyte consisting of an ionic liquid and impurity molecules. The effects of the impurity polarity and molecular size, and its binding energy with the electrode surface or ions on the EDLC capacitance were discussed. Then, we examined the idea of improving the energy storage density in ionophobic pores. The ionophobic environment can be created by introducing impurity molecules inside the pore. Different charge storage mechanisms were found, and the theoretical predictions showed that creating an ionophobic environment at low voltage was beneficial for energy storage. Last, we discussed the importance of pore wettability to the energy storage in porous material. We showed that capillary evaporation may occur for an organic electrolyte in the subnanometer pores. We also demonstrated that the accessibility of micropores depends not only on the ionic diameters but also on the wetting behavior of the electrolyte, which is intrinsically related the vapor-liquid or liquid-liquid phase separation of the bulk ionic system. We hope that the fundamental insights gained in this work will help better understand complex physical processes in EDLC and design of EDLC systems to realize their full potentials.

Table of Contents

List of Figures

Chapter 1. Introduction

Recent years have witnessed a growing interest in developing efficient, cost-effective electric energy storage devices in sizes ranging from hand-held to grid-based.[1] Among many available electric energy storage devices, batteries and electrochemical capacitors (ECs) have been identified by the U.S. Department of Energy (DOE) as two of the most important technologies owing to their potential in high-profile applications such as electric vehicles and grid-scale energy storage.[2] Both technologies are based on electrochemistry; but batteries store energy in the form of chemical reactants capable of generating charge, whereas electrochemical capacitors store electric energy directly as charge. Both systems entail many complex and interrelated chemical and physical processes; understanding these processes is critically important for breaking through existing technology barriers and providing new concepts for future electrical energy storage systems.

In this dissertation, we focus on capacitive energy storage devices, more specifically, the electric double layer capacitors (EDLCs), also known as supercapacitors. Compared to battery technology, electrochemical capacitive storage is a newer technology. The first patent applying the concept of electric double layer capacitor for practical purposed was filed by General Electric's H.I. Becker in 1957, who used porous carbon coated on a metallic current collector immersed in an aqueous electrolyte. [3] The standard EDLC design used today was invented by Robert A. Rightmire.[4] Then the first commercially viable EDLC was patented and sold by Nippon Electric Company (NEC). To date, supercapacitors are widely used in different applications, and the global supercapacitor market is estimated to reach $2.10 billion in 2020.

In comparison with batteries, EDLCs have higher power densities, as well as faster sub-second response times. However, the energy storage densities of EDLCs are typically lower than those for batteries. New materials are needed to improve their charge storage capabilities by

increasing both their energy and power densities. Similarly, advances in electrolytes are needed to increase voltage and conductivity while ensuring stability. A fundamental understanding of the physical processes that take place in the EDLCs - including the electrodes, the electrolytes, and especially their interfaces - will provide essential knowledge to make groundbreaking discoveries that will lead to the next generation of EDLCs. For example, too often the electrolyte is a weak link in EDLCs, limiting both the performance and reliability. There is a need for new electrolytes that have high ionic conductivity in combination with wide electrochemical, chemical, and thermal stability. Ideally, the electrolytes are non-toxic, biodegradable, environment friendly, and/or renewable. Fundamental research about interactions in electrolyte systems- ion-ion, ion-solvent, and ion-electrode - will provide the knowledge base for the formulation of novel electrolytes with enhanced performance and lifetime. New continuum, atomistic, and quantum mechanical models are needed to understand solvents and ions in pores, predict new material chemistries and architectures, and discover new physical phenomena at the electrochemical interfaces. With these breakthroughs, EDLCs have the potential to emerge as a more important energy storage technology in the future.

1.1 Operating Mechanism of Electric Double-Layer Capacitors

In conventional electrochemical capacitors, the capacitance is related to the separation between the two charged plates. Tendering limited charge storage, however, EDLCs can store more energy based on electrical double layer (EDL) principle with similar charge/discharge mechanism as that of the conventional capacitor. In EDLC, charge is stored electrostatically due to reversible adsorption of ions that are electrochemically stable in contact with active electrodes.[5] The double layer capacitance is produced as a consequence of charge separation occurring due to polarization at the electrode-electrolyte interface. The thickness of the double

layer is dependent on the electrolyte concentration and the size of ions. A good understanding of the properties EDL is critically important for EDLC applications.

The Helmholtz model is one of the original models used to describe charge storage via formation of EDL. The concept of the "electrical double layer" originated from this model. The Helmholtz model was first proposed by Hermann von Helmholtz in 1853 while investigating opposite charge distribution at colloidal particle interface.[6] In the Helmholtz model, the electronic surface charge is screened by an adsorbed layer of counterionic charge that is tightly bound to the surface, at a fixed distance set by the size of the ions. According to the Helmholtz model, the capacitance can be computed from:

$$C_H = \frac{\varepsilon_0 \varepsilon_r}{d}, \tag{1.1}$$

where C_H is the double layer capacitance, ε_0 is the permittivity of the vacuum, ε_r is the dielectric constant of the solvent, and d is the thickness of the Helmholtz layer, the range over which the potential drop occurs.

Gouy in 1910[7] and Chapman in 1913[8] independently derived and improved the simple Helmholtz EDL model. The "Gouy-Chapman" (GC) model is the first model that accounts for the thermal energy of ions. In the GC model, ions form a diffuse layer of charge segregate at the interface, and the charge distribution is a function of the distance to the electrode surface. The counter charge is spread through the solution adjacent to the electrode up to a few nanometers, depending on the ion valence, solvent dielectric constant, and ion concentration. The local ion concentration c_i is described by the Boltzmann distribution. Assuming electroneutrality, the GC model predicts the differential capacitance C_{GC} for a symmetrical (Z : Z) electrolyte in contact with a planar electrode

$$C_{GC} = \frac{\varepsilon_0 \varepsilon_r}{\lambda_D} \cosh\left(\frac{Ze\psi_0}{2k_B T}\right), \tag{1.2}$$

where e is unit charge, k_B is Boltzmann constant, T is absolute temperature and ψ_0 is the electrical potential at the electrode. This expression includes the characteristic (Debye) length of the diffuse layer:

$$\lambda_D = \left(\frac{\varepsilon_r \varepsilon_0 k_B T}{2Z^2 e^2 c^0}\right)^{1/2} \tag{1.3}$$

where c^0 is the concentration of each ion in the bulk. The GC model overestimates the capacitance in EDL due to neglecting ion size and electrostatic correlations. Because of the non-physical asymptotic behavior $\lim_{|\psi_0|\to\infty} C_{GC} = \infty$, the GC model also loses its validity for high surface potentials.

Later, Stern[9] combined the Helmholtz model with the GC model to describe the electrode/electrolyte interface: a subset of the ions with finite size adsorb on the surface to form an inner region, which is called the compact layer or "Stern layer"; while others form the diffuse layer region, which is the same as what the GC model defines. This model is known as the "Gouy-Chapman-Stern" (GCS) model. The inner Helmholtz plane (IHP) and outer Helmholtz plane (OHP) are used to distinguish the two types of adsorbed ions. Then capacitance in the EDL (C_S) can be treated as a combination of the capacitance from two regions, the Stern type of compact double layer capacitance (C_H) and the diffusion region capacitance (C_{GC}),

$$\frac{1}{C_S} = \frac{1}{C_H} + \frac{1}{C_{GC}}. \tag{1.4}$$

In the series connection, the smaller contribution dominated the overall capacitance, so the GC part only contribute to the total capacitance for small potentials ψ_0, which otherwise approaches to constant Helmholtz capacitance. This behavior still remains questionable, as it

means that the capacitor is constantly able to accumulate the charge at increasing potential, where some form of decaying differential capacitance by saturating ion layers would be expected. So the GCS model leads to a limited predictive quality for concentrated electrolytes.

In recent years, porous electrode materials and novel designed electrolyte systems, such as ionic liquids (ILs) and organic electrolytes, are widely used in EDLCs to optimize the performance. Ionic liquids are dense ionic systems with strongly correlated electrostatic interactions. A double layer model for these systems should therefore address both the steric and electrostatic interactions between the ions and those with the electrode surface. However, traditional double-layer theories like GCS model fail to capture charge capacitive behavior in these new experimental system. The crucial approximations and problems when applying the GCS model to EDLCs are:[10]

- The mean-field character of the Poisson-Boltzmann theory neglects ion-ion correlations;
- Treatment of the ions as point charges without excluded volume, causing theoretically infinite ion accumulation at the interface;
- Limited validity of the Debye screening length for electrolytes at high ion concentrations;
- Only electrostatic interactions are included in the theories, neglecting chemical properties like specific ion adsorption onto the surface.

In 2007, Kornyshev proposed an alternative mean-field theory to describe the interfacial capacitance of the metal/ionic liquid system by solving the “Poisson-Fermi” equation.[11] This model interprets the solvent particle as voids in the lattice. The expression for the differential capacitance is given by

$$C = C_0 \cdot \frac{\cosh\left(\frac{u_0}{2}\right)}{1+2\gamma\sinh^2\left(\frac{u_0}{2}\right)} \cdot \sqrt{\frac{2\gamma\sinh^2\left(\frac{u_0}{2}\right)}{\ln\left(1+2\gamma\sinh^2\left(\frac{u_0}{2}\right)\right)}}, \tag{1.5}$$

where γ is packing parameter, C_0 is the linear part of the Gouy-Chapman capacitance, and u_0 is surface electric potential in reduced unit. The packing parameter γ is defined as

$$\gamma = \frac{2c_\infty}{c_{\max}}, \tag{1.6}$$

which is the ratio of occupied sites c_∞ to maximal available sites $c_{\max}$ .This model predicts the bell and camel shapes for the differential capacitance versus voltage, decaying as $C \sim V^{-1/2}$, which cannot be captured by the traditional GCS model. The behavior of the differential capacitance predicted by this theory was confirmed by subsequent experiments and simulation.[12, 13] However, this mean-field theory fails to predict the alternate charge layering structure which decays exponential into the bulk liquid, as suggested by experiments[14, 15], simulations [16] and CDFT predictions for ionic liquids.[17] This layering structure, known as overscreening structure, starts with a first layer of counterions that overscreens the surface charge of the electrode, and the charge of the first layer is then overscreened by the co-ions in the second layer and so on for several layers until charge neutrality is reached. In order to capture the overscreening and crowding in dense ionic liquid, Bazant *et al.* proposed a phenomenological modification of the lattice model based on the Landau-Ginzburg theory. [18] This theory predicts that overscreening is pronounced at small voltages and gradually replaced by the formation of a condensed layer of counterions, followed by complete lattice saturation at very large voltages. It has been further improved recently by adding the short-range correlation for the ionic liquid electrolyte.[19] In addition, Bazant *et al.* derived the same analytical solution (Eq.(1.5)) from

solving a modified Poisson-Nernst-Planck (MPNP) equation to describe the ion transport during dynamic charging at large bias voltage.[20, 21]

In spite of the recent experimental and theoretical advancements, there still lacks of an in-depth understanding of the EDL charge storage mechanism. For example, recently a new class of super concentrated electrolyte, called "water-in-salt" electrolyte enables the breakthrough of the limited electrolyte electrochemical stability window of water (1.23V) in conventional aqueous electrolyte, resulting in extended windows up to 4.0V.[22-24] Studies of the interfacial structure of these electrolytes and their capacitive behavior lead to the discovery of a nontrivial structural driven potential dependence of differential capacitance on the applied potential.[25, 26] Temperature dependence of EDLs in neat ionic liquids (ILs) as well as IL-solvent mixtures has also attracted much attention.[27-29] Kondrat *et al*. applied the modified Poisson-Fermi theory to study the capacitance and energy storage in double layers with IL-solvent mixtures close to demixing. [30]The authors unveil a new type of the capacitance shape emerging in such systems and demonstrate that the capacitance and stored energy increase as the system approaches demixing, which can have practical applications.

To sum up, EDL lies at the heart of our understanding of the interfacial behavior of electrolytes, which is critically important for capacitive energy storage in EDLCs. More theoretical and fundamental studies on what happens and how the charge is stored in EDL are desired for future EDLC development.

1.2 Electrode/Electrolyte Material for Electric Double-Layer Capacitors

A practical EDLC is generally made of four main components: electrodes (cathode, anode), electrolytes, separators and current collector. Approximately, the energy E (unit: J) and power P (unit: W) of an EDLC are given by

$$E = \frac{1}{2} C V^2, \tag{1.7}$$

$$P = \frac{V^2}{4R}, \tag{1.8}$$

where C is the capacitance (unit: F), V is the operating voltage (unit: V), and R is the equivalent series resistance (unit: Ω) of the device. Current values for the commercial supercapacitor devices reach 8 Wh/kg ($\approx$250 Wh kg^{-1} for Li-ion batteries) for the energy density and go beyond 10 kW/kg ($\approx$1 kW/kg1 for Li-ion batteries) for the power density. These performance characteristics of EDLC devices typically change little (within 5-20%) for more than 1,000,000 cycles of charge and discharge. [31] Nowadays, many effects are given to increase the energy density of the EDLC devices. As shown by Eq.(1.7), the energy of an EDLC is determined by the double-layer capacitance and the cell voltage. Therefore, the approach for improving the energy of supercapacitors is to search electrolytes with higher electrochemical window, and to increase the double-layer capacitance. In the following, the state-of-art of the electrode and electrolyte material will be discussed.

1.2.1 Carbon Based Electrode Material

An optimal electrode material of EDLC requires high specific surface area (SSA) and good electrical conductivity. Carbon-based material have been widely used as EDLC electrode material since they are light, highly conductive, thermally and chemically stable, and they possess open porosity and high SSA. The versatility of carbon also enables to produce different microstructures and a wide variety of physical and chemical properties can be achieved.[32] According to IUPAC [33], the pore in the materials can be divided in several groups in term of the pore size: micropores (< 2 nm), mesopores (2 nm - 50 nm) and macropores (> 50 nm). Due to the complexity in the pore characteristics, practical electrode material rarely feature a uniform pore size, and the porous electrode materials are usually characterized by their pore size

distributions. From the synthetic viewpoint, parameters such as material dimensionality (i.e., from zero dimensional to three dimensional materials), specific surface area, pore volume, and pore size distribution, particle size, and texture can be easily tuned by controlling the synthetic route parameters (albeit some of those can be difficult to characterize faithfully). In this section, we will give a brief description in carbon materials, mainly activated carbons (AC) and carbide-derived carbons (CDCs). We focus on these two materials because the former is the materials of choice for commercial EDLC devices, and the latter is a model material for fundamental EDL study due to their tunable pore sizes.

1.2.1.1 Activated carbons (ACs)

Activated carbons (ACs) are the material of choice for commercial EDLCs because of their high SSA, relatively facile processability and low cost.[34] ACs display a disordered structure and usually feature a broad pore size distributions (PSD) raging from micropores to macropores. They are derived from carbon-rich organic precursors by either physical and/or chemical activation processes. Physical activation is achieved at high temperature under a mixed inert/oxidizing atmosphere using typically steam or carbon dioxide as activation agents, whereas chemical activation is also performed at high temperature but mixing the carbon precursor with alkalis, carbonates, chlorides, acids, or similar reagents. [35, 36] In general, the higher activation temperature/activation time will lead to the larger porosity as well as the broader PSD. It should be noted that porosity creation often means increasing the amount sp^3-bonding resulting in reduction of carbon conductivity. Therefore, there is a trade-off on porosity and conductivity in ACs activation process. The specific capacitance value of ACs can be as high 180 F g^{-1} and 80 F cm^{-3} in ionic liquid [37] or 200 F g^{-1} and slightly over 60 F cm^{-3} in organic electrolyte [38]. In spite of multiple recent improvements, the key challenge with traditional ACs technology is how

to independently control the SSA, pore volume, pore size and shape in these materials. Thus, alternative synthesis techniques have been developed to address these limitations. [39]

1.2.1.2 Carbide-Derived Carbons (CDCs)

For EDLC application, CDCs are generally produced by extraction of metal form metal carbide precursors (TiC, SiC and VC among others) via physical (e.g. thermal decomposition) or chemical (e.g. halogenation) processes. [40] While various carbon structures can be found in CDC, including nanodiamond, carbononions, graphene, graphite, and very dense vertically aligned carbon nanotubes(CNTs), simple disordered porous carbon was found to be the most attractive and abundant material for EDLC applications. [41, 42] The unique properties of porous CDC, such as a high specific surface area and tunable pore size with a narrow size distribution, make it an ideal material for EDLC electrodes. [43] The CDC structures were also used in a series of molecular dynamics simulations to study ion adsorption from neat ionic liquid and ionic liquid-solvent mixture. CDCs yield capacitance values up to 220 F g^{-1} and 126 F cm^{-3} in KOH and 150 F g^{-1} and 70 F cm^{-3} in organic electrolyte.[31] Commercial EDLCs based on CDC materials offer superior energy densities. High power can be achieved as well, for instance, by introducing mesopore channels for fast ion transport [44] or using nano-felts like CDC electrodes[45]. However, the cost of CDC materials is much higher than that of ACs, which limits their broad commercial applications.

1.2.2 Novel Formulation of Electrolyte as Charge Carrier

The charge storage mechanism in EDLCs relies on ion adsorption onto the surface of porous electrodes. An ideal electrolyte for EDLCs requires:

- High electrochemical stability to ensure a high operating voltage and a broad range of operating temperatures.

- Low viscosity (commonly correlated with high ion mobility) for the fast and efficient storage process.
- High conductivity and environmental friendliness.

In general, the commercial EDLCs use either aqueous or organic-based electrolytes. Aqueous electrolytes are limited to low cell voltage, due to the electrolysis of water. For operating at large electrical windows, organic electrolytes are often preferred. For example, an organic electrolyte consisting of 1 M of tetraethylammonium tetra-fluroroborate (Et_4NBF_4) in acetonitrile (CAN) or propylene carbonate (PC) displays good transport properties, and theses organic electrolytes enable EDLCs to work with a voltage in the order of 2.7–2.8 V and in a rather broad temperature range. However, some studies showed that these organic electrolytes will suffer a dramatic reduction in their cycle life if the EDLC is operated at voltages higher than 2.8-3.0V.[46] As a consequence, the development of innovative electrolytes allowing higher voltages is considered as a priority for the application of EDLC. The two main criteria for electrolyte are (wide) electrochemical window and (high) ionic conductivity. In this section, we introduce two novel electrolytes that may satisfy the requirements: one is the room temperature ionic liquid and their derivatives, and the other is the super concentrated electrolyte, or "Solvent-in-Salt" (SIS) electrolyte.

1.2.2.1 Room temperature ionic liquids and their derivatives

Room temperature ionic liquids (ILs) are generally defined as those salts composed solely of ions (cations and anions) with melting point below $100\,^{\circ}C$.[47] Normally, ILs have several potential advantages including high thermal and chemical stability, wide electrochemical window (~4 V), negligible volatility, and non-flammability (depending on the combination of cations and anions).[48] Furthermore, ILs' physical and chemical properties can be highly tunable due to their large variety (virtually unlimited) of combinations of cations and anions.

Different type of cations, e.g., pyrrolidinium, imidazolium, sulfonium and cyclic sulfonium, and anions, e.g., $TFSI^-$, BF_4^-, and PF_6^- have been investigated for EDLC applications.[31] Despite their great potential, there are several drawbacks with most ILs, such as high viscosity and low ionic conductivity, limiting their practical use in EDLCs. For example, the [EMIM][BF4] electrolyte, which has a relatively high ionic conductivity among the common ILs, its conductivity (14 mS cm^{-1} at 25 °C) is much lower than that of $TEABF_4$/ACN (59.9 mS cm^{-1} at 25 °C),[49] and its viscosity is 41 cp, which is much higher than that of the organic electrolyte (e.g. 0.3 cp for the ACN organic electrolyte). The IL properties (e.g. ionic conductivity, viscosity, and electrochemical window) can be improved by modifying the cations or anions or both, and utilizing a mixture of ILs or with an organic solvent. [46] For example, Lin *et al.* utilized the nanostructured carbon electrode and a eutectic mixture of ionic liquids to dramatically extend the temperature range of electrical energy storage. They demonstrated electrical double layer capacitors able to operate from -50 °C to 100 °C over a wide voltage window (up to 3.7 V) and at very high charge/discharge rates of up to 20 V/s. [50]

It should be pointed out that not all the mixtures of IL and organic solvents provide a benefit to EDLC performance. For example, Palm *et al.* [51] reported the addition of an organic solvent (ACN, PC or GBL) to pure [EMIM][BF4] to compose an electrolyte for EDLCs, and the results showed some negative effects although this mixing strategy could lead to a decreased viscosity and melting point, and increased conductivity when compared to those of pure [EMIM][BF4]. Therefore, attention should be paid to not compromising the important advantages of pure IL when adding solvent into the IL for the electrolyte.

1.2.2.2 "Solvent-in-Salt" (SIS) Electrolyte

The "Solvent-in-Salt" (SIS) is a new class of super concentrated electrolytes. Either the weight or volume ratio of salt-to-solvent exceeds 1.0, the electrolyte can be denoted by "Solvent-

in-salt".[52] This new class of electrolytes was originally used for rechargeable metallic lithium batteries. In 2013, Suo *et al.*[52] reported an electrolyte system containing LiTFSI salt and 1,3-dioxolane(DOL)/dimethoxyethane(DME) (1:1 by volume) as the solvent. In this electrolyte, the salt-to-solvent ratio can be as high as seven. This electrolyte exhibits very good electrochemical performance. It shows an initial specific discharge capacity of 1,041 $mAhg^{-1}$ at a current rate of 0.2 C. A coulombic efficiency nearing 100% and long cycling stability are achieved. It is because the lithium polysulphide dissolution is inhibited, thus SIS overcomes one of today's most challenging technological hurdles, the "polysulphide shuttle phenomenon". The authors then extended this system to aqueous electrolytes.[24] They reported a "Water-in-Salt" (WIS) electrolyte whose electrochemical windows was expanded to ~3.0 V by dissolving LiTFSI extremely high concentrations (molarity > 20 M). And such solution is still "true" liquids at room temperature.

The WIS electrolyte was extended to EDLC applications. Dou *et al.* [53] blended acetonitrile with a typical WIS electrolyte (21 m LiTFST/H_2O) create an "acetonitrile/water in salt"(AWIS) electrolyte. The concentration of AWIS electrolyte is 5 M. This 5 M AWIS electrolyte maintains the wide stability window of ~3.0 V and can still work at -30 ^{o}C . This WIS electrolyte exceeds the limitation of water electrolysis in aqueous electrolyte while keeps a high conductivity. These advantages makes it a very attractive electrolyte candidate for EDLCs. The fundamental understanding in this WIS electrolyte, such as the EDL structure and the capacitive response to voltage is also in demand.

1.3 Recent Progress in Theory and Simulations

Trigged by the recent development and breakthroughs in experimental studies of EDLCs, there have been significant interest from theoretical communities to understand the charge storage in EDLCs.[54]Theory, modeling, and simulation can effectively complement experimental

efforts.[55] Large multiscale computations that integrate methods at different time and length scales have the potential to provide a fundamental understanding of processes such as ion transport in electrolytes, charge transfer at interfaces, and electronic transport in electrodes. Among different method, classical molecular dynamics (MD), Monte Carlo (MC) and classical density functional theory (CDFT) are the favored methods of choice to simulate EDL structure and EDLC performance.

1.3.1 Molecular Dynamics

Molecular Dynamics (MD) simulations have been broadly employed to investigate the structure of EDL and the charging dynamics of EDLCs. There are a couple of aspects of concern regarding the simulation of electrode-electrolyte systems using classical MD: (i) model/force field selection for the electrolyte and (ii) representation of electrode. Recent research point out that the choice of models may influence not only the quantitatively accuracy of simulation prediction, but also the physical aspect studied at a qualitative level.[56]

In MD simulation, electrolytes are usually treated using non-polarizable force fields. For many ionic systems, including room temperature ionic liquids, such an approach provides a reasonable estimate of the EDL structure. However, as shown by Borodin *et al.*[57], inclusion of polarizabilities *via* induced dipoles for electrolytes containing small radius ions can dramatically improve the accuracy of prediction of thermodynamic, structural, and, particularly, dynamic properties. Application of polarizable force field usually means a much higher computational cost.[58] Therefore, there is a trade-off between the accuracy and computational cost when choosing the force fields for electrolytes.

Another challenge in MD simulation of EDLCs is the modeling of electrode. [59] To simulate the charged electrode, two methods have been developed: the constant-charge method and the constant-potential method. In the former case, the electrode atoms are assumed to carry a

uniform fixed charge. The potential associated with each value of surface charging is calculated by solving the Poisson equation. Due to the simplicity of implementation, the constant-charge method has been adopted by most researchers to simulate electrodes with simplified geometries. This method, however, neglects charge fluctuations on the electrode induced by local density fluctuations in the electrolyte solutions. To explicitly take into account such fluctuations, the constant-potential method was developed.[60-62]. The comparisons of these two method has been presented by some researchers. In a recent paper, Merlet *et al.*[63] examined the differences between simulations utilizing these two methods by measuring the relaxation kinetics in EDLC with nanoporous carbide-derived carbon (CDC) electrode, and the electrolyte structure at interface in EDLC with a planar graphite electrode. It shows that constant-potential method predicts more reasonable relaxation time, which is modified by orders of magnitude longer, than the constant-charge method. In their study of the electrolyte structure, there were some quantitative differences between the results of the two methods, but the qualitative features were unchanged for these ionic liquid based EDLCs. Wang *et al.*[59] studied a $LiClO_4$/acetonitrile electrolyte at a graphite electrode. For this system, there are no measurable differences between the results of these two method at low potential differences ($\leq$ 2V); however, at larger potential differences (i.e. 4V) significant qualitative differences emerge in the EDLC ion spatial distribution.

Ideally, MD simulation of supercapacitors would include a realistic representation of the carbon electrode structure, as well as a faithful description of its electronic conductivity. However, this is very challenging since they are both computational expensive. To date, only a few studies have include both of these characteristics.[64] For instance, Péan *et al.*[65] studied the charging of electrified nanoporous CDC electrodes impregnated with a BMI-PF_6 electrolyte and found the charging time depended mainly on the average pore size. In the case of CDC-800,

which has a smaller average pore size compared to CDC-1200 and CDC-950, the charging process is also slower by a factor of 4-8. However, the resistance of the confined electrolyte is still of the same order of magnitude as that of bulk electrolyte, which leads to the charging time of one to ten seconds for a 100 μm thick electrode, indicating the CDC exhibits fast charging dynamics. This confirms that the transport of the ions is not much affected in the porous material, which is in agreement with experiments.

Although a number of challenges have been tackled, MD simulation are valuable as they provide a microscopic picture and fundamental understanding of the EDL structure, charging mechanism, and charge storage in EDLCs. For instance, Feng *et al.* [66] studied a model supercapacitor composed of slit-shaped micropores ranging in size from 0.67 to 1.8 nm in IL [EMIM][TFSI]. They found as pore shirked from 1.0 to 0.7 nm, the capacitance of the micropore increased anomalously, which is in good agreement with the experimental observations. [67] Merlet *et al*.[68] highlighted how the lack of "overscreening" effects in nanoporous electrodes contributes to the anomalous capacitance increase observed in nanometer-sized pores. In nanoporous electrodes, only a single layer (or a few layers) of adsorbed ions is present between the pore wall, which is in stark contrast to planar electrode surfaces. Feng *et al* [69] found strong layering and ordering of solvent molecules near neutral surface and distinct contact adsorption of counterions near the charged surface that cannot be described by the Helmholtz model. They further constructed a model called "countercharge layer in generalized solvents" to describe the structure and capacitance of planar electrode immersed by a mixture of RTILs and organic solvents.[70] Their model predicted that the integral capacitance would increase by less than 10% as the mass fraction of acetonitrile (ACN) in the mixture increases from 0 to 50%. Thompson and coworkers combined MD simulations with neutron scattering and reported that the diffusivity and conductivity of an ionic liquid has a positive correlation with the dipole moment and

concentration of the organic solvent added. [71] MD simulations can also be used to explore new ideas to improve energy storage efficiency in supercapacitors.[64] An interesting example of these hypothetical explorations is the concept of ionophobicity and ionophilicity. MD simulations for single slit pores have shown that ionophobic pores perform better in terms of charging rate.[72] One interesting aspect is that the charging of initially filled pores usually leads to an overfilling of the porosity, corresponding to a temporary state where the density of ions is higher than the final density at the end of charging. This type of phenomena raises the issues of kinetic barriers and the difference between static and dynamic charging of supercapacitors.

1.3.2 Grand Canonical Monte Carlo (GCMC)

Torrie and Valleau are among the first who used Monte Carlo simulation for studying EDL formation at charged interfaces in concentrated electrolytes. Their simulations have shown that the GCS theory is not accurate even for EDL in an aqueous solution when the solvent is assumed to be dielectric continuum. At high concentration of ions in an electrolyte, the charge density in the EDL starts to oscillate. Their pioneering works on modeling EDL in concentrated electrolytes showed apparent limitations of the GCS theory for systems with stronger electrostatic interactions.[73, 74] Skinner *et al.* used MC simulations to examine the capacitance of ionic liquid at a metal surface. The results suggested that the "bell-shaped" capacitance curve appears for a good metal electrode due to the strong attraction between ions and their image charges, while the "camel-shaped" capacitance curve appears for the semi-metal electrode (such as glassy carbon) because the finite screening length shifts the reflection plane for the image charges into the electrode and reduces the attraction.[75]

To understand the charge storage mechanism in nanopores, Kondrat *et al* developed a simple phenomenological model.[76] In their work, the capacitance of the pore monotonously increases with the decrease of the pore width expect for large voltage case. For substantially large

voltage values the differential capacitance vanishes at a pore width larger than the ion diameter. In this case, the ions still can get inside the pore, but because at such voltages the pore is already fully occupied by the counterions (here anions), and the differential capacitance response to further electrode polarization is zero. This indicates a saturation of pores at large voltage. In smaller pores the saturation starts at smaller voltage. For large pores saturation takes place in two steps, preceded by a field-induced phase transition. That transition is responsible for an abrupt expulsion of the cations from the positively charged electrode, passing the phase poor in cations, but in which the amount of anions can still grow till the saturation, and hence the "step" preceding the complete vanishing of the capacitance. This effect is weaker for narrower pores. Following this work, they then performed GCMC simulations for a restrictive primitive model of ionic liquid in slit-like metallic nanopores in which image forces exponentially screen out the ion-ion interactions, and form a "superionic" state. The simulations confirmed several essential predictions of their model, such as the anomalous enhancement of capacitance in narrow pores.[77]

The calculations in Ref.[77] have been performed under an assumption that the ions have a propensity to fill in nonpolarized pores, i.e. there is a substantial reduction in free energy of individual ions when they are transferred from the bulk into the pore. Under an opposite assumption, constant voltage GCMC simulations have been performed by Kiyohara *et al.* for different model electrolyte systems in porous electrode.[78-80] Their simulations also predict a field-induced transition but of a different kind: at low voltages the pore resists to being filled by ions and the response to charging of the electrode is minor; however, at some critical voltage, the counterions abruptly enter the pore. It should be noted that because the simulations are performed with the idealized models, it is difficult to experimentally verify these results. Actually, typical

experimental values lie in between these two simulation results. On should therefore focus only on qualitative correspondence between the simulations and available experimental data.[81]

MC simulations can also be used to explore new strategies to improve energy storage in supercapacitors. Kondrat *et al* showed that by creating "ionophobic" pores with a low or vanishing amount of an ionic liquid inside, the quantity of energy stored is higher than those for conventional ionphilic pores. [82]

1.3.3 Classical Density Functional Theory

Classical density functional theory (CDFT) provides a powerful computational tool to study the structure of electric double layers in aqueous systems[83] as well as in ionic liquids and organic electrolyte solutions.[84] The CDFT approach consistently predicts the camel shape curve at low ionic density and the bell-shaped curve at high ionic density as observed in experiments and as predicted by previous simulation and analytical theories. In case of high ionic density, DFT predicts alternating layer of cations and anions at high polarization for the electrolyte, which is relevant to the structures of ionic liquids at charged substrates. [17] The CDFT is able to establish a structure-capacitance relationship for the EDLC. For instance, Jiang *et al.* [85] predict an oscillatory behavior of capacitance of ionic liquid in different pore size, which is attributed to the interference of the overlapping electric double layers.

The CDFT can also provide the guidance for EDLC design. As discussed in previous sections, organic electrolytes and ionic liquids are widely used in EDLCs. By using CDFT, the influence of the organic solvent on the EDLC performance has been explored. [86] In the coarse-grained CDFT model, the solvent is represented by a dipole. It was found that the weakly polar solvent has a capacitance closer to that of an ionic liquid, while a capacitance maximum can be achieved at an optimal dipole moment of 4.0 Debye. Lian *et al.* studies the capacitance of EMI-TFSI and EMI-BF_4 ionic liquid mixture of different composition with onion-like carbon

electrode. A volcano-shaped trend is identified for the capacitance versus the composition of the ionic liquid. The mixture effect, which makes more counterions pack on and more co-ions leave from the electrode surface, leads to an increase of the counterions density with the EDL and consequently a larger capacitance. The CDFT predications are in good agreement with experimental and offer guidance for designing ionic liquid mixtures for EDLC. Lian *et al.* recently developed a spherical shell model to account for both pore size and curvature effects of amorphous porous material.[87] They showed that, as the inner radius of the shell decrease, the capacitance increased significantly, indicating the significant role of convex surface for the synthesis of new porous electrode to optimize the EDLC performance.

The ion dynamics inside the nanopores during charging can be studied in the framework of the time-dependent density functional theory (TDDFT). TDDFT is an extension of the classical DFT to describe dynamic or time dependent processes based on the assumption of local thermodynamic equilibrium. [88] For ionic liquid in nanopores, TDDFT predict three scenarios of charging behavior, depending on the pore width and voltage: the normal charging, the nonmonotonic charging, and charging inversion. [89] The normal charging refers to a charging process in which the surface charge rises with time monotonic to the equilibrium value, while the nonmonotonic charging refers to the process in which the surface charge rises quickly with time to a maximum and then decays monotonically to the equilibrium value. For both cases, the decline of the electrode charge during the charging process is referred to as kinetic charging inversion. The counterintuitive kinetic charging inversion in ionic liquids is closely affiliated with the local segregation of counterions and co-ions near the electrode surface, leading to formation of layer-by-layer ionic densities. The DDFT predictions further showed that the dispersion interaction between the electrode and ionic liquid will lead to a non-monotonic charging and increase the duration of the charging process. [90]

Within the framework of CDFT, the excluded volume enters via a primitive hard-sphere model for the electrolyte and ion-ion, electrode-ion correlation are included using full electrostatic pair interaction. In this dissertation, we use CDFT as a main theoretical tool and explore the interfacial structure, phase behavior and application of non-aqueous electrolyte to capacitive energy storage. The formulism of DFT will be described in details in Chapter 2.

1.4 Research Objectives and Thesis Outline

This dissertation is focused on the application of classical density functional theory (CDFT) for capacitive energy storage, specifically for ionic liquids and organic electrolytes. Through the computational work, we seek to address the following issues at the frontier of EDLC development:

- How does the electrolyte composition influence the capacitance of EDLC? In particular, what are the effects of ionic liquids mixing with a small amount of additives/impurities?
- How can we design an electrolyte-electrode system to store charge more efficiently? And what is the possible charge storage mechanism in this new model system?
- How does the wettability of the non-aqueous electrolyte influence the performance of the EDLC?

Here we briefly describe the structure and content of the theses:

In **Chapter1,** we introduce the background and research progress in capacitive energy storage. We explain the challenges in EDLC research both in theory and in practice. We summarize development of EDL theory and the state-of-art progress in simulation and modeling. We then summarize our research objectives, and outline of the thesis.

Chapter 2 covers the basic formulism of the Classical Density Functional Theory (CDFT), focusing on the construction of Helmholtz energy and corresponding chemical potential.

We described two functionals that take into account the electrostatic correlation differently. The choice of approximations in CDFT depends on system properties that one would like to investigate. The methodology presented in this chapter will be used throughout the following chapters.

In **Chapter 3** and **Chapter 4**, we analyze how the electrolyte composition influences the charge storage in EDLCs. The porous material is modeled as a simple slit-pore geometry and the electrolyte is represented by a coarse-grained model. The electrolyte mixture consists of an ionic liquid and a small amount of other chemicals, i.e. water or an organic solvent. The properties of such additives/impurities are identified by tuning the size and dipole moment of the molecule, the interaction between the ions or the electrode. We studied the influence of these chemicals on EDL structure and the overall capacitive performance of the EDLC.

Chapter 5 proposed an ideal on how to storage the charge more efficiently. By tuning interaction between the ions and the electrode, we are able to create an equivalent 'ionphobic' pores as originally proposed by Konysheve and co-workers.[72, 82]We analyze the change of capacitance and energy with the voltage and proposed different charging scenarios in this system.

Chapter 6 presents the study of the wettability of the non-aqueous electrolyte on porous carbon material. We study the phase behavior of non-aqueous electrolytes under confinement and demonstrate that the accessibility of micropores depends not only on the ionic diameters (or desolvation) but also on their wetting behavior intrinsically related to the vapor-liquid or liquid-liquid phase separation of the bulk ionic systems.

Finally **Chapter 7** summarizes key conclusions from this dissertation and offers some perspectives for future work.

Bibliography

[1] P. Simon and Y. Gogotsi, "Capacitive energy storage in nanostructured carbon-electrolyte systems," *Acc Chem Res,* vol. 46, no. 5, pp. 1094-103, May 21 2013.

[2] J. B. Goodenough, H. D. Abruna, and M. V. Buchanan, "Basic research needs for electrical energy storage. Report of the basic energy sciences workshop for electrical energy storage. ," 2007.

[3] H. I. Becker, "Low voltage electrolytic capacitor," ed: Google Patents, 1957.

[4] R. A. Rightmire, "Electrical energy storage apparatus," ed: Google Patents, 1966.

[5] M. Winter and R. J. Brodd, "What Are Batteries, Fuel Cells, and Supercapacitors?," *Chemical Reviews,* vol. 104, no. 10, pp. 4245-4270, 2004.

[6] H. Helmholtz, "Ueber einige Gesetze der Vertheilung elektrischer Ströme in körperlichen Leitern, mit Anwendung auf die thierisch-elektrischen Versuche (Schluss.)," *Annalen der Physik und Chemie,* vol. 165, no. 7, pp. 353-377, 1853.

[7] M. Gouy, "Sur la constitution de la charge électrique à la surface d'un électrolyte," *Journal de Physique Théorique et Appliquée,* vol. 9, no. 1, pp. 457-468, 1910.

[8] D. L. Chapman, "LI. A contribution to the theory of electrocapillarity," *The London, Edinburgh, and Dublin Philosophical Magazine and Journal of Science,* vol. 25, no. 148, pp. 475-481, 1913.

[9] O. Stern, "The theory of the electrolytic double-layer," *Z. Elektrochem,* vol. 30, no. 508, pp. 1014-1020, 1924.

[10] K. Breitsprecher, "Simulation studies on electrodes and electrolytes for electric double layer capacitors," 2018.

[11] A. A. Kornyshev, "Double-layer in ionic liquids: paradigm change?," *J Phys Chem B,* vol. 111, no. 20, pp. 5545-57, May 24 2007.

[12] M. T. Alam, M. M. Islam, T. Okajima, and T. Ohsaka, "Measurements of Differential Capacitance at Mercury/Room-Temperature Ionic Liquids Interfaces," *The Journal of Physical Chemistry C,* vol. 111, no. 49, pp. 18326-18333, 2007.

[13] M. M. Islam, M. T. Alam, and T. Ohsaka, "Electrical Double-Layer Structure in Ionic Liquids: A Corroboration of the Theoretical Model by Experimental Results," *The Journal of Physical Chemistry C,* vol. 112, no. 42, pp. 16568-16574, 2008.

[14] M. Mezger *et al.*, "Molecular layering of fluorinated ionic liquids at a charged sapphire (0001) surface," *Science,* vol. 322, no. 5900, pp. 424-8, Oct 17 2008.

[15] R. Hayes, S. Z. El Abedin, and R. Atkin, "Pronounced structure in confined aprotic room-temperature ionic liquids," *J Phys Chem B,* vol. 113, no. 20, pp. 7049-52, May 21 2009.

[16] M. V. Fedorov and A. A. Kornyshev, "Towards understanding the structure and capacitance of electrical double layer in ionic liquids," *Electrochimica Acta,* vol. 53, no. 23, pp. 6835-6840, 2008.

[17] J. Wu, T. Jiang, D.-e. Jiang, Z. Jin, and D. Henderson, "A classical density functional theory for interfacial layering of ionic liquids," *Soft Matter,* vol. 7, no. 23, p. 11222, 2011.

[18] M. Z. Bazant, B. D. Storey, and A. A. Kornyshev, "Double layer in ionic liquids: overscreening versus crowding," *Phys Rev Lett,* vol. 106, no. 4, p. 046102, Jan 28 2011.

[19] Z. A. H. Goodwin, G. Feng, and A. A. Kornyshev, "Mean-Field Theory of Electrical Double Layer In Ionic Liquids with Account of Short-Range Correlations," *Electrochimica Acta,* vol. 225, pp. 190-197, 2017.

[20] M. S. Kilic, M. Z. Bazant, and A. Ajdari, "Steric effects in the dynamics of electrolytes at large applied voltages. I. Double-layer charging," *Phys Rev E Stat Nonlin Soft Matter Phys,* vol. 75, no. 2 Pt 1, p. 021502, Feb 2007.

[21] M. S. Kilic, M. Z. Bazant, and A. Ajdari, "Steric effects in the dynamics of electrolytes at large applied voltages. II. Modified Poisson-Nernst-Planck equations," *Phys Rev E Stat Nonlin Soft Matter Phys,* vol. 75, no. 2 Pt 1, p. 021503, Feb 2007.

[22] H. Tomiyasu, H. Shikata, K. Takao, N. Asanuma, S. Taruta, and Y. Y. Park, "An aqueous electrolyte of the widest potential window and its superior capability for capacitors," *Sci Rep,* vol. 7, p. 45048, Mar 21 2017.

[23] V. A. Azov, K. S. Egorova, M. M. Seitkalieva, A. S. Kashin, and V. P. Ananikov, ""Solvent-in-salt" systems for design of new materials in chemistry, biology and energy research," *Chem Soc Rev,* vol. 47, no. 4, pp. 1250-1284, Feb 21 2018.

[24] L. Suo *et al.*, ""Water-in-salt" electrolyte enables high-voltage aqueous lithium-ion chemistries," *Science,* vol. 350, no. 6263, pp. 938-43, Nov 20 2015.

[25] M. McEldrew, Z. A. H. Goodwin, A. A. Kornyshev, and M. Z. Bazant, "Theory of the Double Layer in Water-in-Salt Electrolytes," *J Phys Chem Lett,* vol. 9, no. 19, pp. 5840-5846, Oct 4 2018.

[26] Z. Li, G. Jeanmairet, T. Méndez-Morales, B. Rotenberg, and M. Salanne, "Capacitive Performance of Water-in-Salt Electrolytes in Supercapacitors: A Simulation Study," *The Journal of Physical Chemistry C,* vol. 122, no. 42, pp. 23917-23924, 2018.

[27] J. Wang *et al.*, ""Thermal Charging" Phenomenon in Electrical Double Layer Capacitors," *Nano Lett,* vol. 15, no. 9, pp. 5784-90, Sep 9 2015.

[28] M. Janssen and R. van Roij, "Reversible Heating in Electric Double Layer Capacitors," *Phys Rev Lett,* vol. 118, no. 9, p. 096001, Mar 3 2017.

[29] M. Chen, Z. A. H. Goodwin, G. Feng, and A. A. Kornyshev, "On the temperature dependence of the double layer capacitance of ionic liquids," *Journal of Electroanalytical Chemistry,* vol. 819, pp. 347-358, 2018.

[30] C. Cruz, A. Ciach, E. Lomba, and S. Kondrat, "Electrical Double Layers Close to Ionic Liquid–Solvent Demixing," *The Journal of Physical Chemistry C,* vol. 123, no. 3, pp. 1596-1601, 2018.

[31] Z. Lin *et al.*, "Materials for supercapacitors: When Li-ion battery power is not enough," *Materials Today,* vol. 21, no. 4, pp. 419-436, 2018.

[32] Y. Zhai, Y. Dou, D. Zhao, P. F. Fulvio, R. T. Mayes, and S. Dai, "Carbon materials for chemical capacitive energy storage," *Adv Mater,* vol. 23, no. 42, pp. 4828-50, Nov 9 2011.

[33] A. D. McNaught and A. D. McNaught, *Compendium of chemical terminology*. Blackwell Science Oxford, 1997.

[34] M. Sevilla and R. Mokaya, "Energy storage applications of activated carbons: supercapacitors and hydrogen storage," *Energy Environ. Sci.,* vol. 7, no. 4, pp. 1250-1280, 2014.

[35] L. Wei, M. Sevilla, A. B. Fuertes, R. Mokaya, and G. Yushin, "Hydrothermal Carbonization of Abundant Renewable Natural Organic Chemicals for High-Performance Supercapacitor Electrodes," *Advanced Energy Materials,* vol. 1, no. 3, pp. 356-361, 2011.

[36] L. Wei and G. Yushin, "Nanostructured activated carbons from natural precursors for electrical double layer capacitors," *Nano Energy,* vol. 1, no. 4, pp. 552-565, 2012.

[37] E. Redondo *et al.*, "Outstanding room-temperature capacitance of biomass-derived microporous carbons in ionic liquid electrolyte," *Electrochemistry Communications,* vol. 79, pp. 5-8, 2017.

[38] A. Jänes, H. Kurig, and E. Lust, "Characterisation of activated nanoporous carbon for supercapacitor electrode materials," *Carbon,* vol. 45, no. 6, pp. 1226-1233, 2007.

[39] W. Gu and G. Yushin, "Review of nanostructured carbon materials for electrochemical capacitor applications: advantages and limitations of activated carbon, carbide-derived carbon, zeolite-templated carbon, carbon aerogels, carbon nanotubes, onion-like carbon, and graphene," *Wiley Interdisciplinary Reviews: Energy and Environment,* vol. 3, no. 5, pp. 424-473, 2014.

[40] V. Presser, M. Heon, and Y. Gogotsi, "Carbide-Derived Carbons - From Porous Networks to Nanotubes and Graphene," *Advanced Functional Materials,* vol. 21, no. 5, pp. 810-833, 2011.

[41] Y. Gogotsi, S. Welz, D. A. Ersoy, and M. J. McNallan, "Conversion of silicon carbide to crystalline diamond-structured carbon at ambient pressure," *Nature,* vol. 411, no. 6835, p. 283, 2001.

[42] Z. G. Cambaz, G. Yushin, S. Osswald, V. Mochalin, and Y. Gogotsi, "Noncatalytic synthesis of carbon nanotubes, graphene and graphite on SiC," *Carbon,* vol. 46, no. 6, pp. 841-849, 2008.

[43] J. Chmiola, G. Yushin, R. Dash, and Y. Gogotsi, "Effect of pore size and surface area of carbide derived carbons on specific capacitance," *Journal of Power Sources,* vol. 158, no. 1, pp. 765-772, 2006.

[44] Y. Korenblit *et al.,* "High-rate electrochemical capacitors based on ordered mesoporous silicon carbide-derived carbon," *ACS Nano,* vol. 4, no. 3, pp. 1337-44, Mar 23 2010.

[45] Y. Gao *et al.,* "High power supercapacitor electrodes based on flexible TiC-CDC nano-felts," *Journal of Power Sources,* vol. 201, pp. 368-375, 2012.

[46] C. Zhong, Y. Deng, W. Hu, J. Qiao, L. Zhang, and J. Zhang, "A review of electrolyte materials and compositions for electrochemical supercapacitors," *Chem Soc Rev,* vol. 44, no. 21, pp. 7484-539, Nov 7 2015.

[47] R. D. Rogers and G. A. Voth, "Ionic liquids," *Acc Chem Res,* vol. 40, no. 11, pp. 1077-8, Nov 2007.

[48] M. Armand, F. Endres, D. R. MacFarlane, H. Ohno, and B. Scrosati, "Ionic-liquid materials for the electrochemical challenges of the future," *Nat Mater,* vol. 8, no. 8, pp. 621-9, Aug 2009.

[49] J. G. Huddleston, A. E. Visser, W. M. Reichert, H. D. Willauer, G. A. Broker, and R. D. Rogers, "Characterization and comparison of hydrophilic and hydrophobic room temperature ionic liquids incorporating the imidazolium cation," *Green Chemistry,* vol. 3, no. 4, pp. 156-164, 2001.

[50] R. Lin *et al.,* "Capacitive Energy Storage from −50 to 100 °C Using an Ionic Liquid Electrolyte," *The Journal of Physical Chemistry Letters,* vol. 2, no. 19, pp. 2396-2401, 2011.

[51] R. Palm, H. Kurig, K. Tõnurist, A. Jänes, and E. Lust, "Influence of Different Organic Solvent Additives on 1-ethyl-3-methylimidazolium Tetrafluoroborate Electrolyte Based Electrical Double Layer Capacitors," *Journal of The Electrochemical Society,* vol. 160, no. 10, pp. A1741-A1745, 2013.

[52] L. Suo, Y. S. Hu, H. Li, M. Armand, and L. Chen, "A new class of Solvent-in-Salt electrolyte for high-energy rechargeable metallic lithium batteries," *Nat Commun,* vol. 4, p. 1481, 2013.

[53] Q. Dou *et al.*, "Safe and high-rate supercapacitors based on an “acetonitrile/water in salt” hybrid electrolyte," *Energy & Environmental Science,* vol. 11, no. 11, pp. 3212-3219, 2018.

[54] C. Zhan *et al.*, "Computational Insights into Materials and Interfaces for Capacitive Energy Storage," *Adv Sci (Weinh),* vol. 4, no. 7, p. 1700059, Jul 2017.

[55] J. Huang, B. G. Sumpter, and V. Meunier, "Theoretical model for nanoporous carbon supercapacitors," *Angew Chem Int Ed Engl,* vol. 47, no. 3, pp. 520-4, 2008.

[56] J. Vatamanu and O. Borodin, "Ramifications of Water-in-Salt Interfacial Structure at Charged Electrodes for Electrolyte Electrochemical Stability," *J Phys Chem Lett,* vol. 8, no. 18, pp. 4362-4367, Sep 21 2017.

[57] O. Borodin, "Polarizable force field development and molecular dynamics simulations of ionic liquids," *J Phys Chem B,* vol. 113, no. 33, pp. 11463-78, Aug 20 2009.

[58] M. Salanne, "Simulations of room temperature ionic liquids: from polarizable to coarse-grained force fields," *Phys Chem Chem Phys,* vol. 17, no. 22, pp. 14270-9, Jun 14 2015.

[59] Z. Wang, Y. Yang, D. L. Olmsted, M. Asta, and B. B. Laird, "Evaluation of the constant potential method in simulating electric double-layer capacitors," *J Chem Phys,* vol. 141, no. 18, p. 184102, Nov 14 2014.

[60] J. I. Siepmann and M. Sprik, "Influence of surface topology and electrostatic potential on water/electrode systems," *The Journal of chemical physics,* vol. 102, no. 1, pp. 511-524, 1995.

[61] S. K. Reed, O. J. Lanning, and P. A. Madden, "Electrochemical interface between an ionic liquid and a model metallic electrode," *J Chem Phys,* vol. 126, no. 8, p. 084704, Feb 28 2007.

[62] T. R. Gingrich and M. Wilson, "On the Ewald summation of Gaussian charges for the simulation of metallic surfaces," *Chemical Physics Letters,* vol. 500, no. 1-3, pp. 178-183, 2010.

[63] C. Merlet, C. Pean, B. Rotenberg, P. A. Madden, P. Simon, and M. Salanne, "Simulating Supercapacitors: Can We Model Electrodes As Constant Charge Surfaces?," *J Phys Chem Lett,* vol. 4, no. 2, pp. 264-8, Jan 17 2013.

[64] A. C. Forse, C. Merlet, J. M. Griffin, and C. P. Grey, "New Perspectives on the Charging Mechanisms of Supercapacitors," *J Am Chem Soc,* vol. 138, no. 18, pp. 5731-44, May 11 2016.

[65] C. Pean *et al.*, "On the dynamics of charging in nanoporous carbon-based supercapacitors," *ACS Nano,* vol. 8, no. 2, pp. 1576-83, Feb 25 2014.

[66] G. Feng and P. T. Cummings, "Supercapacitor Capacitance Exhibits Oscillatory Behavior as a Function of Nanopore Size," *The Journal of Physical Chemistry Letters,* vol. 2, no. 22, pp. 2859-2864, 2011.

[67] C. Largeot, C. Portet, J. Chmiola, P. L. Taberna, Y. Gogotsi, and P. Simon, "Relation between the ion size and pore size for an electric double-layer capacitor," *J Am Chem Soc,* vol. 130, no. 9, pp. 2730-1, Mar 5 2008.

[68] C. Merlet *et al.*, "On the molecular origin of supercapacitance in nanoporous carbon electrodes," *Nat Mater,* vol. 11, no. 4, pp. 306-10, Mar 4 2012.

[69] G. Feng, J. Huang, B. G. Sumpter, V. Meunier, and R. Qiao, "Structure and dynamics of electrical double layers in organic electrolytes," *Phys Chem Chem Phys,* vol. 12, no. 20, pp. 5468-79, 2010.

[70] G. Feng, J. Huang, B. G. Sumpter, V. Meunier, and R. Qiao, "A "counter-charge layer in generalized solvents" framework for electrical double layers in neat and hybrid ionic liquid electrolytes," *Phys Chem Chem Phys,* vol. 13, no. 32, pp. 14723-34, Aug 28 2011.

[71] N. C. Osti *et al.*, "Solvent Polarity Governs Ion Interactions and Transport in a Solvated Room-Temperature Ionic Liquid," *J Phys Chem Lett,* vol. 8, no. 1, pp. 167-171, Jan 5 2017.

[72] S. Kondrat, P. Wu, R. Qiao, and A. A. Kornyshev, "Accelerating charging dynamics in subnanometre pores," *Nat Mater,* vol. 13, no. 4, pp. 387-93, Apr 2014.

[73] G. M. Torrie and J. P. Valleau, "Electrical double layers. I. Monte Carlo study of a uniformly charged surface," *The Journal of Chemical Physics,* vol. 73, no. 11, pp. 5807-5816, 1980.

[74] G. M. Torrie, J. P. Valleau, and G. N. Patey, "Electrical double layers. II. Monte Carlo and HNC studies of image effects," *The Journal of Chemical Physics,* vol. 76, no. 9, pp. 4615-4622, 1982.

[75] M. S. Loth, B. Skinner, and B. I. Shklovskii, "Anomalously large capacitance of an ionic liquid described by the restricted primitive model," *Phys Rev E Stat Nonlin Soft Matter Phys,* vol. 82, no. 5 Pt 2, p. 056102, Nov 2010.

[76] S. Kondrat and A. Kornyshev, "Corrigendum: Superionic state in double-layer capacitors with nanoporous electrodes," *Journal of Physics: Condensed Matter,* vol. 25, no. 11, p. 119501, 2013.

[77] S. Kondrat, N. Georgi, M. V. Fedorov, and A. A. Kornyshev, "A superionic state in nano-porous double-layer capacitors: insights from Monte Carlo simulations," *Phys Chem Chem Phys,* vol. 13, no. 23, pp. 11359-66, Jun 21 2011.

[78] K. Kiyohara, T. Sugino, and K. Asaka, "Phase transition in porous electrodes," *J Chem Phys,* vol. 134, no. 15, p. 154710, Apr 21 2011.

[79] K. Kiyohara, H. Shioyama, T. Sugino, and K. Asaka, "Phase transition in porous electrodes. II. Effect of asymmetry in the ion size," *J Chem Phys,* vol. 136, no. 9, p. 094701, Mar 7 2012.

[80] K. Kiyohara *et al.*, "Phase transition in porous electrodes. III. For the case of a two component electrolyte," *J Chem Phys,* vol. 138, no. 23, p. 234704, Jun 21 2013.

[81] M. V. Fedorov and A. A. Kornyshev, "Ionic liquids at electrified interfaces," *Chem Rev,* vol. 114, no. 5, pp. 2978-3036, Mar 12 2014.

[82] S. Kondrat and A. A. Kornyshev, "Pressing a spring: what does it take to maximize the energy storage in nanoporous supercapacitors?," *Nanoscale Horizons,* vol. 1, no. 1, pp. 45-52, 2016.

[83] Z. Li and J. Wu, "Density functional theory for planar electric double layers: closing the gap between simple and polyelectrolytes," *J Phys Chem B,* vol. 110, no. 14, pp. 7473-84, Apr 13 2006.

[84] D.-e. Jiang, D. Meng, and J. Wu, "Density functional theory for differential capacitance of planar electric double layers in ionic liquids," *Chemical Physics Letters,* vol. 504, no. 4-6, pp. 153-158, 2011.

[85] D. E. Jiang, Z. Jin, and J. Wu, "Oscillation of capacitance inside nanopores," *Nano Lett,* vol. 11, no. 12, pp. 5373-7, Dec 14 2011.

[86] D. E. Jiang and J. Wu, "Unusual effects of solvent polarity on capacitance for organic electrolytes in a nanoporous electrode," *Nanoscale,* vol. 6, no. 10, pp. 5545-50, May 21 2014.

[87] C. Lian, D.-e. Jiang, H. Liu, and J. Wu, "A Generic Model for Electric Double Layers in Porous Electrodes," *The Journal of Physical Chemistry C,* vol. 120, no. 16, pp. 8704-8710, 2016.

[88] S. L. Zhao and J. Wu, "Self-consistent equations governing the dynamics of nonequilibrium colloidal systems," *J Chem Phys,* vol. 134, no. 5, p. 054514, Feb 7 2011.

[89] J. Jiang, D. Cao, D. E. Jiang, and J. Wu, "Kinetic Charging Inversion in Ionic Liquid Electric Double Layers," *J Phys Chem Lett,* vol. 5, no. 13, pp. 2195-200, Jul 3 2014.

[90] C. Lian, S. Zhao, H. Liu, and J. Wu, "Time-dependent density functional theory for the charging kinetics of electric double layer containing room-temperature ionic liquids," *J Chem Phys,* vol. 145, no. 20, p. 204707, Nov 28 2016.

Chapter 2. General Formulism of Classical Density Functional Theory

This chapter introdcues the basic concepts and formulism of classical density functional theory (CDFT), which are common ingredients of the following chapters. CDFT is a standard approach to calculate the structure, the thermodynamic properties and the phase behavior of confined fluids. In essence, CDFT is able to quantitatively predict the microscopic structural and thermodynamic properties of complex molecular system with accuracy comparable to that inherited from semi-empirical force filed but at a computational cost lower than molecular simulations up to several orders of magnitude. [1] Practical application of CDFT requires various approximations for the free energy functional in terms of the one-body density profile underlying the microscopic structure of molecular systems.

2.1 Background

The theoretical basis underpinning all kinds of DFT method can be established within the framework of the Hohenberg-Kohn-Mermin (HKM) theory. In 1964, Hohenberg and Kohn established the Density Functional Theory (DFT) in a quantum-mechanical framework.[2] Their formulation relates to the ground-state energy of electrons in the presence of external fields. That work was later generalized by Mermin to finite temperatures, demonstrating that the thermodynamic free energy was minimized by the equilibrium electronic number density.[3] The central idea of HKM theorem is that the external potential of a multi-body system is uniquely determined by the one-body density profile. CDFT has its origins in the density functional treatment for the ground state of an inhomogeneous electro gas. Whereas in electronic DFT the fundamental variable is the electron density, in classical DFT this is the average one-body ‘particle’ density where the particles refer to atoms or ions, tackled at the Angstrom scale, or to colloidal particles at the micron length scale.[4]

One might also argue that van der Waals' 1893 treatment of the liquid-gas interface,[5] which used the particle density as a basic variable, and Onsager's treatment of the isotropic to nematic transition in hard-rod model fluids, which used particle position and orientation as fundamental variable,[6] were early example of classical DFT. However, without the fundamental variation principle of HKM, the basis of classical DFT would be questionable. The first application of classical DFT as a general methodology to classical systems was reported in 1976-7 by Ebner *et al.*[7] [8] for modeling the surface tension of the liquid–gas interface and the density profile of a repulsive wall-liquid interface for a simple Lennard–Jones fluid. In the same year, Yang *et al*[9] without knowing about the HKM formalism for electrons, independently published a formal derivation of square-gradient theory for a fluid interface and introduced a Legendre transformation from external potential as variable to particle density as variable - which is now considered as a key ingredient of DFT. A more detailed historical discussion can be found in several review and introductory articles. [4, 10-12]

2.2 Density Profile

We first present a brief introduction to the DFT formalism using a one-component monatomic system as an example. Similar equations are applicable to multicomponent molecular/ionic systems. For a system containing N identical particles, the instantaneous total density $\hat{\rho}(\mathbf{r})$, which counts the number of particles at a position $\mathbf{r}$ can be represented by a three-dimensional Dirac- δ function:

$$\hat{\rho}(\mathbf{r}) = \sum_{i=1}^{N} \delta(\mathbf{r} - \mathbf{r}_i), \tag{2.1}$$

The Dirac-δ function is zero everywhere but infinite at the location of the particle. The Dirac-δ function is subject to the normalization condition:

$$\int d\mathbf{r}\,\delta(\mathbf{r} - \mathbf{r}_i) = 1. \tag{2.2}$$

The density profile is defined as an ensemble average of the instantaneous density:

$$\rho(\mathbf{r}) = <\hat{\rho}(\mathbf{r})> = \left\langle \sum_{i=1}^{N} \delta(\mathbf{r} - \mathbf{r}_i) \right\rangle. \tag{2.3}$$

Because the Dirac-δ function specifies the probability density of finding a single particle, the density profile $\rho(\mathbf{r})$ represent the average distribution of all particles in space.

To connect thermodynamic properties with the one-body density $\rho(\mathbf{r})$, we consider an open system at fixed temperature T and volume V. The grand partition function Ξ is given by:

$$\Xi = \sum_{N} \frac{1}{N!\Lambda^{3N}} \int d\mathbf{r}^N \exp\left\{ -\beta \left[\Gamma(\mathbf{r}^N) + \sum_{i=1}^{N} \varphi(\mathbf{r}_i) \right] \right\}, \tag{2.4}$$

where Λ is the thermal wavelength, $\Gamma(\mathbf{r}^N)$ stands for the total interaction potential of N particles at configuration $\mathbf{r}^N = (\mathbf{r}_1, \mathbf{r}_2, \ldots, \mathbf{r}_N)$, and $\beta = 1/(k_B T)$ with k_B is the Boltzmann constant. The one-body potential $\varphi(\mathbf{r})$ combines the chemical potential μ and the external potential $v(\mathbf{r})$:

$$\varphi(\mathbf{r}) \equiv v(\mathbf{r}) - \mu. \tag{2.5}$$

The grand partition function is a function of T and volume V but a functional of the one-body potential $\varphi(\mathbf{r})$.

By substituting Eq.(2.4) into Eq.(2.3), the one-body density profile $\rho(\mathbf{r})$ is related to the grand partition function:

$$\rho(\mathbf{r}) = \frac{1}{\Xi} \sum_{N} \frac{1}{N!\Lambda^{3N}} \int d\mathbf{r}^N \sum_{i=1}^{N} \delta(\mathbf{r} - \mathbf{r}_i) \exp\left\{ -\beta \left[\Gamma(\mathbf{r}^N) + \sum_{i=1}^{N} \varphi(\mathbf{r}_i) \right] \right\} = -\frac{1}{\beta \Xi} \frac{\delta \Xi}{\delta \varphi(\mathbf{r})}, \tag{2.6}$$

where $\delta\Xi / \delta\varphi(\mathbf{r})$ represents a functional derivative. In terms of the grand potential Ω :

$$\beta\Omega \equiv -\ln \Xi. \tag{2.7}$$

The one-body density $\rho(\mathbf{r})$ can be expressed as:

$$\rho(\mathbf{r}) = \frac{\delta\Omega}{\delta\varphi(\mathbf{r})}. \tag{2.8}$$

We may define the intrinsic Helmholtz energy by using the Legendre transformation:

$$F \equiv \Omega - \int d\mathbf{r}\varphi(\mathbf{r})\rho(\mathbf{r}). \tag{2.9}$$

Based on Eq.(2.8), the Legendre transform ensures that the intrinsic Helmholtz energy F is a functional of the one-body density profiles $\rho(\mathbf{r})$, i.e. $F = F[\rho(\mathbf{r})]$.

At equilibrium, the grand potential functional is minimized by the one-body density:

$$\frac{\delta\Omega\left[\rho(\mathbf{r})\right]}{\delta\rho(\mathbf{r})} = 0, \tag{2.10}$$

Combining Eq.(2.5), Eq. (2.9) and Eq.(2.10) , we have

$$\frac{\delta F\left[\rho(\mathbf{r})\right]}{\delta\rho(\mathbf{r})} = \mu - v(\mathbf{r}). \tag{2.11}$$

Given the chemical potential μ, the external potential $v(\mathbf{r})$, and an expression for the intrinsic Helmholtz energy functional $F[\rho(\mathbf{r})]$, we can solve for the equilibrium density profile $\rho(\mathbf{r})$ from the Euler-Lagrange equation (*viz*., (2.11)). The equilibrium density can then be used to determine the grand potential and all pertinent thermodynamic properties.[13]

In a nutshell, the knowledge of the functional $F\left[\rho(\mathbf{r})\right]$ reduces the problem of calculating the equilibrium density profile and the grand potential of inhomogeneous fluids to a functional minimization problem, representing a simplification over the direct evaluation of the grand partition function Ξ.

We can generalize the above procedure to a multi-component system consisting of mixture of polymeric molecules and monomers with varying intermolecular and intramolecular

interactions at temperature T, total volume V, and bulk chemical potential of polymeric molecules μ_M and that of monomers μ_a. By using a coarse-grained model, polymeric molecules are represented by freely joined spherical segments with M segments. Within this model, the bond length is defined by the segment diameters, the monomers are represented by spherical particles. [14] The grand potential can be then expressed as:

$$\begin{aligned}\Omega\left[\rho_M(\mathbf{R}),\{\rho_a(\mathbf{r})\}\right] = F\left[\rho_M(\mathbf{R}),\{\rho_a(\mathbf{r})\}\right] + \int\left[V_M(\mathbf{R})-\mu_M\right]\rho_M(\mathbf{R})d\mathbf{R} \\ +\sum_a\int\left[V_a(\mathbf{r})-\mu_a\right]\rho_a(\mathbf{r})d\mathbf{r}',\end{aligned} \tag{2.12}$$

in which $d\mathbf{R} = d\mathbf{r}_1 d\mathbf{r}_2 \cdots d\mathbf{r}_M$ represents a set of differential volumes, $\rho_M(\mathbf{R})$ is a multi-dimensional molecular density profile as a function of the configuration $\mathbf{R}$, $\rho_a(\mathbf{r})$ is the segmental distribution of monomers, $V_M(\mathbf{R})$ is the summation of the external potential of segments, i.e. $V_M(\mathbf{R}) = \sum_{i=1}^{M} v_i(\mathbf{r}_i)$, and $V_a(\mathbf{r})$ is the external potential of monomers.

2.3 Intrinsic Helmholtz Free Energy

Formally, the intrinsic Helmholtz free energy can be decomposed into an ideal-gas term F^{id} and an excess term F^{ex},

$$F\left[\rho_M(\mathbf{R}),\{\rho_a(\mathbf{r})\}\right] = F^{id}\left[\rho_M(\mathbf{R}),\{\rho_a(\mathbf{r})\}\right] + F^{ex}\left[\rho_M(\mathbf{R}),\{\rho_a(\mathbf{r})\}\right]. \tag{2.13}$$

The ideal part represents the contribution of an ideal gas where all non-bonded interactions are turned off. The ideal-gas term is known exactly

$$\begin{aligned}F^{id}\left[\rho_M(\mathbf{R}),\{\rho_a(\mathbf{r})\}\right] = \int\left[\ln\rho_M(\mathbf{R})-1\right]\rho_M(\mathbf{R})d\mathbf{R} + \beta\int V_B(\mathbf{R})\rho_M(\mathbf{R})d\mathbf{R} \\ +\sum_a\int\left[\ln\rho_a(\mathbf{r})-1\right]\rho_a(\mathbf{r})d\mathbf{r}.\end{aligned} \tag{2.14}$$

where $V_B(\mathbf{R})$ stands for the bond potential. Here, we set $V_B(\mathbf{R})$ equal to the bare bonding potential though other choices are possible. Different choices for $V_B(\mathbf{R})$ will necessarily alter the

expression for the excess free energy. For rigid bonds in the freely jointed chain of equal size, the bare bonding potential is given by the following relation,

$$\exp\left[-\beta V_B\left(\mathbf{R}\right)\right]=\prod_{i=1}^{M-1}\frac{\delta\left(\left|\mathbf{r}_{i+1}-\mathbf{r}_i\right|-\sigma_p\right)}{4\pi\sigma_p{}^2}. \tag{2.15}$$

where σ_p is the segment diameter. Note that we have assumed the bonding potential has an additive constant, which normalized the Boltzmann factor. This constant can be physically interpreted as an entropic contribution due to free bond rotation.

While the ideal Helmholtz free energy functional F^{id} is known exactly, the excess term F^{ex} is not known in general and one has to reply on approximations. The representations and approximations about the excess Helmholtz free energy will be described in details in the following.

2.4 Excess Helmholtz Free Energy

The excess Helmholtz free energy F^{ex} arises from the thermodynamic non-ideality due to inter- and intra-molecular interactions. This functional is unknown for most systems of practical interest. However, it can be approximately formulated by rigorous mathematical analysis and, more important, by physical insights for the specific system under consideration.[10] For the system considered in this dissertation, the excess Helmholtz free energy can be expressed as:

$$F^{ex}=F_{hs}^{ex}+F_{ch}^{ex}+F_C^{ex}+F_{el}^{ex}, \tag{2.16}$$

where each term indicating a contribution to the excess Helmholtz free energy, i.e., contributions due to hard-sphere repulsion (F_{hs}^{ex}), chain connectivity (F_{ch}^{ex}), direct Coulomb energy (F_C^{ex}) , and the electrostatic correlations (F_{el}^{ex}), respectively. Different versions of CDFT choose different approximations to formulate the excess Helmholtz free energy functional. The functional

derivative of excess Helmholtz free energy with respect to the density profile yields the excess chemical potential:

$$\begin{aligned}\beta\mu^{ex}(\mathbf{r}) &= \frac{\delta\beta F^{ex}}{\delta\rho(\mathbf{r})} \\ &= \frac{\delta\beta F_{hs}^{ex}}{\delta\rho(\mathbf{r})} + \frac{\delta\beta F_{ch}^{ex}}{\delta\rho(\mathbf{r})} + \frac{\delta\beta F_{C}^{ex}}{\delta\rho(\mathbf{r})} + \frac{\delta\beta F_{el}^{ex}}{\delta\rho(\mathbf{r})} \\ &= \beta\mu_{hs}^{ex}(\mathbf{r}) + \beta\mu_{ch}^{ex}(\mathbf{r}) + \beta\mu_{C}^{ex}(\mathbf{r}) + \beta\mu_{el}^{ex}(\mathbf{r}).\end{aligned} \tag{2.17}$$

In the following subsections, we will present the detail expression for the excess Helmholtz free energies and the corresponding excess chemical potentials.

2.4.1 Short-range Repulsion

In statistical mechanics, the short-range repulsion between molecules can be represented by an effective the hard-sphere model, which assumes that each particle has a physical volume prohibiting overlap with other spheres. Such an excluded-volume effect plays a pivotal role in determining the structure and thermodynamic properties of condensed materials. The hard-sphere potential between two spherical particles is given by

$$\beta u(\mathbf{r}_i, \mathbf{r}_j) = \begin{cases} 0, & |\mathbf{r}_i - \mathbf{r}_j| \geq \frac{1}{2}(\sigma_i + \sigma_j) \\ \infty, & |\mathbf{r}_i - \mathbf{r}_j| < \frac{1}{2}(\sigma_i + \sigma_j) \end{cases}, \tag{2.18}$$

where $\mathbf{r}_i$ and $\mathbf{r}_j$ are particle positions; σ_i and σ_j are the particle diameters.

Because of its theoretical importance, a number of analytical theories have been published for representing the structure and thermodynamic properties of hard spheres, including Percus-Yevck (PY) integral equation,[15] the scaled particle theory (SPT),[16] and the Boublik–Mansoori–Carnahan–Starling–Leland (BMCSL) equation of state.[17, 18] Among these theories, the fundamental measure theory (FMT), which is originally proposed by Roesnfeld,[19] has been the most effective approach. Within the framework of FMT, the free energy density is taken to be

a function not just of one but of several weighted densities that defined by geometrical characteristics of the particles. In principle, FMT can be applied to not only spherical particles systems but also to systems containing non-spherical particles.

A number of modifications of FMT have been proposed since it was first published in 1989.[20] Because the accuracy of FMT is similar to that of the scaled-particle theory or Percus–Yevick theory for bulk hard spheres,[21] its numerical performance can be further improved by using the quasi-exact BMCSL equation of state for bulk hard-sphere fluids.[22, 23]This version of FMT is called modified FMT (MFMT) or the White Bear Version.[23] According to MFMT, the excess Helmholtz energy functional is given by:

$$\begin{aligned}\beta F_{hs}^{ex} &= \int \Phi_{hs}^{ex}\left[\left\{n_\alpha(\mathbf{r})\right\}\right]d\mathbf{r} \\ &= \int d\mathbf{r}\left\{-n_0\ln(1-n_3)+\frac{n_1 n_2-\vec{\mathbf{n}}_{V1}\cdot\vec{\mathbf{n}}_{V2}}{1-n_3}\right. \\ &\left.+\left(n_2{}^3-3n_2\vec{\mathbf{n}}_{V2}\cdot\vec{\mathbf{n}}_{V2}\right)\frac{n_3+(1-n_3)^2\ln(1-n_3)}{36\pi n_3{}^2(1-n_3)^2}\right\},\end{aligned} \tag{2.19}$$

where Φ_{hs}^{ex} is the excess Helmholtz free energy density, and $\{n_\alpha\}$ stand for weighted densities defined as:

$$n_\alpha(\mathbf{r})=\sum_i n_{\alpha,i}(\mathbf{r})=\sum_i\int\rho_i(\mathbf{r}')\omega_i^{(\alpha)}\left(|\mathbf{r}-\mathbf{r}'|\right)d\mathbf{r}'. \tag{2.20}$$

The weight function $\omega^{(\alpha)}(\mathbf{r})$ characterize the geometry of a hard sphere , and are expressed in terms of four scalar and two vector-weighted densities, as introduced by Rosenfeld.[19] The integration of two scalar weight functions $\omega_i^{(2)}(r)$ and $\omega_i^{(3)}(r)$ with respect to the position yields the particle surface area and volume, and the integration of the vector weight function $\vec{\boldsymbol{\omega}}_i^{(V2)}(\mathbf{r})$ gives the gradient across the sphere in **r** direction. These three weight functions can be expressed as

$$\omega_i^{(2)}(r) = \delta(\sigma_i/2 - r)\ , \tag{2.21}$$

$$\omega_i^{(3)}(r) = \theta(\sigma_i/2 - r)\ , \tag{2.22}$$

$$\vec{\omega}_i^{(V2)}(\mathbf{r}) = (\mathbf{r}/r)\delta(\sigma_i/2 - r)\ , \tag{2.23}$$

The other weight functions are proportional to those three functions,

$$\omega_i^{(0)}(r) = \frac{\omega_i^{(2)}(r)}{\pi\sigma_i^{\,2}}, \tag{2.24}$$

$$\omega_i^{(1)}(r) = \frac{\omega_i^{(2)}(r)}{2\pi\sigma_i}, \tag{2.25}$$

$$\vec{\omega}_i^{(V1)}(\mathbf{r}) = \frac{\vec{\omega}_i^{(V2)}(\mathbf{r})}{2\pi\sigma_i}. \tag{2.26}$$

In Eq. (2.21)-(2.26), σ_i is the hard-sphere diameter, $\delta(r)$ is the Dirac delta function, and $\theta(r)$ is the Heaviside step functions.

In the case of systems with one-dimensional inhomogeneity, the weighted densities is reduced to one-dimensional integration. For system with slab geometry, the weighted densities are expressed as

$$n_{2,i}(z) = \pi\sigma_i \int_{z-\sigma_i/2}^{z+\sigma_i/2} dz'\,\rho_i(z') \tag{2.27}$$

$$n_{3,i}(z) = \pi \int_{z-\sigma_i/2}^{z+\sigma_i/2} dz' \left[\frac{\sigma_i^{\,2}}{4} - (z'-z)^2\right]\rho_i(z') \tag{2.28}$$

$$\vec{\mathbf{n}}_{V2,i}(z) = -\frac{\mathbf{z}}{z}\pi\sigma_i \int_{z-\sigma_i/2}^{z+\sigma_i/2} dz'(z'-z)\rho_i(z') \tag{2.29}$$

$$n_{0,i}(z) = \frac{2n_{1,i}(z)}{\sigma_i} = \frac{n_{2,i}(z)}{\pi\sigma_i^{\,2}} \tag{2.30}$$

$$\vec{\mathbf{n}}_{V1,i}(\mathbf{r}) = \frac{\vec{\mathbf{n}}_{V2,i}(\mathbf{r})}{2\pi\sigma_i} \tag{2.31}$$

The vector-weighted densities, $\vec{\mathbf{n}}_{V1}$ and $\vec{\mathbf{n}}_{V2}$, vanish in the limit of a bulk fluid. For a uniform fluid, the vector-weighted densities disappear due to the homogeneity in every direction. In that case, Eq.(2.19) reduces to the excess Helmholtz energy from BMCSL equation of state. While the modified FMT preserves the advantages of the original theory, it improves the numerical performance, in particular, for highly asymmetric hard-sphere systems.[24]

The functional derivative of excess Helmholtz free energy due to the hard-sphere repulsion yields the excess chemical potential $\mu_{hs,i}^{ex}$,

$$\begin{aligned}\beta\mu_{hs,i}^{ex}(\mathbf{r}) &= \frac{\delta\beta F_{hs}^{ex}}{\delta\rho_i(\mathbf{r})} \\ &= \int d\mathbf{r}' \frac{\delta\Phi_{hs}^{ex}}{\delta\rho_i(\mathbf{r})} \\ &= \sum_\alpha \int d\mathbf{r}' \frac{\partial\Phi_{hs}^{ex}}{\partial n_\alpha(\mathbf{r}')} \frac{\delta n_\alpha(\mathbf{r}')}{\delta\rho_i(\mathbf{r})} \\ &= \sum_\alpha \int d\mathbf{r}' \frac{\partial\Phi_{hs}^{ex}}{\partial n_\alpha(\mathbf{r}')} \omega_i^{(\alpha)}(\mathbf{r}'-\mathbf{r}).\end{aligned} \tag{2.32}$$

A set of $\delta\Phi_{hs}^{ex} / \delta n_\alpha(\mathbf{r})$ from MFMT are given by

$$\frac{\partial\Phi_{hs}^{ex}}{\partial n_0(\mathbf{r})} = -\ln(1-n_3), \tag{2.33}$$

$$\frac{\partial\Phi_{hs}^{ex}}{\partial n_1(\mathbf{r})} = \frac{n_2}{1-n_3}, \tag{2.34}$$

$$\frac{\partial\Phi_{hs}^{ex}}{\partial n_2(\mathbf{r})} = \frac{n_1}{1-n_3} + \left[\frac{\ln(1-n_3)}{n_3} + \frac{1}{(1-n_3)^2}\right]\frac{n_2^2 - \vec{\mathbf{n}}_{V2}^2}{12\pi n_3}, \tag{2.35}$$

$$\begin{aligned}\frac{\partial\Phi_{hs}^{ex}}{\partial n_3(\mathbf{r})} = &-\left[\frac{\ln(1-n_3)}{12\pi n_3^3} + \frac{1-3n_3+(1-n_3)^2}{36\pi n_3^2\left((1-n_3)^3\right)}\right]\left(n_2^3 - 3n_2\vec{\mathbf{n}}_{V2}^2\right) \\ &+ \frac{n_0}{1-n_3} + \frac{n_1 n_2 - \vec{\mathbf{n}}_{V1}\vec{\mathbf{n}}_{V2}}{(1-n_3)^2},\end{aligned} \tag{2.36}$$

$$\frac{\partial \Phi_{hs}^{ex}}{\partial \vec{\mathbf{n}}_{V1}(\mathbf{r})} = -\frac{\vec{\mathbf{n}}_{V2}}{1-n_3}, \tag{2.37}$$

$$\frac{\partial \Phi_{hs}^{ex}}{\partial \vec{\mathbf{n}}_{V2}(\mathbf{r})} = -\frac{\vec{\mathbf{n}}_{V1}}{1-n_3} - \left[\frac{\ln(1-n_3)}{n_3} + \frac{1}{(1-n_3)^3}\right]\frac{n_2 \vec{\mathbf{n}}_{V2}}{6\pi n_3}. \tag{2.38}$$

2.4.2 Thermodynamic Perturbation Theory for Chain Connectivity

The excess Helmholtz free energy due to chain connectivity is taken into account only for polymeric fluids. Application of CDFT to polymeric systems was first discussed by Chandler, McCoy, and Singer (CMS) in 1986.[25] Early versions of polymer DFT were heavily influenced by the self-consistent field theory and by the Landau expansions for the selection of the reference system or for the formulation of the free-energy functional. Most recent applications of CDFT, however, adopt segment-level intermolecular forces following either the CMS theory or the generalized thermodynamic perturbation theory(TPT).[26]

The generalized thermodynamic perturbation theory was initially introduced by Kierlik and Rosinburg,[26] who built on earlier work by Woodward.[27, 28] In this approach, the Helmholtz energy functional includes an exact formalism for the ideal chains that retains the details of bond connectivity and an excess part accounting for the contributions from all non-bonded inter- and intramolecular interactions. The excess Helmholtz energy functional is expressed in terms of a weighted-density approximation for short range forces and a first-order perturbation theory for chain correlations.[29, 30]

The excess Helmholtz free energy can also be represented in terms of free energy density,

$$\beta F_{ch}^{ex} = \int \Phi_{ch}^{ex}\left[\{n_\alpha(\mathbf{r})\}\right] d\mathbf{r}, \tag{2.39}$$

where $\{n_\alpha\}$ stands for weighted densities and the expressions can be found in previous discussion.

To be more specific, we consider a mixture consisting of homo-polyelectrolytes and ions in a solvent which is treated as dielectric continuum with dielectric constant ε . Polyelectrolyte is a charged hard-sphere chain with electric charge $Z_p e$ on each segments, and ions are charged hard spheres with electric charge $Z_+ e$ or $Z_- e$. Here e is the elementary charge. According to Wertheim's first-order perturbation theory for a bulk fluid, the Helmholtz energy density due to chain connectivity is given by

$$\Phi_{ch}^{ex,b} = \frac{1-M}{M} \rho_{p,b} \ln y_{pp}^{b}\left(\sigma_p\right), \tag{2.40}$$

where $\rho_{p,b}$ is the bulk polymer segment density, and $y_{pp}^{b}\left(\sigma_p\right)$ is the contact value of the cavity correlation functional (CCF) between segments, both in bulk. The CCF is given by

$$y(r) \equiv g(r) \exp\left[\beta u(r)\right], \tag{2.41}$$

in which $g(r)$ is the pair distribution function (PDF), and $u(r)$ is the pair interaction potential. The pair potential for system with charged hard spheres is given by

$$\beta u_{ij}(r) = \begin{cases} \infty, & r < \sigma_{ij} \\ l_B \dfrac{Z_i Z_j}{r}, & r \geq \sigma_{ij} \end{cases}, \tag{2.42}$$

where $l_B = \beta e^2 / \varepsilon$ is the Bjerrum length.

In case of hard-sphere chains, the pair potential is $u(r)= 0$ for $r \geq \sigma_P$, the contact value of CCF is equal to the contact value of PDF. However, for a polyelectrolyte solution, the pair potential does not vanish at contact and the exact PDF is difficult to obtain, it is more subtle to get the free energy density. In previous work, [31] $y_{pp}\left(\sigma_p\right)$ is estimated from the hypernetted chain (HNC) approximation which has been proved reliable in the system, especially with electrostatic interaction:

$$y_{pp}\left(\sigma_p\right)=\exp\left[g_{pp}^{MSA}\left(\sigma_p\right)-1-c_{pp}^{MSA}\left(\sigma_p\right)\right], \tag{2.43}$$

where $g_{pp}^{MSA}\left(\sigma_p\right)$ and $c_{pp}^{MSA}\left(\sigma_p\right)$, respectively, are the contact value of the PDF function and correlation function from Blum's mean-spherical approximation (MSA),

$$g_{pp}^{MSA}\left(\sigma_p,n_\alpha\right)=\frac{1}{1-n_3}+\frac{n_2\sigma_p\left(1-\vec{\mathbf{n}}_{V2}\cdot\vec{\mathbf{n}}_{V2}/n_2^{\,2}\right)}{4\left(1-n_3\right)^2}-\frac{\Gamma^2 a_p^{\,2}}{4\pi\sigma_p l_B}, \tag{2.44}$$

$$c_{pp}^{MSA}\left(\sigma_p\right)=-\beta u_{pp}\left(\sigma_p\right), \tag{2.45}$$

where

$$\Gamma^2=\pi l_B\sum_{i=p,+,-}n_{0i}\left(\frac{1}{1+\Gamma\sigma_i}\right)^2\left(Z_i-\frac{\pi P_n\sigma_i^{\,2}}{2\left(1-n_3\right)}\right)^2, \tag{2.46}$$

$$a_i=\frac{2\pi l_B\left(Z_i-\dfrac{\pi P_n\sigma_i^2}{2\left(1-n_3\right)}\right)}{\Gamma\left(1+\Gamma\sigma_i\right)} \tag{2.47}$$

with

$$P_n=\frac{\displaystyle\sum_{i=p,+,-}\frac{2n_{1i}Z_i}{1+\Gamma\sigma_i}}{1+\dfrac{3}{1-n_3}\displaystyle\sum_{i=p,+,-}\frac{n_{3i}}{1+\Gamma\sigma_i}}. \tag{2.48}$$

The parameter Γ and a_i can be solved by an iterative procedure, and the weighted densities obtained from FMT is applied to those equations. The pair potential at contact value for the polyelectrolyte solution is given by

$$u_{pp}\left(\sigma_p\right)=\frac{l_B Z_p^{\,2}}{\sigma_p}. \tag{2.49}$$

According to the definition of the CCF (Eq.(2.41), however, $y_{pp}\left(\sigma_p\right)$ may be estimated from

$$y_{pp}\left(\sigma_p, n_\alpha\right) = g_{pp}^{MSA}\left(\sigma_p, n_\alpha\right)\exp\left(\frac{l_B {Z_p}^2}{\sigma_p}\right). \tag{2.50}$$

It has been recognized that $g_{pp}^{MSA}\left(\sigma_p, n_\alpha\right)$ given by the MSA is not very accurate for high coupling and low density; in some cases, negative values may appear, and these have no physical meaning. There are several methods to improve this deficiency, and a simple one is the EXP approximation as follow: [32, 33]

$$g_{pp}^{EXP}\left(\sigma_p, n_\alpha\right) = g_{pp}^{hs}\left(\sigma_p, n_\alpha\right)\exp\left[g_{pp}^{MSA}\left(\sigma_p, n_\alpha\right) - g_{pp}^{hs}\left(\sigma_p, n_\alpha\right)\right], \tag{2.51}$$

where $g_{pp}^{hs}\left(\sigma_p, n_\alpha\right)$ is the pair correlation function for hard sphere at contact, given by

$$g_{pp}^{hs}\left(\sigma_p, n_\alpha\right) = \frac{1}{1-n_3} + \frac{n_2\sigma_p\left(1-\vec{\mathbf{n}}_{V2}\cdot\vec{\mathbf{n}}_{V2}/{n_2}^2\right)}{4\left(1-n_3\right)^2}. \tag{2.52}$$

The EXP gives better structural properties than the MSA, and has been applied widely for the Lennard-Jones(LJ) fluid,[34, 35] the Yukawa fluid,[36] and electrolyte solutions.[37]

Using Eq. (2.51) and Eq.(2.52), we can rewrite Eq. (2.50) as

$$y_{pp}\left(\sigma_p, n_\alpha\right) = \left[\frac{1}{1-n_3} + \frac{n_2\sigma_p\left(1-\vec{\mathbf{n}}_{V2}\cdot\vec{\mathbf{n}}_{V2}/{n_2}^2\right)}{4\left(1-n_3\right)^2}\right]\times\exp\left(-\frac{\Gamma^2 {a_p}^2}{4\pi\sigma_p l_B}\right)\exp\left(\frac{l_B {Z_p}^2}{\sigma_p}\right). \tag{2.53}$$

For inhomogeneous fluids, both the bulk density and CCF are replaced by the weighted densities used in FMT. Thus, the free energy density for inhomogeneous homo-polyelectrolyte solution is expressed as:

$$\Phi_{ch}^{ex} = \frac{1-M}{M} n_{0p}\zeta_p \ln y_{pp}\left(\sigma_p, n_\alpha\right), \tag{2.54}$$

with $\zeta_p = 1-\vec{\mathbf{n}}_{V2p}\cdot\vec{\mathbf{n}}_{V2p}/{n_{2p}}^2$.

We can also extend the expression for the excess Helmholtz energy density for the hetero-polyelectrolytes, e.g. polyatomic molecules composed of segments with different charges and sizes. Although throughout this thesis, we only consider a simple case of dimer composed of opposite charge and same size, here we will discuss the general expression for the hetero-polyelectrolyte case. Assuming a mixture is composed by m_p species of block copolymer and m_a species of monomers. Each block polymer contains p_k blocks of polymerized monomers. In the case of the *k*-th species of block copolymer, each block contain M_i^k segments with diameter σ_i^k and valence Z_i^k ($i = 1, 2, \cdots, p_k$). In the *k*-th species of block copolymer, there will be $M_i^k - 1$ number of $B_i^k - B_i^k$ bonds for identical bead *i*, and $p_k - 1$ number of $B_i^k - B_{i+1}^k$ bonds for consecutive segments .[14]

The free energy density regarding the *k*-th species of block copolymer $\Phi_{ch,k}^{ex}$ is given by

$$\Phi_{ch,k}^{ex} = -\frac{n_0^k \zeta^k}{\sum_{i=1}^{p_k} M_i^k}\left[\sum_{i=1}^{p_k}\left(M_i^k - 1\right)\ln y_{i,i}^k\left(\sigma_{i,i}^k, n_\alpha\right) + \sum_{i=1}^{p_k - 1}\ln y_{i,i+1}^k\left(\sigma_{i,i+1}^k, n_\alpha\right)\right], \tag{2.55}$$

where

$$n_0^k = \sum_{i=1}^{p_k} n_{0,i}^k, \tag{2.56}$$

$$\zeta^k = 1 - \frac{\vec{\mathbf{n}}_{V2}^k \cdot \vec{\mathbf{n}}_{V2}^k}{n_2^k \times n_2^k} = 1 - \frac{\sum_{i=1}^{p_k} \vec{\mathbf{n}}_{V2,i}^k \cdot \sum_{i=1}^{p_k} \vec{\mathbf{n}}_{V2,i}^k}{\left(\sum_{i=1}^{p_k} n_{2,i}^k\right)^2}, \tag{2.57}$$

$$\sigma_{i,j}^k = \frac{1}{2}\left(\sigma_i^k + \sigma_j^k\right). \tag{2.58}$$

The CCF in Eq.(2.55) is given by

$$y_{i,j}^{k}\left(\sigma_{i,j}^{k},n_{\alpha}\right)=\left[\frac{1}{1-n_3}+\frac{n_2\sigma_i^k\sigma_j^k\left(1-\vec{\mathbf{n}}_{V2}\cdot\vec{\mathbf{n}}_{V2}/n_2^{\,2}\right)}{4\left(1-n_3\right)^2\sigma_{i,j}^{k}}\right]\times\exp\left(-\frac{\Gamma^2a_i^ka_j^k}{4\pi^2\sigma_{i,j}^{k}l_B}\right)\exp\left(\frac{l_BZ_i^kZ_j^k}{\sigma_{i,j}^{k}}\right) \tag{2.59}$$

The total free energy density is a sum of all species of block copolymer:

$$\Phi_{ch}^{ex}=\sum_{k=1}^{m_p}\Phi_{ch,k}^{ex}. \tag{2.60}$$

The functional derivative of excess Helmholtz free energy due to chain connectivity yields the excess chemical potential $\mu_{\mathrm{ch,t}}^{ex}$,

$$\beta\mu_{ch,t}^{ex}\left(\mathbf{r}\right)=\frac{\delta\beta F_{ch}^{ex}}{\delta\rho_t\left(\mathbf{r}\right)}=\sum_{\alpha}\int d\mathbf{r}'\frac{\partial\Phi_{ch}^{ex}}{\partial n_{\alpha,t}\left(\mathbf{r}'\right)}\omega_t^{(\alpha)}\left(\mathbf{r}'-\mathbf{r}\right). \tag{2.61}$$

In Eq.(2.61), *t* applies to all species in the system, including both block copolymer segments and monomers, and the corresponding $n_{\alpha,t}\left(\mathbf{r}\right)$ refers to weighted densities of the *t*-th species, not the total weighted densities. The detailed expressions of $\mu_{\mathrm{ch,t}}^{ex}$ is given in Appendix A of Ref [14].

2.4.3 Excess Helmholtz Energy Due to Direct Coulomb Interaction

The excess Helmholtz energy due to the electrostatic interactions include two parts: one is the direct Coulomb interaction as appeared in the Poisson-Boltzmann (PB) equation, and the second part accounts for the correlation of charge distributions. The mean-field Coulomb excess free energy functional βF_C^{ex} reads

$$\beta F_C^{ex}=\frac{l_B}{2}\sum_{i,j=p,+,-}\iint d\mathbf{r}d\mathbf{r}'\frac{Z_iZ_j\rho_i\left(\mathbf{r}\right)\rho_j\left(\mathbf{r}'\right)}{\left|\mathbf{r}-\mathbf{r}'\right|}. \tag{2.62}$$

The factor $1/2$ in Eq. (2.62) prevent double counting. The Coulomb functional contains an artificial divergence for $\mathbf{r}\to\mathbf{r}'$, which is absent in Coulomb energy but appears when the

discrete sum over all particle pairs $i \neq j$ is transformed to an integral over the complete volume. To avoid the numerical problem, the electrostatic energy is often calculated from the local electrostatic potential,

$$\psi(\mathbf{r}) = \int d\mathbf{r}' \sum_{j=p,+,-} \frac{Z_j e \rho_j(\mathbf{r}')}{4\pi\varepsilon|\mathbf{r}-\mathbf{r}'|}. \tag{2.63}$$

This local mean electrostatic potential satisfied the Poisson equation

$$\nabla^2\psi(\mathbf{r}) = -\frac{4\pi e}{\varepsilon}\rho_c(\mathbf{r}), \tag{2.64}$$

where $\rho_c(\mathbf{r}) = \sum_{i=p,+,-} Z_i\rho_i(\mathbf{r})$ .The Poisson Equation can be solved analytically for a one-dimensional system with appropriate boundary conditions. For a case of slit-like geometry, the density profile and electrostatic potential is only *z* dependent. In that case, Eq.(2.64) can be simplified as

$$\frac{d}{dz}\left(\frac{d\psi(z)}{dx}\right) = -\frac{4\pi e}{\varepsilon}\rho_c(z). \tag{2.65}$$

Eq.(2.65) can be solved with the boundary condition that require surface potential fixed at a given value. Assuming the slit has a pore size of *H*:

$$\psi(0) = \psi(H) = \psi_s, \tag{2.66}$$

where ψ_s is the external surface electrostatic potential. Integration of Eq.(2.65) yields

$$\psi(z) - \psi(0) - C_1(z-0) = -\frac{4\pi e}{\varepsilon}\int_0^z (z-z')\rho_c(z')dz', \tag{2.67}$$

where C_1 in Eq.(2.67) is an integration constant and can be obtained by using boundary condition (2.66)

$$C_1 = \frac{1}{H}\left(-\frac{4\pi e}{\varepsilon}\right)\int_0^H (H-z')\rho_c(z')dz'. \tag{2.68}$$

We rewrite the Coulomb functional Eq.(2.62) as

$$\beta F_C^{ex} = \frac{1}{2}\int dz \beta Z_i \rho_i(z)\psi(z) \tag{2.69}$$

The functional derivative of βF_C^{ex} yields

$$\beta\mu_{C,i}^{ex}(z) = \frac{\delta\beta F_C^{ex}}{\delta\rho_i(z)} = \beta Z_i e\psi(z) \tag{2.70}$$

2.4.4 Electrostatic Correlation

Electrostatic interactions play a dominant role in electric double layer (EDL) systems, different versions of DFT methods are often distinguished by different ways to formulate F_{el}^{ex} , the excess Helmholtz energy affiliated with electrostatic correlations. Common approximations include the bulk fluid density (BFD) method,[38-40] the reference fluid density (RFD) method,[41-43] and the weighted correlation approach (WCA)[44, 45]. All these approximations are able to account for exclude volume effects and electrostatic correlations neglected in the conventional Poisson-Boltzmann (PB) equation. Among these approaches, two methods are used in this thesis and will be discussed in this subsections: the bulk fluid density (BFD) method and the reference fluid density (RFD) method.

2.4.4.1 Bulk Fluid Density Perturbation

A “classical” approximation for the electrostatic part of the excess Helmholtz energy is represented by quadratic functional expansion relative to that of a reference system of uniform ionic densities by neglecting all higher-order terms. The bulk fluid density (BFD) method was used in the early application of DFT to inhomogeneous electrolytes and remain popular nowadays.[39, 40, 46]

In BFD method, the excess Helmholtz free energy F_{el}^{ex} is given by[47]

$$\begin{aligned}\beta F_{el}^{ex}\left[\left\{\rho_i(\mathbf{r})\right\}\right] = \beta F_{el}^{ex}\left[\left\{\rho_i^b\right\}\right] - \int d\mathbf{r} \sum_{i=+,-} C_i^{(1)el}\left[\rho_i(\mathbf{r}) - \rho_i^b\right] \\ -\frac{1}{2}\int\int d\mathbf{r}d\mathbf{r}' \sum_{j=+,-}\sum_{i=+,-} C_{ij}^{(2)el}\left(|\mathbf{r}-\mathbf{r}'|\right)\left[\rho_i(\mathbf{r}) - \rho_i^b\right]\left[\rho_j(\mathbf{r}') - \rho_j^b\right]\end{aligned} \tag{2.71}$$

where the direct correlation functions (DCFs) are defined as

$$C_i^{(1)el} = -\left.\frac{\delta\beta F_{el}^{ex}}{\delta\rho_i(\mathbf{r})}\right|_b, \tag{2.72}$$

$$C_{ij}^{(2)el}\left(|\mathbf{r}-\mathbf{r}'|\right) = -\left.\frac{\delta\beta F_{el}^{ex}}{\delta\rho_i(\mathbf{r})\delta\rho_j(\mathbf{r}')}\right|_b. \tag{2.73}$$

In writing Eq. (2.71), it is assumed that the effect of chain connectivity on the electrostatic part of the DCF can be neglected.[48]

The first term of the right-hand side of Eq.(2.71) corresponds to the electrostatic part of excess Helmholtz energy for a uniform fluid, the second term equals to the bulk excess chemical potential due to electrostatic correlation, and the third term takes into account correlations among ion distributions. Since the direct Coulomb term is explicitly taken into account in Eq. (2.62), the two-body excess direct correlation function can be calculated from mean-spherical approximation (MSA) [47]

$$C_{ij}^{(2)el}(r) = C_{ij}(r) - C_{ij}^{C}(r) - C_{ij}^{hs}(r), \tag{2.74}$$

where $C_{ij}(r)$ is the total DCF, $C_{i,j}^{C}(r) = -l_B Z_i Z_j / r$ is the DCF due to direct Coulomb interaction, and $C_{ij}^{hs}(r)$ is that due to hard-sphere repulsion from PY approximation.[49] For $r > (\sigma_i + \sigma_j)/2$, C_{ij} is given by [50]

$$C_{ij}(r) \approx -\frac{l_B Z_i Z_j}{r}. \tag{2.75}$$

In that case, $C_{ij}^{(2),el}(r)$ vanishes in this region. For $0 \le r \le \left|\sigma_j - \sigma_i\right|/2$, the two-body direct correlation function from MSA for asymmetric electrolytes is given by [51, 52]

$$C_{ij}(r) - C_{ij}^{hs}(r) = -2l_b\left[-Z_i N_j + X_i\left(N_i + \Gamma X_i\right) - \left(\sigma_i/3\right)\left(N_i + \Gamma X_i\right)^2\right]. \tag{2.76}$$

The parameters X_i, N_i, and Γ are calculated numerically from

$$X_i \equiv \frac{Z_i}{1+\Gamma\sigma_i} - \frac{c\sigma_i^2}{1+\Gamma\sigma_i}\frac{\sum_i \frac{\rho_j^b \sigma_j Z_j}{1+\Gamma\sigma_j}}{1+c\sum_i \frac{\rho_j^b \sigma_j^3}{1+\Gamma\sigma_j}}, \tag{2.77}$$

$$X_i = Z_i + N_i\sigma_i, \tag{2.78}$$

$$\Gamma^2 = \pi l_B \sum_i \rho_i^b X_i^2, \tag{2.79}$$

where

$$c = \frac{\pi}{2\left[1 - \frac{\pi}{6}\sum_i \rho_i^b \sigma_i^3\right]}. \tag{2.80}$$

For $\left|\sigma_i-\sigma_j\right|/2\le r\le\left(\sigma_i+\sigma_j\right)/2$,

$$rC_{ij}\left(r\right)-rC_{ij}^{hs}\left(r\right)=l_B\left(\begin{array}{c}\left(\sigma_i-\sigma_j\right)\left\{\begin{array}{c}\frac{\left(X_i+X_j\right)}{4}\left[\left(N_i+\Gamma X_i\right)-\left(N_j+\Gamma X_j\right)\right]\\-\frac{\left(\sigma_i-\sigma_j\right)}{16}\left[\left(N_i+\Gamma X_i+N_j+\Gamma X_j\right)^2-4N_iN_j\right]\end{array}\right\}\\-r\left\{\begin{array}{c}\left(X_i-X_j\right)\left(N_i-N_j\right)+\left(X_i^2+X_j^2\right)\Gamma+\left(\sigma_i+\sigma_j\right)N_iN_j\\-\frac{1}{3}\left[\sigma_i\left(N_i+\Gamma X_i\right)^2+\sigma_j\left(N_j+\Gamma X_j\right)^2\right]\end{array}\right\}\\+r^2\left\{\begin{array}{c}\frac{X_i}{\sigma_i}\left(N_i+\Gamma X_i\right)+\frac{X_j}{\sigma_j}\left(N_j+\Gamma X_j\right)+N_iN_j\\-\frac{1}{2}\left[\left(N_i+\Gamma X_i\right)^2+\left(N_j+\Gamma X_j\right)^2\right]\end{array}\right\}\\+r^4\left\{\frac{\left(N_i+\Gamma X_i\right)^2}{6\sigma_i^2}+\frac{\left(N_j+\Gamma X_j\right)^2}{6\sigma_j^2}\right\}\end{array}\right). \qquad (2.81)$$

The excess chemical potential due to electrostatic correlation is given by

$$\beta\mu_{el,i}^{ex}\left(\mathbf{r}\right)=\frac{\delta\beta F_{el}^{ex}}{\delta\rho_i\left(\mathbf{r}\right)}=\beta\mu_i^{el}\left[\left\{\rho_i^b\right\}\right]-\sum_{j=+,-}\int d\mathbf{r}'C_{ij}^{(2),el}\left(\left|\mathbf{r}-\mathbf{r}'\right|;\left\{\rho_i^b\right\}\right)\left[\rho_j\left(\mathbf{r}'\right)-\rho_j^b\right]. \qquad (2.82)$$

While the BFD method works well for a wide of variety of inhomogeneous electrolyte systems, its performance is rather disappointing for the electrolyte near a weakly charged surface. [46, 53]

2.4.4.2 Reference Fluid Density Perturbation

The reference system in the perturbation expansion is not restricted to a bulk fluid with uniform ionic densities. Unfortunately, an early attempt with a perturbation expansion around position-dependent weighted densities did not generate numerical results much different from those from the BFD method. More recently, Gillespie and co-workers introduce a quadratic expansion relative to position-dependent reference fluid densities (RFD) that satisfy local charge neutrality.[42, 43] In comparison with the simulation results, the RFD expansion shows

significant improvements over the BFD method for asymmetric electrolyte near a neutral or weakly charged surface.

In RFD method, the excess Helmholtz free energy F_{el}^{ex} is virtually identical to that from BFD (see Eq.(2.71))

$$\begin{aligned}\beta F_{el}^{ex}\left[\left\{\rho_k(\mathbf{y})\right\}\right] \approx \beta F_{el}^{ex}\left[\left\{\rho_k^{ref}(\mathbf{y})\right\}\right] - \int d\mathbf{x} \sum_{i=+,-} C_i^{(1),el}(\mathbf{x})\Delta\rho_i(\mathbf{x}) \\ -\frac{1}{2}\sum_{ij}\int\int d\mathbf{x}d\mathbf{x}' C_{ij}^{(2),el}(\mathbf{x},\mathbf{x}')\Delta\rho_i(\mathbf{x})\rho_j(\mathbf{x}'),\end{aligned} \tag{2.83}$$

with

$$\Delta\rho_i(\mathbf{x}) = \rho_i(\mathbf{x}) - \rho_i^{ref}(\mathbf{x}), \tag{2.84}$$

except $\rho_i^{ref}(\mathbf{x})$ is a ionic density of a locally defined reference fluid at point **x**. The RFD approach makes the reference fluid densities functional of the particle densities $\rho_i(\mathbf{x})$:

$$\rho_k^{ref}(\mathbf{y}) = \bar{\rho}_k\left[\left\{\rho_i(\mathbf{x})\right\};\mathbf{y}\right]. \tag{2.85}$$

$\bar{\rho}_k\left[\left\{\rho_i(\mathbf{x}')\right\};\mathbf{x}\right]$ is the RFD functional, recalling its origin as 'reference fluid density'. It should be noted that the fluid with densities $\bar{\rho}_k\left[\left\{\rho_i(\mathbf{x}')\right\};\mathbf{x}\right]$ does not have to be physically real fluid; the functional $\bar{\rho}_k\left[\left\{\rho_i(\mathbf{x}')\right\};\mathbf{x}\right]$ is a mathematical construction that one is free to choose.[41]To determine the $\bar{\rho}_k$, we define

$$\bar{\rho}_k\left[\left\{\rho_i(\mathbf{x}');\mathbf{x}\right\}\right] = \int d\mathbf{x}'\alpha_i(\mathbf{x}')\rho_i(\mathbf{x}')w(\mathbf{x},\mathbf{x}'), \tag{2.86}$$

where if $Z_i \geq 0$

$$\alpha_i(\mathbf{x}) = A(\mathbf{x}) \tag{2.87}$$

and if $Z_i < 0$,

$$\alpha_i(\mathbf{x}) = A(\mathbf{x})B(\mathbf{x}), \tag{2.88}$$

with

$$A(\mathbf{x}) = \frac{\sum_i Z_i^2 \rho_i(\mathbf{x})}{\sum_{Z_i \geq 0} Z_i^2 \rho_i(\mathbf{x}) + B(\mathbf{x}) \sum_{Z_i < 0} Z_i^2 \rho_i(\mathbf{x})} \tag{2.89}$$

and

$$B(\mathbf{x}) = \frac{\sum_{Z_i \geq 0} Z_i \rho_i(\mathbf{x})}{\sum_{Z_i < 0} |Z_i| \rho_i(\mathbf{x})}. \tag{2.90}$$

This choice of scaling factor $\alpha_i(\mathbf{x})$ ensures that the fluid with densities $\{\alpha_i(\mathbf{x})\rho_i(\mathbf{x})\}$ is charge neutral and has the same ionic strength at each position **x** as the fluid with densities $\{\rho_i(\mathbf{x})\}$. The weighted function is given by

$$w(\mathbf{x}', \mathbf{x}) = \frac{\theta(|\mathbf{x}' - \mathbf{x}| - R_{el}(\mathbf{x}))}{\frac{4\pi}{3} R_{el}^3(\mathbf{x})}, \tag{2.91}$$

where θ is the unit step function. The radius of the sphere $R_{el}(\mathbf{x})$ over which we average is the local electrostatic length scale, and is approximated as the sum of average ion radii R_i and the local screening length $s(\mathbf{x})$:

$$R_{el}(\mathbf{x}) \approx \frac{\sum_i \alpha_i(\mathbf{x}) \rho_i(\mathbf{x}) R_i}{\sum_i \alpha_i(\mathbf{x}) \rho_i(\mathbf{x})} + s(\mathbf{x}). \tag{2.92}$$

The screening length $s(\mathbf{x})$ is defined as:

$$s(\mathbf{x}) = \frac{1}{2\Gamma(\mathbf{x})}, \tag{2.93}$$

where $\Gamma(\mathbf{x})$ is the MSA screening length that has been calculated at every point *x* with densities $\{\rho_i^{ref}(\mathbf{x})\}$. This then define the capacitance length of each ion species:

$$\lambda_i(\mathbf{x}) = R_i + s(\mathbf{x}). \tag{2.94}$$

The first-order DCF, $C_i^{(1),el}(\mathbf{x})$, is estimated by using a bulk formulation (specifically the MSA) at each point $\mathbf{x}$ with densities $\rho_i^{ref}(\mathbf{x})$. Similar, the second-order DCF $C_{ij}^{(2),el}(\mathbf{x},\mathbf{x}')$ is estimated by using an approximation of the MSA DCF:

$$C_{ij}^{(2),el}(x,x') = -\frac{l_B Z_i Z_j}{2}\frac{1}{|x-x'|}\left(|x-x'|\frac{\lambda_i+\lambda_j}{\lambda_i\lambda_j} - \frac{|x-x'|^2}{2\lambda_i\lambda_j} - \frac{(\lambda_i-\lambda_j)^2}{2\lambda_i\lambda_j}\right). \tag{2.95}$$

Similar to Eq.(2.82), the excess chemical potential due to electrostatic correlation in RFD method is expressed as

$$\beta\mu_{el,i}^{ex}(\mathbf{r}) = \beta\mu_i^{el}\left[\{\rho_i^{ref}(\mathbf{r})\}\right] - \sum_{j=+,-}\int d\mathbf{r}' C_{ij}^{(2),el}\left(|\mathbf{r}-\mathbf{r}'|;\{\rho_j^{ref}(\mathbf{r}')\}\right)\Delta\rho_j^{ref}(\mathbf{r}'). \tag{2.96}$$

2.5 Computational Details for Density Profile Calculation

In this thesis, most of the calculations are performed in a slit-pore geometry. In this case, the density profile varies only in z direction, i.e., the direct perpendicular to the surface. The density distributions of monomers and polymeric segments are given by:

$$\rho_a(z) = \exp\left[\beta\mu_a - \beta V_a(z) - \frac{\delta\beta F^{ex}}{\delta\rho_a(z)}\right], \tag{2.97}$$

$$\rho_p(z) = \exp(\beta\mu_M)\sum_{j=1}^{M}\exp\left[-\beta\lambda_j(z_j)\right]G^i(z)G^{M+1-i}(z) \tag{2.98}$$

where $V_a(z)$ stands for the external potential of monomer, $\lambda_j(z_j)$ represents an effective one-body potential

$$\lambda_j(z_j) = V_j(z_j) + \frac{\delta F^{ex}}{\delta \rho_p(z_j)}, \tag{2.99}$$

the propagator function $G^i(z)$ arise from the connection of the polymeric segments due to the bond connectivity. They are identical to the Green functions used in a typical polymer self-consistent field theory (SCFT) [54].

The propagator functions are determined from the recurrence relation[55]

$$G^i(z) = \int dz' \exp\left[-\beta\lambda_i(z')\right] \frac{\theta\left(\sigma_p - |z - z'|\right)}{2\sigma_p} G^{i-1}(z'), \tag{2.100}$$

for $i = 2,\ldots,M$ with $G^1(z) = 1$. If the chain length approaches infinity, the effect of end segments becomes less significant and all segments in polymeric molecule are indistinguishable,

$$G^i(z) = G(z), \tag{2.101}$$

and Eq. (2.98) can be simplified as

$$\rho_p(z) = M \exp\left(\beta\mu_M - \beta\lambda(z)\right)\left[G(z)\right]^2. \tag{2.102}$$

For mixture of polymeric species and monomers, the chemical potentials of both components can be extended from Wertheim's TPT1 equation of state for bulk hard-sphere-chain fluids[56]

$$\begin{aligned}\beta\mu_a = {} & \ln\rho_a^b + \beta\mu_a^{hs}\left(\rho_a^b, \rho_p^b\right) + \beta\mu_a^C + \beta\mu_a^{el} \\ & + \frac{1-M}{M}\rho_p^b \frac{\partial \ln y_{pp}^b\left(\sigma_a, \sigma_p\right)}{\partial \rho_a^b},\end{aligned} \tag{2.103}$$

$$\beta\mu_M = \ln\rho_M^b + M\beta\mu_M^{hs}\left(\rho_a^b,\rho_p^b\right) + M\beta\mu_M^C + \beta\mu_a^{el} + (1-M)\left[\ln y_{pp}^b\left(\rho_a^b,\rho_p^b\right) + \rho_p^b\frac{\partial\ln y_{pp}^b\left(\sigma_a,\sigma_p\right)}{\partial\rho_p^b}\right]. \quad (2.104)$$

To be noted, both $\beta\mu_a^C$ and $\beta\mu_M^C$ vanish due to charge neutrality of the bulk fluid.

A typical DFT calculation follow an iterative (Picard) scheme. The densities are defined on a grid of points in the spatial region to be solved, where the number of points used will be determined by the length-scale of the expected structural variation. In a simple Picard iteration scheme:

1. The initial guess is made for density profiles $\{\rho_i(z)\}$ of polymer segments and monomers ((i.e. bulk densities). The effective field $\lambda_i(z)$ and the Green function $G^i(z)$ can be obtained from Eq. (2.100) for short polymer and from Eq. (2.101) for long polymer where end effect can be neglected.

2. The new set of density profiles $\{\rho_i^{new}(z)\}$ obtained from Eq. (2.97) and Eq. (2.98) or Eq.(2.102) .

3. The set $\{\rho_i^{new}(z)\}$ is then mixed with the previous set (labelled as $\{\rho_i^{old}(z)\}$) according to,

$$\rho_i(z) = f_{mix}\cdot\rho_i^{new}(z) + (1-f_{mix})\rho_i^{old}(z), \quad (2.105)$$

where $f_{mix} < 1$.

4. Step 2 and 3 are repeated until the difference between consecutive iteration drops bellows a present tolerance (i.e. 1×10^{-6}) at all spatial points for all species.

After obtaining the equilibrium density profile, we can derive all thermodynamic properties as discussed above.

Bibliography

[1] J. Wu, "Classical Density Functional Theory for Molecular Systems," in *Variational Methods in Molecular Modeling*, J. Wu, Ed. Singapore: Springer Singapore, 2017, pp. 65-99.

[2] P. Hohenberg and W. Kohn, "Inhomogeneous Electron Gas," *Physical Review,* vol. 136, no. 3B, pp. B864-B871, 1964.

[3] N. D. Mermin, "Thermal Properties of the Inhomogeneous Electron Gas," *Physical Review,* vol. 137, no. 5A, pp. A1441-A1443, 1965.

[4] R. Evans, M. Oettel, R. Roth, and G. Kahl, "New developments in classical density functional theory," *J Phys Condens Matter,* vol. 28, no. 24, p. 240401, Jun 22 2016.

[5] J. D. van der Waals, "The thermodynamic theory of capillarity under the hypothesis of a continuous variation of density," *Journal of Statistical Physics,* vol. 20, no. 2, pp. 200-244, 1979.

[6] L. Onsager, "The Effects of Shape on the Interaction of Colloidal Particles," *Annals of the New York Academy of Sciences,* vol. 51, no. 4, pp. 627-659, 1949.

[7] C. Ebner, W. F. Saam, and D. Stroud, "Density-functional theory of simple classical fluids. I. Surfaces," *Physical Review A,* vol. 14, no. 6, pp. 2264-2273, 1976.

[8] W. F. Saam and C. Ebner, "Density-functional theory of classical systems," *Physical Review A,* vol. 15, no. 6, pp. 2566-2568, 1977.

[9] A. J. M. Yang, P. D. Fleming, and J. H. Gibbs, "Molecular theory of surface tension," *The Journal of Chemical Physics,* vol. 64, no. 9, pp. 3732-3747, 1976.

[10] J. Wu, "Density functional theory for chemical engineering: From capillarity to soft materials," *AIChE Journal,* vol. 52, no. 3, pp. 1169-1193, 2006.

[11] R. Roth, "Fundamental measure theory for hard-sphere mixtures: a review," *J Phys Condens Matter,* vol. 22, no. 6, p. 063102, Feb 17 2010.

[12] H. Löwen, "Density functional theory of inhomogeneous classical fluids: recent developments and new perspectives," *Journal of Physics: Condensed Matter,* vol. 14, no. 46, p. 11897, 2002.

[13] J. Wu, "Density functional theory for liquid structure and thermodynamics," 2008.

[14] Z. Jin, "A hybrid density functional theory for solvation and solvent-mediated interactions," UC Riverside, 2012.

[15] J. K. Percus and G. J. Yevick, "Analysis of Classical Statistical Mechanics by Means of Collective Coordinates," *Physical Review,* vol. 110, no. 1, pp. 1-13, 1958.

[16] H. Reiss, H. L. Frisch, and J. L. Lebowitz, "Statistical Mechanics of Rigid Spheres," *The Journal of Chemical Physics,* vol. 31, no. 2, pp. 369-380, 1959.

[17] T. Boublík, "Hard-Sphere Equation of State," *The Journal of Chemical Physics,* vol. 53, no. 1, pp. 471-472, 1970.

[18] G. Mansoori, N. F. Carnahan, K. Starling, and T. Leland Jr, "Equilibrium thermodynamic properties of the mixture of hard spheres," *The Journal of Chemical Physics,* vol. 54, no. 4, pp. 1523-1525, 1971.

[19] Y. Rosenfeld, "Free-energy model for the inhomogeneous hard-sphere fluid mixture and density-functional theory of freezing," *Phys Rev Lett,* vol. 63, no. 9, pp. 980-983, Aug 28 1989.

[20] J. A. Cuesta, Y. Martínez-Ratón, and P. Tarazona, "Close to the edge of fundamental measure theory: a density functional for hard-sphere mixtures," *Journal of Physics: Condensed Matter,* vol. 14, no. 46, p. 11965, 2002.

[21] S. M. Oversteegen and R. Roth, "General methods for free-volume theory," *J Chem Phys,* vol. 122, no. 21, p. 214502, Jun 1 2005.

[22] Y.-X. Yu and J. Wu, "Structures of hard-sphere fluids from a modified fundamental-measure theory," *The Journal of Chemical Physics,* vol. 117, no. 22, pp. 10156-10164, 2002.

[23] R. Roth, R. Evans, A. Lang, and G. Kahl, "Fundamental measure theory for hard-sphere mixtures revisited: the White Bear version," *Journal of Physics: Condensed Matter,* vol. 14, no. 46, p. 12063, 2002.

[24] R. D. Groot, J. P. van der Eerden, and N. M. Faber, "The direct correlation function in hard sphere fluids," *The Journal of Chemical Physics,* vol. 87, no. 4, pp. 2263-2270, 1987.

[25] D. Chandler, J. D. McCoy, and S. J. Singer, "Density functional theory of nonuniform polyatomic systems. I. General formulation," *The Journal of Chemical Physics,* vol. 85, no. 10, pp. 5971-5976, 1986.

[26] E. Kierlik and M. Rosinberg, "A perturbation density-functional theory for polyatomic fluids. I. Rigid molecules," *The Journal of chemical physics,* vol. 97, no. 12, pp. 9222-9239, 1992.

[27] C. E. Woodward, "A density functional theory for polymers: Application to hard chain–hard sphere mixtures in slitlike pores," *The Journal of Chemical Physics,* vol. 94, no. 4, pp. 3183-3191, 1991.

[28] C. E. Woodward and A. Yethiraj, "Density functional theory for inhomogeneous polymer solutions," *The Journal of Chemical Physics,* vol. 100, no. 4, pp. 3181-3186, 1994.

[29] J. W. Jiang, L. Blum, O. Bernard, and J. M. Prausnitz, "Thermodynamic properties and phase equilibria of charged hard sphere chain model for polyelectrolyte solutions," *Molecular Physics,* vol. 99, no. 13, pp. 1121-1128, 2001.

[30] Y.-X. Yu and J. Wu, "Density functional theory for inhomogeneous mixtures of polymeric fluids," *The Journal of chemical physics,* vol. 117, no. 5, pp. 2368-2376, 2002.

[31] J. Jiang, H. Liu, Y. Hu, and J. M. Prausnitz, "A molecular-thermodynamic model for polyelectrolyte solutions," *The Journal of chemical physics,* vol. 108, no. 2, pp. 780-784, 1998.

[32] H. C. Andersen and D. Chandler, "Optimized Cluster Expansions for Classical Fluids. I. General Theory and Variational Formulation of the Mean Spherical Model and Hard Sphere Percus-Yevick Equations," *The Journal of Chemical Physics,* vol. 57, no. 5, pp. 1918-1929, 1972.

[33] H. C. Andersen, D. Chandler, and J. D. Weeks, "Optimized Cluster Expansions for Classical Fluids. III. Applications to Ionic Solutions and Simple Liquids," *The Journal of Chemical Physics,* vol. 57, no. 7, pp. 2626-2631, 1972.

[34] G. Stell and J. J. Weis, "Structure and thermodynamics of a simple fluid," *Physical Review A,* vol. 21, no. 2, pp. 645-657, 1980.

[35] Y. Tang and B. C. Y. Lu, "Analytical description of the Lennard-Jones fluid and its application," *AIChE Journal,* vol. 43, no. 9, pp. 2215-2226, 1997.

[36] D. Henderson, E. Waisman, J. L. Lebowitz, and L. Blum, "Equation of state of a hard-core fluid with a Yukawa tail," *Molecular Physics,* vol. 35, no. 1, pp. 241-255, 1978.

[37] Y. Zhou, S. Yeh, and G. Stell, "Criticality of charged systems. I. The restricted primitive model," *The Journal of Chemical Physics,* vol. 102, no. 14, pp. 5785-5795, 1995.

[38] L. Mier-y-Teran, S. Suh, H. S. White, and H. Davis, "A nonlocal free-energy density-functional approximation for the electrical double layer," *The Journal of Chemical Physics,* vol. 92, no. 8, pp. 5087-5098, 1990.

[39] E. Kierlik and M. L. Rosinberg, "Density-functional theory for inhomogeneous fluids: Adsorption of binary mixtures," *Physical Review A,* vol. 44, no. 8, pp. 5025-5037, 1991.

[40] Y. Rosenfeld, "Free energy model for inhomogeneous fluid mixtures: Yukawa-charged hard spheres, general interactions, and plasmas," *The Journal of Chemical Physics,* vol. 98, no. 10, pp. 8126-8148, 1993.

[41] D. Gillespie, W. Nonner, and R. S. Eisenberg, "Density functional theory of charged, hard-sphere fluids," *Phys Rev E Stat Nonlin Soft Matter Phys,* vol. 68, no. 3 Pt 1, p. 031503, Sep 2003.

[42] D. Gillespie, M. Valiskó, and D. Boda, "Density functional theory of the electrical double layer: the RFD functional," *Journal of Physics: Condensed Matter,* vol. 17, no. 42, pp. 6609-6626, 2005.

[43] D. Gillespie, W. Nonner, and R. S. Eisenberg, "Coupling Poisson Nernst Planck and density functional theory to calculate ion flux," *Journal of Physics: Condensed Matter,* vol. 14, no. 46, pp. 12129-12145, 2002.

[44] Z. Wang, L. Liu, and I. Neretnieks, "The weighted correlation approach for density functional theory: a study on the structure of the electric double layer," *J Phys Condens Matter,* vol. 23, no. 17, p. 175002, May 4 2011.

[45] Z. Wang, L. Liu, and I. Neretnieks, "A novel method to describe the interaction pressure between charged plates with application of the weighted correlation approach," *J Chem Phys,* vol. 135, no. 24, p. 244107, Dec 28 2011.

[46] G. Yang and L. Liu, "A systematic comparison of different approaches of density functional theory for the study of electrical double layers," *J Chem Phys,* vol. 142, no. 19, p. 194110, May 21 2015.

[47] Z. Li and J. Wu, "Density-functional theory for the structures and thermodynamic properties of highly asymmetric electrolyte and neutral component mixtures," *Phys Rev E Stat Nonlin Soft Matter Phys,* vol. 70, no. 3 Pt 1, p. 031109, Sep 2004.

[48] Z. Li and J. Wu, "Density functional theory for planar electric double layers: closing the gap between simple and polyelectrolytes," *J Phys Chem B,* vol. 110, no. 14, pp. 7473-84, Apr 13 2006.

[49] M. S. Wertheim, "Exact Solution of the Percus-Yevick Integral Equation for Hard Spheres," *Physical Review Letters,* vol. 10, no. 8, pp. 321-323, 1963.

[50] L. L. Lee, *Molecular thermodynamics of nonideal fluids*. Butterworth-Heinemann, 2016.

[51] K. Hiroike, "Supplement to Blum's theory for asymmetric electrolytes," *Molecular Physics,* vol. 33, no. 4, pp. 1195-1198, 1977.

[52] L. Blum, "Mean spherical model for asymmetric electrolytes," *Molecular Physics,* vol. 30, no. 5, pp. 1529-1535, 1975.

[53] J. Jiang, D. Cao, D. Henderson, and J. Wu, "Revisiting density functionals for the primitive model of electric double layers," *J Chem Phys,* vol. 140, no. 4, p. 044714, Jan 28 2014.

[54] G. Fredrickson, *The equilibrium theory of inhomogeneous polymers*. Oxford University Press on Demand, 2006.

[55] Z. Jin, S. Zhao, and J. Wu, "Entropic forces of single-chain confinement in spherical cavities," *Phys Rev E Stat Nonlin Soft Matter Phys,* vol. 82, no. 4 Pt 1, p. 041805, Oct 2010.

[56] M. S. Wertheim, "Thermodynamic perturbation theory of polymerization," *The Journal of Chemical Physics,* vol. 87, no. 12, pp. 7323-7331, 1987.

Chapter 3. Boosting the Performance of Ionic-Liquid-Based Supercapacitors with Polar Additives

In this chapter, we study the effects of polar additives on EDLC capacitance using the classical density functional theory within the framework of a coarse-grained model for the microscopic structure of the porous electrodes and room-temperature ionic liquids. The theoretical results indicate that a highly polar, low-molecular-weight additive is able to drastically increase the EDLC capacitance at low bulk concentration. Additionally, the additive is able to dampen the oscillatory dependence of the capacitance on the pore size thereby boosting the performance of amorphous electrode materials. The theoretical predictions are directly testable with experiments and provide new insights into the additive effects on EDL properties.

3.1 Introduction

A major effort for the ongoing research on supercapacitors is to address the limitation of their moderate energy density.[1, 2] One of the key strategies is to identify electrolyte-electrode pairs that can optimize the equilibrium and transport properties of the charge carriers.[3-6] Because the EDLC performance is directly related to preferential adsorption of cations or anions into the micropores of the electrodes, an appropriate combination of the electrode material and the working electrolyte plays a pivotal role for the rational design and optimization of supercapacitors.[7-10]

Whereas a wide variety of porous materials, with tuned pore size distributions, morphology, architecture and functionality, has been proposed as the supercapacitor electrodes,[11, 12] most porous electrodes in practical use are made of carbon materials such as activated carbon, templated carbons, carbon aerogels, carbide-derived carbons, carbon nanotubes and graphenes.[13]Porous carbons are attractive owing to relatively low cost, easy processing, non-toxicity, high chemical stability, large electrical conductivity, and large specific surface area.

Meanwhile, diverse electrolytes have been tested to enhance the EDLC performance.[5]Although existing supercapacitors are mostly based on conventional electrolytes such as aqueous or organic solutions of small ions, room-temperature ionic liquids (ILs) are promising for future applications because they enable electric charging at a much higher voltage, thus greatly increase the energy density.[14] Besides, ILs have the advantages of low vapor pressure and non-flammability, allowing them to be used safely over a wide temperature range.[15, 16]

Although porous carbons with a broad spectrum of pore sizes and shapes have been investigated as the electrodes, previous studies are mostly focused on pure ionic liquids, i.e., electrolytes consisting of one type of cation and one type of anion. The effect of electrolyte composition and electrode structure on the EDLC performance is not completely understood.[17]For example, a number of experimental and theoretical reports indicate that the surface-area-normalized capacitance may be drastically increased as the pore size becomes comparable to the dimensionality of the ionic species.[18-24]But complications often arise from the experimental side in terms of how the values of the surface area and the pore size distribution are determined and how the effects of the pore size dispersity are taken into account for realistic electrodes.[25]While both theory and molecular simulations predict an oscillatory dependence of the capacitance on the electrode pore size, [26-28] direct validation of the theoretical results with experimental measurements is difficult due to the lack of a precise control of the electrode pore size. Contradictory results have also been reported on the effects of electrolyte composition on the EDL structure and capacitance. Based on molecular dynamics (MD) simulations, Feng et al. found that the EDL capacitance increases only slightly for 1-butyl-3-methylimidazolium tetrafluoroborate ([BMIM][BF4]) near either a positive or a negative electrode when it is diluted with acetonitrile (ACN) up to 50% in the mass fraction.[29] However, simulation results by Shim et al. indicate that the capacitance of 1-ethyl-3-methylimidazolium tetrafluoroborate

([EMIM][BF4]), a similar ionic liquid, is higher than that in a binary mixture of IL and acetonitrile by 55–60%.32 Recent experiment and theoretical studies show that solvent addition to an IL may lead to a significant increase of the capacitance and that an optimum composition can be identified to maximize the EDLC performance. [30, 31]

Built upon our previous studies of the structure and capacitance of electrolyte/electrode interfaces,[26] we investigate in this work the effects of polar additives on IL-based EDLCs by using the classical density functional theory (CDFT). While the solvent effects were studied in our previous publications,[24, 32] the additives interact with the electrode surface and ionic species in unique ways such that they may have drastic effects on supercapacitor performance even at very low concentration. To our knowledge, the special additive effects have not been investigated before but could open up a new direct of research for design and optimization of EDLCs. We demonstrate that the oscillatory dependence of the capacitance on the pore size can be strongly alleviated by the use of a polar additive, in addition to an overall increase of the capacitance. The theoretical results open up new perspectives on additive effects and may usher in new experimental studies on the use of low-concentration additives.

3.2 Molecular Model and Methods

We consider the additive effects on the performance of electric double layer (EDL) capacitors consisting of porous carbons and room-temperature ionic liquids. Because the carbon material has a dielectric constant not much different from that of a typical ionic liquid (~10-20), the polarizability effect or "electronic screening" is relatively insignificant for such systems. Like our previous studies, we use a slit-pore model for the porous electrode, which is fully consistent with that typically used for the characterization of amorphous porous materials in experiments. For simplicity, the restricted primitive model is used to represent cations and anions in an ionic liquid. The cations and anions have the same diameter ($\sigma_i = 0.5\,\text{nm}$) but opposite valence (

$Z_i = \pm 1$). Approximately, the model parameters match those corresponding to 1-ethyl-3-methylimidazolium bis(trifluoromethyl-sulfonyl)imide (EMIM-TFSI), an ionic liquid commonly used in electrochemical devices. At 298 K and 1 bar, the molar volume of EMIM-TFSI is 259 cm^3/mol, corresponding to a reduced number density of $\rho_i \sigma_i^3 = 0.29$ for both cations and anions.

The additive molecules are represented by two tangentially connected spheres of the same size but opposite charges. While the simple model does not reveal atomic details as provided by realistic force fields used in molecular dynamics simulations, it captures the essential features important for understanding the charging behavior of ionic liquids. In particular, it accounts for electrostatic correlations and ionic excluded volume effects important for understanding the supercapacitor performance but neglected in conventional electric double layer (EDL) theories. Similar models have been extensively used to study a broad range of parameters such as pore size, ion and solvent densities, ionic valences, surface energy and electric potential.

As in the primitive model for aqueous electrolyte solutions, the pair potential between charged spheres i and j is given by

$$\beta u_{ij}(r) = \begin{cases} \infty, & r < \sigma_{ij}/2 \\ Z_i Z_j l_B / r, & r \geq \sigma_{ij}/2 \end{cases} \tag{3.1}$$

where $\beta = 1/(k_B T)$ with k_B and T being the Boltzmann constant and the absolute temperature (fixed at 298 in this work), respectively, r is the center-to-center distance between particles i and j, and $\sigma_{ij} = (\sigma_i + \sigma_j)/2$. Parameter l_B is the Bjerrum length, which is equal to 556.9 Å, a value that corresponds to electrostatic interaction in vacuum at 298 K. We assume that dielectric constant is unity because the IL model accounts for pair interactions among all components explicitly.

The porous electrode is modeled as a slit pore with two symmetric hard walls. Inside the slit pore, the electrical field due to the surface charge density is uniform. As a result, each ionic species experiences a constant external potential in the direction perpendicular to the surface:

$$\beta V_i(z) = \begin{cases} -2\pi l_B Z_i HQ/e, & \sigma_i/2 \le z \le H - \sigma_i/2 \\ \infty & \text{otherwise} \end{cases}, \tag{3.2}$$

where z is the perpendicular distance of the center of the sphere from the surface, Q is the surface charge density (C/m^2), and H stands for the surface-to-surface separation (or pore width).

The theoretical details of the classical density functional theory (CDFT) have been reported in previous publications.[33] Here we recapitulate only the key equations and refer the readers to our earlier articles for the details. Intuitively, one may understand CDFT as a formal generalization of the Poisson-Boltzmann (PB) equation to account for ionic excluded volume effects and electrostatic correlations that are not negligible for ionic liquids. For given bulk densities of the ions and the additive molecules, temperature, the pore size, and the surface potential, we solve for the one-dimensional density profiles of cations and anions, $\rho_a(z)$ with $a = \pm 1$, as well as the additive segments, $\rho_\gamma(z)$ with $\gamma = \delta\pm$, across the slit pore by minimizing the grand potential:[34, 35]

$$\Omega = F\left[\rho_0(\mathbf{R}), \rho_a(\mathbf{r})\right] + \int d\mathbf{R}\rho_0(\mathbf{R})\left[V_0(\mathbf{R}) - \mu_0\right] + \sum_a \int d\mathbf{r}\rho_a(\mathbf{r})\left[V_a(\mathbf{r}) - \mu_a\right] \tag{3.3}$$

where $\mathbf{R} \equiv (\mathbf{r}_{\delta+}, \mathbf{r}_{\delta-})$ are two coordinates specifying the positions of two additive segments, μ_a is the chemical potential of the ions , μ_0 is the chemical potential of the additive, $V_a(\mathbf{r})$ stands for the external potential of cations and ions, and $V_0(\mathbf{R})$ is the external potential for additive molecule, i.e. $V_0(\mathbf{R}) = V_{\delta+}(\mathbf{r}_{\delta+}) + V_{\delta-}(\mathbf{r}_{\delta-})$.

The number densities of the positive and negative segments $\rho_{\delta+}(\mathbf{r})$ and $\rho_{\delta-}(\mathbf{r})$ are calculated from

$$\rho_{\delta+}(\mathbf{r}_{\delta+}) = \int d\mathbf{R}\delta\left(\mathbf{r} - \mathbf{r}_{\delta+}\right)\rho_0(\mathbf{R}), \tag{3.4}$$

$$\rho_{\delta-}(\mathbf{r}_{\delta-}) = \int d\mathbf{R}\delta\left(\mathbf{r} - \mathbf{r}_{\delta-}\right)\rho_0(\mathbf{R}), \tag{3.5}$$

where $\delta(r)$ is the Dirac function. The excess Helmholtz free energy arising from the thermodynamic non-ideality (viz. due to the exclude-volume effect and electrostatic interactions). In this work, we use the modified fundamental measure theory to account for the hard-sphere repulsion, the first-order thermodynamic perturbation theory to account for the chain connectivity, and a quadratic functional expansion to account for the electrostatic correlations.[36-39]In previous publications,[34]we have calibrated the theoretical performance of the course-grained model and the CDFT calculations with experimental results for both the capacitance and the ionic distributions.

3.3 Results and Discussion

To capture the generic features of the additive effects, we assume that a polar additive can be represented by two tangentially connected hard spheres that have the same diameter but opposite charges. The dipole moment can be tuned by changing either the partial charge or the diameter for each segment (e.g., two hard-sphere segments that have a diameter of 0.2 nm and an opposite charge of 0.208 e yield an electrical dipole moment of 2.0 D). To investigate the additive effects, we fix the mole fraction of the additive molecules in the bulk at a small value

$$x_0 = \frac{\rho_0}{\rho_0 + \rho_+ + \rho_-} = 10^{-4} \tag{3.6}$$

where ρ_0, ρ_+ and ρ_- are the number densities of polar additives, cations and anions in the bulk, respectively.

We began our analysis of the additive effect by examining its influence on the microstructure of EDLs in a single nanopore. Figure 3.1 presents the CDFT predictions for the local number densities of different species across a 1.2 nm slit pore. For all cases, the additive molecules are assumed to have the same segment diameter of 0.2 nm but with different dipole moments. When the electrode is grounded (viz., 0 V at the surface), the distributions of the positive and negative particles are identical, as shown in Figure 3.1(a-d), due to the symmetry in the model parameters. While cations and anions are found to accumulate primarily near the electrode surface, the additive molecules form a multilayer structure owing to its smaller segment size. Despite its low bulk concentration, $x_0 = 10^{-4}$, a significant amount of additive molecules are accumulated inside the neutral pore, and the additive enrichment is enhanced when its dipole moment increases. Even without any direct attraction from the surface, the average ion density inside the pore is significantly larger than that in the bulk, and the dipole-ion correlations are mainly responsible for the enrichment of the additive molecules. From the density profiles, we can calculate the partition coefficient for the additive molecules, defined as its average concentration inside the pore divided by that in the bulk, and find that it increases from 2.67 to 675 when the additive dipole moment is raised from 2.0 to 3.5 D. The tremendous increase in the partition coefficient indicates the importance of electrostatic correlations for the confined electrolyte.

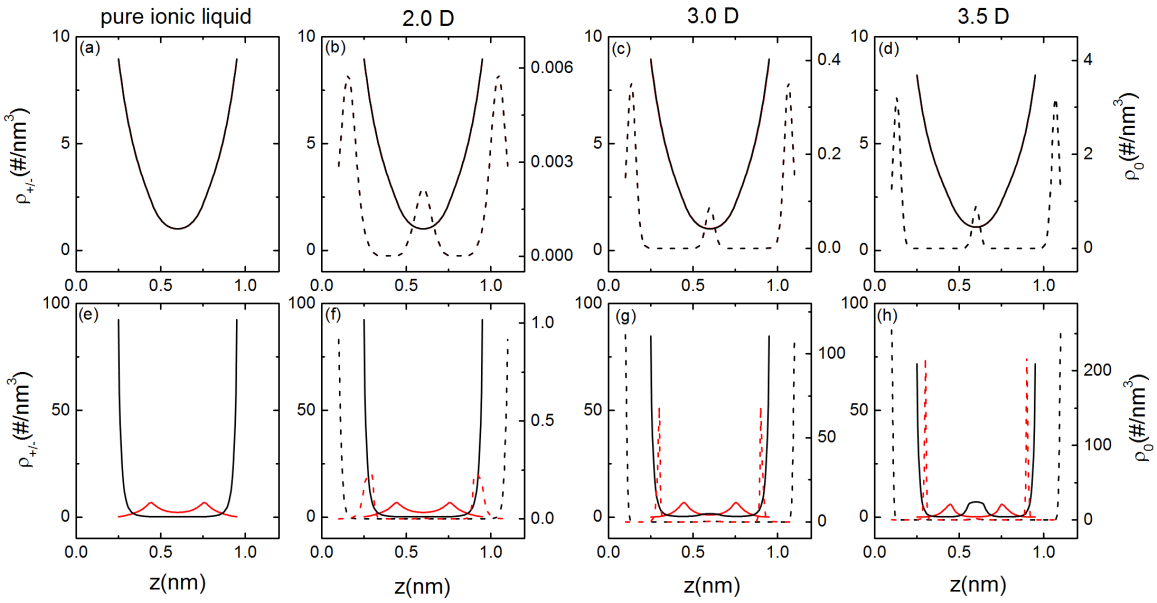

Figure 3.1 Number densities of anions (black solid lines) and cations (red solid lines), $\rho_{\pm}$, and the number densities of the negative (black dashed lines) and the positive segments (red dashed lines) of the additive molecules, ρ_0, across a 1.2 nm slit pore. Here the surface electrical potential is 0 V for panel a−d and +1.5 V for panel e−h. In all cases, the mole fraction of the polar additive in the bulk is fixed at $x_0 = 10^{-4}$. The four columns correspond to a pure ionic liquid (3.8 M) and those with an additive of dipole moment of 2.0, 3.0, and 3.5 D, respectively.

Figure 3.1 (e-h) shows the EDL structure in the presence of a surface electrical potential (+1.5 V). In Figure 3.1(f-h), the peak positions between the density profiles of anions and the positive segment of the polar additive are less than 0.5 Å apart because both types of particles are distributed close to the surface. Because the electric potential at the pore surface is fixed at +1.5 V, the additives have little effects on coion (cation) distributions. The surface charge leads to alternating layering of cations and anions in the slit pore, regardless of the dipole moment of the additives. The ion distributions, especially the density profile for anions (counterions in this case), are noticeably affected by the presence of additive molecules. One can see that the EDL consists of not only a layer of counterions but also a layer of additive molecules. The polar molecules accumulate mainly on the electrode surface and its adsorption inside the pore is strongly

correlated with the dipole moment. The density profile for the positive segment of the additive molecules becomes much more localized as the dipole moment increases and followed by a strong layer of the negative segments, suggesting that the polar molecules are aligned perpendicular to the surface, in contrast to that near a neutral surface.

One important question about the additive effects is how they change the energy density for the charge storage or, more specifically, the surface charge and the EDL capacitance. The net electrical charge of the electrode includes several contributions: adsorption of counterions, swapping of coions for counterions, and desorption of coions from the porous electrode.[40, 41] For a given electrode and an electrolyte pair, all these contributions depend on the electrode voltage. To identify these different contributions to the surface charge density, we present in Figure 3.2 the influence of the electrode potential on the contact densities of counterions and the negative segments of the additive molecules. Here the contact number density of each species is defined as

$$\rho_{c,i} = \rho_i(z = \sigma_i / 2) \tag{3.7}$$

where σ_i is the diameter of particle i. The composition of the contact layer reflects a competition between the counterions and the additive molecules.

At a low surface electrical potential, the additive effect on the adsorption of counterions is insignificant because its density in the contact layer is negligible compared to that of the counterions. When the surface electrical potential is beyond a threshold, however, the additive density in the contact layer dramatically increases with the electrical potential. Because the contact densities are defined in terms of the particle radii, the electric potential for the negative segment of the additive molecules is much larger than that for the counterions (anions). Besides, the electric potential at the contact position of the additive segments is not screened by ionic species due to the excluded-volume effects. As a result, the contact density for the negative

segment of the additive molecules increases more drastically with the surface electric potential in comparison to that for the counterions. For similar reasons, the polarity has little effect on the counterion density even though the contact density for the additive is sensitive to its dipole moment. Nevertheless, the contact density of the counterions is noticeably reduced due to the adsorptions of additive molecules. As shown in Figure 3.1(h), their strong alignment at the surface leads to the formation of a counterion layer at the center of the slit pore, and the additional layer results an increase in the overall surface charge density. Figure 3.2 indicates that the additive effect is most significant under conditions of large dipole moment and high electrical potentials.

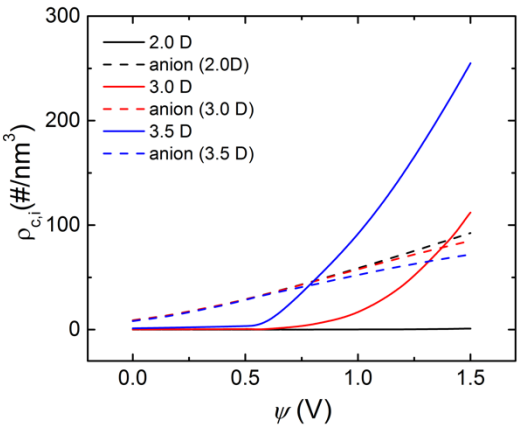

Figure 3.2 Contact densities of the anions (dashed lines) and the negative segment of the additive molecule (solid lines) versus the surface electrical potential. Here the pore width is fixed at 1.2 nm, the solid lines correspond to the additives with a dipole moment of 2.0, 3.0, and 3.5 D, respectively.

To elucidate the effect of polar additives on the integral capacitance, we consider two key parameters in our coarse-grained model – dipole moment and segment size. Figure 3.3(a) shows the dependence of the integral capacitance versus the dipole moment while the segment diameter is fixed at σ_0 = 0.2 nm and the partial charge on each segment is treated as a variable. For three representative pores of different sizes, the integral capacitance increases as we raise the dipole

moment. In all three pores, a similar trend is observed on the effect of integral capacitance on the dipole moment. The increased capacitance can be attributed to stronger ion-dipole correlations and electrostatic attractions of additive molecules with the electrode. We find that adsorption of additives depletes more coions than counterions from the slit pore, leading to the drastic increase of the integral capacitance. The additives are mainly distributed at the pore center when the dipole moment is small but strongly accumulate at the electrode surface as the dipole moment increases (Figure 3.2). Such transition is clearly noticeable in a small pore as shown in Figure 3.3(a). As the pore size increases, the additive has little effects on the ionic distributions if the dipole moment is very small (see Figure 3.3(a), H =1.7 nm). For additives with a strong polarity, however, their accumulation at the electrode surface results in a drastic increase of the capacitance because of the formation of multilayer structures concomitant to surface alignment. Interestingly, the capacitance appears independent of the pore size when the additives have a dipole moment of about 3.4 D. As discussed later, similar capacitances at these pores are resulted from the oscillatory dependence on the pore size.

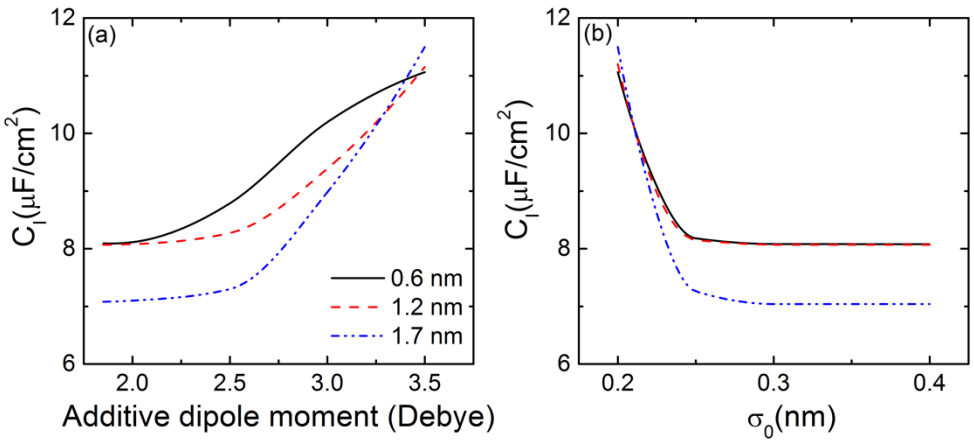

Figure 3.3 (a) Integral capacitance versus the dipole moment for additives of the same segment diameter (σ_0 = 0.2 nm). Here the surface potential is fixed at +1.5 V, and different lines correspond to three representative pore widths. (b) The same as (a) but for additives of the same dipole moment of 3.5 D but different segment diameters (σ_0) in three pores.

Evidently, the additive size also plays an important role. If we fix the dipole moment of the additives as 3.5 D but vary the diameter of the additive molecules, the trend is quite different. As shown in Figure 3.3(b), the integral capacitance remains almost constant as the segment size increases beyond some threshold point (~ 0.25 nm). Beyond this segment size, the segment size has little effect on the integral capacitance. At a fixed dipole moment, the partial charge on each segment of the dimer will be reduced as the segment size increases thus the electrostatic attraction from the charged surface is reduced. While the increase in molecular volume hinders the additive entering the slit pore, the excluded volume effect becomes insignificant because of the low concentration of the additive molecules.

So far our calculations have been based on a single pore size, i.e., 1.2 nm slit pore. However, practical electrodes are mostly amorphous porous materials that do not have a precise control of the pore size distribution. One natural question is how the additive affects the pore size dependence of the capacitance.[42] To address this question, we present in Figure 3.4 the integral capacitance versus the slit pore width for the pure ionic liquid and its mixtures with additives of different dipole moments. It shows that the oscillatory dependence of the capacitance on the pore size is unaffected in the presence of a weakly polar additive at low concentration. In this case, the capacitance is hardly changed compared to that for the pure ionic liquid due to the negligible accumulation of additive molecules inside the pore. For additives with a larger dipole moment (3.0 D or 3.5 D), however, their accumulation inside the pore leads to a significant depletion of counterions (Figure 3.2) from the contact layer and thus dampens the oscillatory dependence of the integral capacitance on the pore size. From Figure 3.4, we see that two distinctive features stand out for highly polar additives: (a) the capacitance is drastically increased across the entire range of the pore size; and (b) capacitance oscillation in response to the changing pore size is greatly depressed.

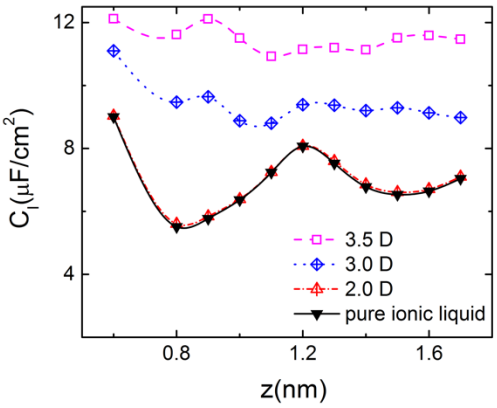

Figure 3.4 Integral capacitance versus the pore size for the pure ionic liquid and its mixture with additives of different dipole moments. Here the surface potential is fixed at +1.5 V, and the segment diameter of the additive molecules is σ_0 = 0.2 nm.

To further understand the additive effects on the integral capacitance, we analyze the density profiles of all chemical species in different pores. Figure 3.5 shows that, regardless of the pore size, addition of polar molecules leads to not only drastic changes in the EDL structure, as evidenced in their strong alignment near the surface, but also depletion of coions from the pore. Such effects become more pronounced as the dipole moment of the additive increases. The coion depletion explains the increase in the integral capacitance as shown in Figure 3.4. For a given additive (viz., the same dipole moment), the EDL structures are essentially the same as the pore size changes (such 0.9 nm and 1.5 nm), explaining why the addition of additives inhibits the oscillatory dependence of the capacitance with the pore size.26 The weak variation of the integral capacitance with the pore size can be attributed to the insensitivity of the EDL structure when it consists of a mixture of counterions and additive molecules. In the smaller pores, the depletion of coions contributes a larger net charge at the surface and disturbs the layer-by-layer ionic distributions. As a result, the oscillatory dependence of the integral capacitance on the pore size diminishes.

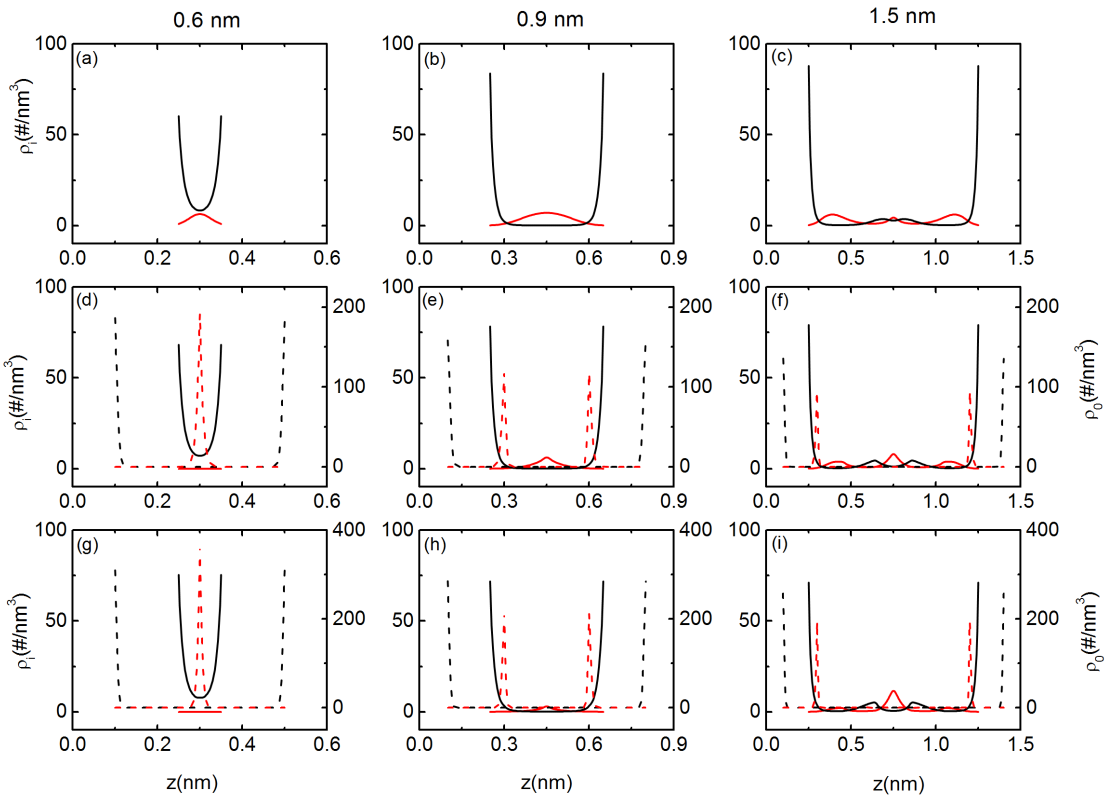

Figure 3.5 Density profiles of anions (black solid lines), cations (red solid lines), the negative segments (black dashed lines), and the positive segments (red dashed lines) of the additive molecules across slit pores of three representative widths. In all cases, the surface potential is fixed at +1.5 V; the three rows correspond to pure ionic liquid (~3.8 M) and ionic liquids with additive molecules of 3.0 and 3.5 D in dipole moment, respectively.

3.4 Conclusions

We have studied how polar additives may influence the layering structure and the integral capacitance of ionic-liquid-based supercapacitors with porous electrodes. Due to the electrostatic attraction from the ionic species and the electrode, the additive molecules of low molecular weight and strong polarity can accumulate in the nanopores even at a very low bulk density. The competitive adsorption of counterion and additive molecules alters the EDL structure and the net charge at the electrode surface, leading to a drastic increase of the integral capacitance. Importantly, the additive may inhibit the pore size effect thereby enabling broader usage of low-cost amorphous electrodes without scarifying the performance. The theoretical results suggesting

that the energy density of supercapacitors can be significantly improved by introducing highly polar additive should be testable with experiments or more elaborate theoretical investigations such as atomistic simulations.

Bibliography

[1] P. Simon and Y. Gogotsi, "Capacitive energy storage in nanostructured carbon-electrolyte systems," *Acc Chem Res,* vol. 46, no. 5, pp. 1094-103, May 21 2013.

[2] J. Vatamanu and D. Bedrov, "Capacitive Energy Storage: Current and Future Challenges," *J Phys Chem Lett,* vol. 6, no. 18, pp. 3594-609, Sep 17 2015.

[3] S. Kondrat, P. Wu, R. Qiao, and A. A. Kornyshev, "Accelerating charging dynamics in subnanometre pores," *Nat Mater,* vol. 13, no. 4, pp. 387-93, Apr 2014.

[4] K. L. Van Aken, M. Beidaghi, and Y. Gogotsi, "Formulation of ionic-liquid electrolyte to expand the voltage window of supercapacitors," *Angew Chem Int Ed Engl,* vol. 54, no. 16, pp. 4806-9, Apr 13 2015.

[5] C. Zhong, Y. Deng, W. Hu, J. Qiao, L. Zhang, and J. Zhang, "A review of electrolyte materials and compositions for electrochemical supercapacitors," *Chem Soc Rev,* vol. 44, no. 21, pp. 7484-539, Nov 7 2015.

[6] C. Lian *et al.*, "Enhancing the Capacitive Performance of Electric Double-Layer Capacitors with Ionic Liquid Mixtures," *ACS Energy Letters,* vol. 1, no. 1, pp. 21-26, 2016.

[7] M. T. Alam, M. Mominul Islam, T. Okajima, and T. Ohsaka, "Measurements of differential capacitance in room temperature ionic liquid at mercury, glassy carbon and gold electrode interfaces," *Electrochemistry Communications,* vol. 9, no. 9, pp. 2370-2374, 2007.

[8] A. A. Kornyshev, "Double-layer in ionic liquids: paradigm change?," *J Phys Chem B,* vol. 111, no. 20, pp. 5545-57, May 24 2007.

[9] G. Feng, J. S. Zhang, and R. Qiao, "Microstructure and Capacitance of the Electrical Double Layers at the Interface of Ionic Liquids and Planar Electrodes," *The Journal of Physical Chemistry C,* vol. 113, no. 11, pp. 4549-4559, 2009.

[10] A. Uysal *et al.*, "Interfacial ionic 'liquids': connecting static and dynamic structures," *J Phys Condens Matter,* vol. 27, no. 3, p. 032101, Jan 28 2015.

[11] G. Wang, L. Zhang, and J. Zhang, "A review of electrode materials for electrochemical supercapacitors," *Chem Soc Rev,* vol. 41, no. 2, pp. 797-828, Jan 21 2012.

[12] P. Simon and Y. Gogotsi, "Materials for electrochemical capacitors," *Nat Mater,* vol. 7, no. 11, pp. 845-54, Nov 2008.

[13] E. Frackowiak, Q. Abbas, and F. Béguin, "Carbon/carbon supercapacitors," *Journal of Energy Chemistry,* vol. 22, no. 2, pp. 226-240, 2013.

[14] A. Balducci *et al.*, "High temperature carbon–carbon supercapacitor using ionic liquid as electrolyte," *Journal of Power Sources,* vol. 165, no. 2, pp. 922-927, 2007.

[15] M. Galiński, A. Lewandowski, and I. Stępniak, "Ionic liquids as electrolytes," *Electrochimica Acta,* vol. 51, no. 26, pp. 5567-5580, 2006.

[16] M. Armand, F. Endres, D. R. MacFarlane, H. Ohno, and B. Scrosati, "Ionic-liquid materials for the electrochemical challenges of the future," *Nat Mater,* vol. 8, no. 8, pp. 621-9, Aug 2009.

[17] C. Lian, D.-e. Jiang, H. Liu, and J. Wu, "A Generic Model for Electric Double Layers in Porous Electrodes," *The Journal of Physical Chemistry C,* vol. 120, no. 16, pp. 8704-8710, 2016.

[18] C. Largeot, C. Portet, J. Chmiola, P. L. Taberna, Y. Gogotsi, and P. Simon, "Relation between the ion size and pore size for an electric double-layer capacitor," *J Am Chem Soc,* vol. 130, no. 9, pp. 2730-1, Mar 5 2008.

[19] J. Huang, B. G. Sumpter, and V. Meunier, "Theoretical Model for Nanoporous Carbon Supercapacitors," *Angewandte Chemie,* vol. 120, no. 3, pp. 530-534, 2008.

[20] J. Huang, B. G. Sumpter, and V. Meunier, "A universal model for nanoporous carbon supercapacitors applicable to diverse pore regimes, carbon materials, and electrolytes," *Chemistry,* vol. 14, no. 22, pp. 6614-26, 2008.

[21] T. A. Centeno, O. Sereda, and F. Stoeckli, "Capacitance in carbon pores of 0.7 to 15 nm: a regular pattern," *Phys Chem Chem Phys,* vol. 13, no. 27, pp. 12403-6, Jul 21 2011.

[22] Y. Shim and H. J. Kim, "Nanoporous carbon supercapacitors in an ionic liquid: a computer simulation study," *ACS Nano,* vol. 4, no. 4, pp. 2345-55, Apr 27 2010.

[23] S. Kondrat, N. Georgi, M. V. Fedorov, and A. A. Kornyshev, "A superionic state in nano-porous double-layer capacitors: insights from Monte Carlo simulations," *Phys Chem Chem Phys,* vol. 13, no. 23, pp. 11359-66, Jun 21 2011.

[24] D. E. Jiang, Z. Jin, D. Henderson, and J. Wu, "Solvent Effect on the Pore-Size Dependence of an Organic Electrolyte Supercapacitor," *J Phys Chem Lett,* vol. 3, no. 13, pp. 1727-31, Jul 5 2012.

[25] N. Jäckel *et al.*, "Anomalous or regular capacitance? The influence of pore size dispersity on double-layer formation," *Journal of Power Sources,* vol. 326, pp. 660-671, 2016.

[26] D. E. Jiang and J. Wu, "Microscopic Insights into the Electrochemical Behavior of Nonaqueous Electrolytes in Electric Double-Layer Capacitors," *J Phys Chem Lett,* vol. 4, no. 8, pp. 1260-7, Apr 18 2013.

[27] G. Feng and P. T. Cummings, "Supercapacitor Capacitance Exhibits Oscillatory Behavior as a Function of Nanopore Size," *The Journal of Physical Chemistry Letters,* vol. 2, no. 22, pp. 2859-2864, 2011.

[28] D. E. Jiang, Z. Jin, and J. Wu, "Oscillation of capacitance inside nanopores," *Nano Lett,* vol. 11, no. 12, pp. 5373-7, Dec 14 2011.

[29] G. Feng, J. Huang, B. G. Sumpter, V. Meunier, and R. Qiao, "A "counter-charge layer in generalized solvents" framework for electrical double layers in neat and hybrid ionic liquid electrolytes," *Phys Chem Chem Phys,* vol. 13, no. 32, pp. 14723-34, Aug 28 2011.

[30] Y. Shim, Y. Jung, and H. J. Kim, "Graphene-Based Supercapacitors: A Computer Simulation Study," *The Journal of Physical Chemistry C,* vol. 115, no. 47, pp. 23574-23583, 2011.

[31] D. J. Bozym *et al.*, "Anomalous Capacitance Maximum of the Glassy Carbon-Ionic Liquid Interface through Dilution with Organic Solvents," *J Phys Chem Lett,* vol. 6, no. 13, pp. 2644-8, Jul 2 2015.

[32] D. E. Jiang and J. Wu, "Unusual effects of solvent polarity on capacitance for organic electrolytes in a nanoporous electrode," *Nanoscale,* vol. 6, no. 10, pp. 5545-50, May 21 2014.

[33] Z. Li and J. Wu, "Density functional theory for planar electric double layers: closing the gap between simple and polyelectrolytes," *J Phys Chem B,* vol. 110, no. 14, pp. 7473-84, Apr 13 2006.

[34] J. Wu, T. Jiang, D.-e. Jiang, Z. Jin, and D. Henderson, "A classical density functional theory for interfacial layering of ionic liquids," *Soft Matter,* vol. 7, no. 23, p. 11222, 2011.

[35] Z. Li and J. Wu, "Density functional theory for polyelectrolytes near oppositely charged surfaces," *Phys Rev Lett,* vol. 96, no. 4, p. 048302, Feb 3 2006.

[36] J. W. Jiang, L. Blum, O. Bernard, and J. M. Prausnitz, "Thermodynamic properties and phase equilibria of charged hard sphere chain model for polyelectrolyte solutions," *Molecular Physics,* vol. 99, no. 13, pp. 1121-1128, 2001.

[37] J. Jiang, H. Liu, Y. Hu, and J. M. Prausnitz, "A molecular-thermodynamic model for polyelectrolyte solutions," *The Journal of chemical physics,* vol. 108, no. 2, pp. 780-784, 1998.

[38] R. Roth, R. Evans, A. Lang, and G. Kahl, "Fundamental measure theory for hard-sphere mixtures revisited: the White Bear version," *Journal of Physics: Condensed Matter,* vol. 14, no. 46, pp. 12063-12078, 2002.

[39] Y.-X. Yu and J. Wu, "A fundamental-measure theory for inhomogeneous associating fluids," *The Journal of Chemical Physics,* vol. 116, no. 16, pp. 7094-7103, 2002.

[40] J. M. Griffin *et al.*, "Ion counting in supercapacitor electrodes using NMR spectroscopy," *Faraday Discuss*, vol. 176, pp. 49-68, 2014.

[41] A. C. Forse, C. Merlet, J. M. Griffin, and C. P. Grey, "New Perspectives on the Charging Mechanisms of Supercapacitors," *J Am Chem Soc*, vol. 138, no. 18, pp. 5731-44, May 11 2016.

[42] N. Mehio, S. Dai, J. Wu, and D.-e. Jiang, "Theoretic Insights into Porous Carbon-Based Supercapacitors," *Nanocarbons for Advanced Energy Storage*, vol. 1, pp. 361-378, 2015.

Chapter 4. Impurity Effects on Ionic-liquid-based Supercapacitors

Small amounts of an impurity may affect the key properties of an ionic liquid and such effects can be dramatically amplified when the electrolyte is under confinement. In this chapter, the classical density functional theory is employed to investigate the impurity effects on the microscopic structure and the performance of ionic-liquid-based electrical double-layer capacitors, also known as supercapacitors. Using a primitive model for ionic species, we study the effects of an impurity on the double layer structure and the integral capacitance of a room temperature ionic liquid in model electrode pores and find that an impurity strongly binding to the surface of a porous electrode can significantly alter the electric double layer structure and dampen the oscillatory dependence of the capacitance with the pore size of the electrode. Meanwhile, a strong affinity of the impurity with the ionic species affects the dependence of the integral capacitance on the pore size. Up to 30% increase in the integral capacitance can be achieved even at a very low impurity bulk concentration. By comparing with an ionic liquid mixture containing modified ionic species, we find that the cooperative effect of the bounded impurities is mainly responsible for the significant enhancement of the supercapacitor performance.

4.1 Introduction

When RTILs are used as the electrolyte for EDLCs, impurity becomes one important issue in both well controlled laboratory systems as well as for practical applications.[1-3] Some previous studies demonstrated that impurities in RTILs, which are very common in commercial RTILs (even in apparently ultrapure quality), can easily and strongly alter surface electrochemical processes, potentially leading to misinterpretations.[4] Impurities in RTILs – such as traces of water, acids, halide ions, residual solvents and unreacted volatile organic compounds arising from synthesis and purification processes– can have a pronounced impact on the physical, spectroscopic and chemical characteristics of the ionic system.[5, 6]Despite their ubiquitous

presence in RTILS, it remains to be understood how these impurity molecules distribute in the inhomogeneous electric field, in particular in the vicinity of an electrode surface, and how they influence the performance of supercapacitors. Although much effort has been made to remove impurity or contaminant from ionic liquids, a complete removal is practically impossible.[7] Meanwhile the storage of ionic liquids also requires a strict environment because even hydrophobic RTILs can absorb a certain amount of water from the atmosphere and water absorption will cause a performance loss for the supercapacitors.[8-10]

Electric double layers (EDLs) are microscopic structures formed at electrolyte-electrode interfaces due to the inhomogeneous distributions of ionic species. Because the interfacial structure plays an essential role in determining the performance of EDLCs, the properties of EDLs have been extensively investigated by both experimental and theoretical methods. While such literature is abundant, previous studies are mostly concerned with pure ionic liquids, i.e. electrolytes consisting of one type of cations and one type of anions.[11-14] The role of impurities in RTILs near an electrified surface has been rarely examined until recently.[15, 16] The experiment tools such as X-ray reflectometry and atomic force microscopy (AFM) were used to study the EDLs in a hybrid RTIL containing impurity species at the electrode surface.[17-19] Computational methods, such as molecular dynamics (MD) simulations, were also used to investigate the distribution of impurities near electrified interfaces.[20] One of the key difficulties to attain a fundamental understanding of hybrid electrolytes is that the impurity effect is manifested at extremely dilute bulk concentrations. Because of the potential importance of an impurity on the EDLC performance, we expect more efforts will be devoted to understanding the nanoscale structure of EDLs containing RTILs in the presence of an impurity (or additive).

In the past decades, many theoretical efforts have been devoted to studying the equilibrium and dynamic properties of inhomogeneous ionic mixtures. [21, 22] Classical density

functional theory (CDFT) represents a popular choice to investigate inhomogeneous electrolyte systems within the framework of coarse-grained models at different levels of microscopic details and approximations. For example, the primitive model has been employed to study size selectivity, ion distribution, exclusion coefficient and separation factor of electrolytes in cylindrical nanopores.[23, 24] Oleksy and Hansen used a semi-primitive model and a 'civilized' model with explicit solvent effects to study the wetting and drying behavior of the ionic solutions near a single wall or between charged walls.[25-28] CDFT has also been successfully applied to investigating the EDL structure and the capacitances of ionic liquids and organic electrolyte systems.[29-32] It has been shown that CDFT predictions are able to capture the essential features of experimental and simulation results and provide microscopic insights into the electrochemical behavior of ionic liquids as the working electrolytes for supercapacitors.[33-37] In this chapter, we use CDFT to examine the structure and the capacitance of EDLCs in RTIL electrolytes under confinement containing a small amount of an impurity. The impurity effects on the integral capacitance as well as the ionic distributions in model porous electrodes of various pore sizes are investigated by varying the surface energies of the impurity molecules as well as the intermolecular potential between the impurity and ionic species. We show that, with different surface energies or intermolecular potentials, small amounts of impurities can notably alter the EDL structure in micropores, which may have profound impacts on the electrochemical performance of supercapacitors.

4.2 Model and Method

We consider a generic model for EDL capacitors consisting of porous carbons and RTILs. Because the carbon material has a dielectric constant not much different from that of a typical ionic liquid, the polarizability effect or electronic screening is relatively insignificant for such systems.[38, 39] Figure 4.1 shows the model EDLC system we consider in this study. The

porous carbon electrode is represented by a slit pore consisting of two symmetric hard walls of equal surface charge density. The restricted primitive model is used for the RTIL: both cations and anions are represented by hard spheres of equal size (0.5 nm in diameter) and monovalent charge ($Z_+ = -Z_- = 1$). We assume that the electrical charges of cations and anions are located at the geometrical center of the spherical particles. Approximately, the model electrolyte mimics an RTIL consisting of 1-ethyl-3-methylimidazolium bis(tri-fluoromethylsulfonyl)imide ([Emim][TFSI]) (259 cm^3/mol at 298 K and 1 bar), which has been widely used in experimental studies. The impurity molecules are represented as neutral particles with the same size as the ions ($\sigma_0 = \sigma_{+/-} = 0.5\,\mathrm{nm}$). The difference in chemical details of the impurity is reflected in their interactions with the electrode, i.e. the non-electrostatic surface energy acting on the impurity.

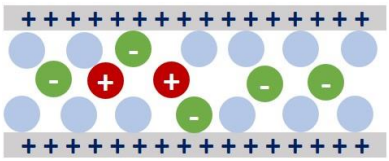

Figure 4.1 The restricted primitive model of an ionic liquid (charged spheres) and an impurity (neutral spheres) inside a slit pore. The impurity molecules may accumulate inside the pore due to strong surface affinity.

While this simple coarse-grained model does not reveal atomic details as provided by semi-empirical force fields used in MDs simulations, it captures the essential features important for understanding the charging behavior of RTIL. In particular, it accounts for electrostatic correlations and ionic excluded volume effects that are important to describe EDLC performance but neglected in conventional EDL theories. Similar models have been extensively used to study a broad range of parameters such as pore size, ion and solvent densities, ionic valences and surface potential.[40]

For systems with a uniform dielectric background, the Coulomb interactions between ionic species are not affected by the electrode polarizability. As a result, the pair potential between ionic species is given by

$$\beta u_{ij}(r) = \begin{cases} \infty, & r < \sigma_{ij} \\ Z_i Z_j l_B / r, & r \geq \sigma_{ij} \end{cases} \tag{4.1}$$

where $\beta = 1/(k_B T)$, with k_B and T being the Boltzmann constant and the absolute temperature (fixed at 298 K in this work), respectively; r is the center-to-center distance between particles i and j ; Z_i is the valence of a particle of species i and σ_{ij} is defined as $\sigma_{ij} = (\sigma_i + \sigma_j)/2$. Here σ_i is the diameter of particle i . Parameter $l_B = \beta e^2/(4\pi\varepsilon_0\varepsilon_r)$ denotes the Bjerrum length, which is taken as 55.69 nm, a value that corresponds to electrostatic interactions in a vacuum at 298 K. The parameter e represents the elementary charge, and ε_0 stands for the permittivity of the free space. The chosen value of l_B corresponds to room temperature with the environment of the ions having a dielectric constant, ε_r, of unity because we have considered all components explicitly. It should be noted that, in this work, we assume the dielectric constant for the model porous carbon electrode and for the ionic liquid is uniform. Recent theoretical works of Kornyshev and co-workers reveal the importance of 'electronic screening' for ionic interactions near a metallic surface and in conducting nanoconfinement.[41] However, the polarizability effect or electronic screening is relatively insignificant because the carbon material has a dielectric constant not much different from that of a typical ionic liquid. In other words, the primitive model used in this work ignores the dielectric relaxation due to ion polarizability, which may lead to an effective dielectric constant.

The slit pore model was used to represent porous carbon electrodes in numerous previous investigations on the effects of pore size on the capacitance. The same model is adopted in this

work to illustrate how an impurity may affect the EDL performance. Inside the slit pore, the electrical field due to the surface charge density is uniform. As a result, each ionic species experiences a constant external potential in the direction perpendicular to the surface:

$$\beta V_i(z) = \begin{cases} -2\pi l_B Z_i HQ/e, & \sigma_i/2 \le z \le H - \sigma_i/2 \\ \infty, & \text{otherwise} \end{cases}, \tag{4.2}$$

where z is the perpendicular distance of the center of the sphere from the lower surface, Q is the surface charge density (C/m^2) of the electrode and H is the surface-to- surface separation (or pore width). Whereas the total interaction potential between ionic species might be more accurately described by an atomistic model, it is commonly assumed that the non-electrostatic interaction play only a secondary role in the interfacial behavior of ionic liquids.[30]

The external potential, or surface energy, acting on the impurity particles is represented by the square-well (SW) potential

$$V_w(z) = \begin{cases} \infty, & z < \sigma_i/2 \text{ or } z > H - \sigma_i/2 \\ 0, & \sigma_i/2 + w < z < H - \sigma_i/2 + w, \\ -\varepsilon_w, & \text{otherwise} \end{cases} \tag{4.3}$$

where w denotes the range of attraction, or the width of the (attractive) wall. In this study, w is equal to $0.1\sigma_i$; ε_w > 0 represents an attractive energy from the surface. The intermolecular potential between the ionic species and impurity is also described by the SW potential $V_{ij}(r)$,

$$V_w(z) = \begin{cases} \infty, & r < \sigma_{ij} \\ -\varepsilon_w, & \sigma_{ij} \le r \le \sigma_{ij} + w. \\ 0, & \text{otherwise} \end{cases} \tag{4.4}$$

It is worth noting that the self-energy and image forces are irrelevant if the dielectric constant is uniform throughout the system.[42]As explained above, the uniform dielectric background assumed in this work can be justified from both physics considerations and in terms of the specific aims pursued in this work.

The details of classical density functional theory (cDFT) can be found in Chapter 2. At a given temperature, T , and a set of electrolyte concentration in the bulk, cDFT predicts the particle distributions inside the slit pore as

$$\rho_i(z) = \rho_i^0(z)\exp\left[-\beta V_i^{ext}(z) - \beta Z_i e\psi(z) - \beta\Delta\mu_i^{ex}(z)\right], \tag{4.5}$$

where $V_i^{ext}(z)$ is a potential other than the direct Coulomb forces, $\Delta\mu_i^{ex}(z)$ accounts for electrostatic correlations and ionic excluded volume effects, and the electrical potential, $\psi(z)$, is related to the local charge density by the Poisson equation.

It has come to our attention that the overall charge neutrality in small pores may be violated according to recent experiment with nuclear magnetic resonance (NMR) techniques.[43] In agreement with this experimental observation, the theoretical work by Colla *et al* also indicates that the confined electrolyte system may not satisfy the overall charge neutrality. [44] In this work, we assume that the surface potential of porous electrodes is fixed by connection with an external power. As discussed above, the constant voltage at the surface effectively forces the overall charge neutrality.

4.3 Result and Discussion

4.3.1 Effect of Surface Energy V_w on the Structure and Capacitance of EDLs

The size dependence of the integral capacitance (CI) has been investigated before by both experimental and theoretical means.[31, 45, 46] The integral capacitance is defined as the ratio of the charge to the electrical potential at the electrode surface, that is, $C_I = Q/\psi_s$. By modelling the microscopic environment of porous carbon electrodes as slit pores, CDFT predicts an oscillatory dependence of C_I on the pore size (H), resembling that for the potential of mean force between two charged surfaces surrounded by an RTIL.[31] For a pure ionic liquid in a slit pore with the width less than 10 times the ion diameter, we expect significant overlap of the

EDLs from the two charged walls. The peak capacitance appears when the EDLs near the two surfaces have the most constructive interference. If the RTIL contains an impurity, how is the $C_I - H$ curve different from that of a pure ionic liquid?

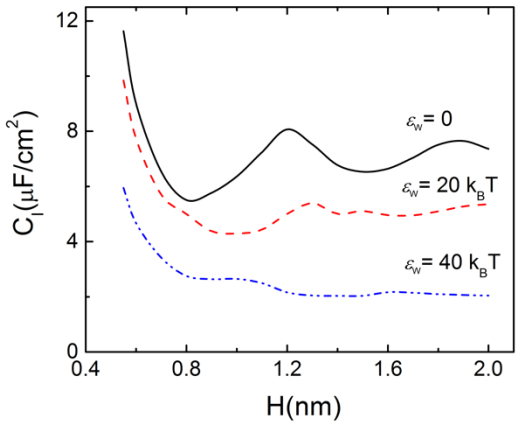

Figure 4.2 The integral capacitance (C_I) versus the pore size (H). Here, the surface electrical potential is ψ_s = 1.5 V; the bulk mole fraction of the impurity, $x_0 = \rho_0^b / \left(\rho_0^b + \rho_+^b + \rho_-^b\right)$, is 10^{-4}. The lines correspond to different surface energy ε_w.

Figure 4.2 shows C_I as a function of H when the surface potential ψ_s is fixed at 1.5V. Here the impurity is modelled as inert particles except that they can bind to the surface, i.e. ε_{ij} = 0 for the interaction between the impurity segments with all ionic species. Throughout this work, the parameters and the bulk concentration for the ionic liquid are fixed, approximately corresponding to those for Emim-TFSI at 298 K and 1 bar (σ = 0.5 nm, ρ = 2.32 nm^{-3}). In the range of pore size about 1–4 times the ion diameter, the integral capacitance becomes remarkably different when the binding energy increases from 0 to 40 k_BT . If there is no surface binding energy, that is, ε_w = 0, the impurity has negligible influence on the capacitance due to its extremely low bulk concentration. In this case, the $C_I - H$ curve is almost identical to that of a pure ionic liquid: the capacitance displays multiple peaks with a decaying envelope and the peaks

appear at the positions corresponding to the layer-by-layer ionic distributions. When the surface binding energy increases to $20\,k_BT$, the integral capacitance is significantly reduced, in particular for large pores, while the oscillation in the $C_I - H$ curve is weakened. A maximum reduction of ~38% (at H = 1.1 nm) can be observed in the $C_I - H$ curve. Further increasing the surface energy to $40\,k_BT$, which is about the same order of magnitude for the energy of a covalent bond, the capacitance is reduced to an even lower value, and no oscillation can be observed in the $C_I - H$ curve. The reduction in capacitance varies from ~48% to ~72%, depending on the pore size. Compared to the case in which ε_w = 0, strong adsorption of impurity leads to a drastic decrease of the integral capacitance and the disappearance of its oscillatory dependence on the pore size.

Why does the impurity generate such a drastic reduction of the integral capacitance and make the oscillatory profile vanishing? To address this question, we first analyze the composition of the contact layer to explain this harmful effect of an impurity. For convenience, here the contact layer is defined within a region of 0.30 nm from the surface, which corresponds to the ion radius (0.25 nm) plus the range of the surface attraction (0.05 nm). Ions or impurity molecules in this region can be considered as in direct contact with the electrode. The composition of the contact layer is described by the fraction of each segment, ϕ_i^s , inside the contact layer:

$$\phi_i^s = \frac{\rho_i^s}{\rho_0^s + \rho_+^s + \rho_-^s} \tag{4.6}$$

where ρ_0^s , ρ_+^s and ρ_-^s are the surface number density (nm^{-2}) of the impurity, cations (counterion in this case) and anions (co-ions) in the contact layer, respectively.

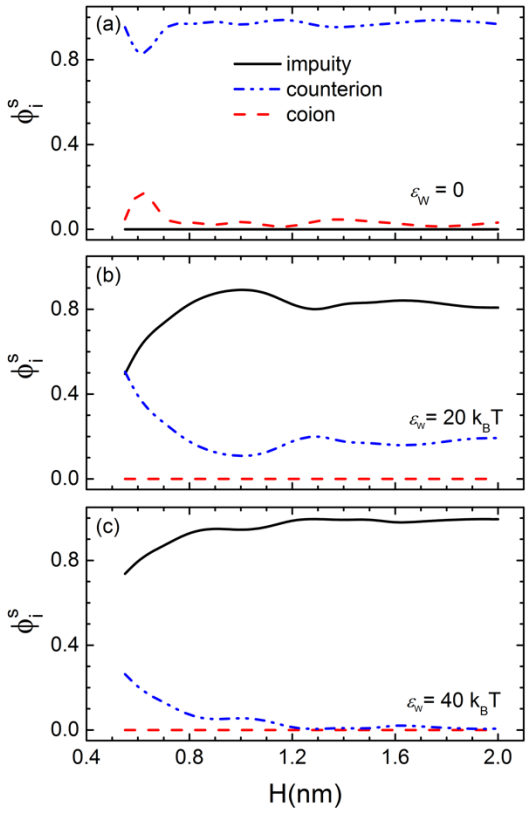

Figure 4.3 The composition of the contact layer versus the pore size at ψ_s =1.5 V. The impurity bulk mole fraction is fixed at with x_0 =10^{-4}. From top to bottom, the surface energy acting on the impurity is ε_w = 0, 20 and 40 k_BT , respectively.

Figure 4.3 shows the composition of the contact layer for the three ionic systems discussed above. One can see that the adsorption of impurity on the electrode can be greatly enhanced and the degree of enhancement depends on the surface energy and the pore size. For the case with no surface binding energy for the impurity molecules, the interfacial region is mainly dominated by counterions due to the strong electrostatic attraction. With the surface binding energy, the impurity is also able to be enriched in the contact layer. Due to the competition of the surface energy and the electrostatic potential, the contact layer, or the interfacial region, is eventually dominated by the impurity instead of the counterions as the binding energy increases.

Essentially, the oscillation of the capacitance is the result of the interference of alternating cations and anions layers. When the contact layer is occupied by the neutral impurity, the effective surface charge density within the first ionic layer becomes significantly smaller, making the layering structure less distinctive. Therefore, the oscillation of the capacitance with the pore size vanishes. For the same magnitude of the surface binding energy, the depletion of the counterions is stronger in larger pores than in smaller pores. In contrast to the electrostatic potential, the surface binding energy is short-ranged. In a small pore, the confinement effect is responsible for the strong overlap of the electrostatic potential. A large binding energy is required for the impurity molecules to overcome the energy barrier and accumulate at the electrode surface. Even when the surface binding energy is as large as $40\,k_BT$, the counterions still contribute up to ~30% of the contact layer. In large pores, the overlap of the electrostatic potential from the surface becomes less distinctive so the impurities are much easily enriched at the interface. The smaller effective surface charge density as well as the excluded volume effects contribute to the reduction of the capacitance for large pores.

To better understand the effect of adsorbed impurity, we extend our analysis of the ion distributions to the entire pore. For the pore size comparable to the ion diameter, the ions can only form a monolayer. The composition of the contact layer can be deduced from the ionic distributions. Therefore, here we focus on a larger pore, such as 2.0 nm to delineate the EDL structure in detail: the distributions of ions and impurity molecules near the interface and their mutual effects on each other. Figure 4.4(a–c) shows the ionic distributions across the pore. Similar to prior studies, cations and anions form alternating layers near the electrode surface. However, the oscillation of the ionic density profiles varies in response to the change in the surface binding energy. For the hybrid RTIL containing an impurity but without the surface energy, the influence of the impurity is negligible. In that case, the contact layer is mainly

composed of counterions. As the surface energy changes from0 to $40\,k_BT$, the contact layer evolves into two parts: counterions and the impurities, while both the counterions and co-ions tend to accumulate primarily at the central plane of the slit. The depletion of counterions from the electrode surface can be attributed to the competition between the surface energy and the electrostatic potential.

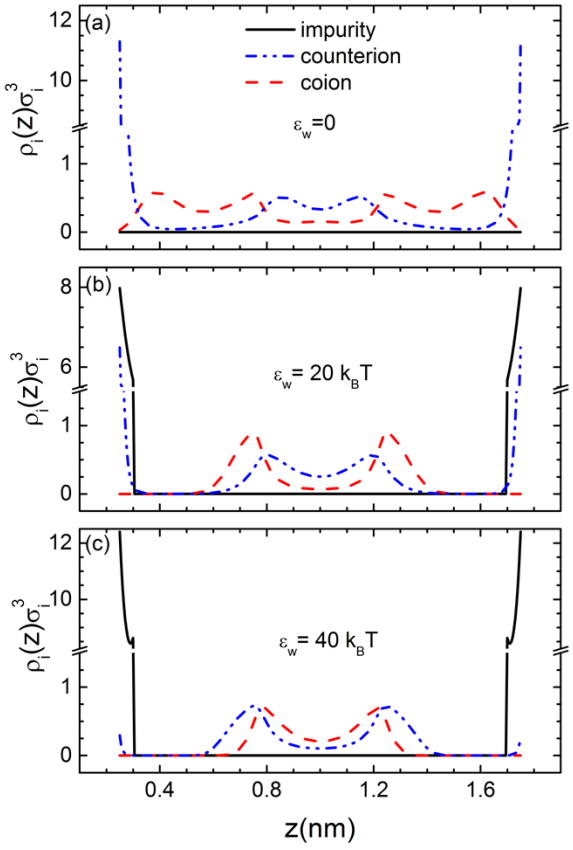

Figure 4.4 Density distributions of the counterions, co-ions and impurity molecules across a 2.0 nm pore at ψ_s = 1.5 V. The impurity bulk mole fraction is x_0 =10^{-4}. From top to bottom, the surface energy acting on the impurity is ε_w = 0, 20 and $40\,k_BT$, respectively.

Figure 4.5 shows the effect of surface energy on the integral capacitance and the contact layer composition in various pore sizes. One can see that both the capacitance and the interfacial region composition are sensitive to the surface energy of impurity molecules. For all three pores,

the impurity molecules need to overcome an energy barrier, around 10 k_BT for the given electrical potential, to enter the slit pore. Increasing the surface energy from 10 to 40 k_BT, the capacitance decreases monotonically with the surface energy. This implies that the impurity molecules begin to interfere the EDL structure and change the ionic density profiles in the pore. Meanwhile, the impurity molecules eventually accumulate inside the porous electrode until saturation. For the larger pores of H =1.2 and 2.0 nm, increasing the surface energy to 10 k_BT or more, both the capacitance and the contact layer composition show little changes. It means that, in these cases, the surface energy plays a more important role than the pore size effects.

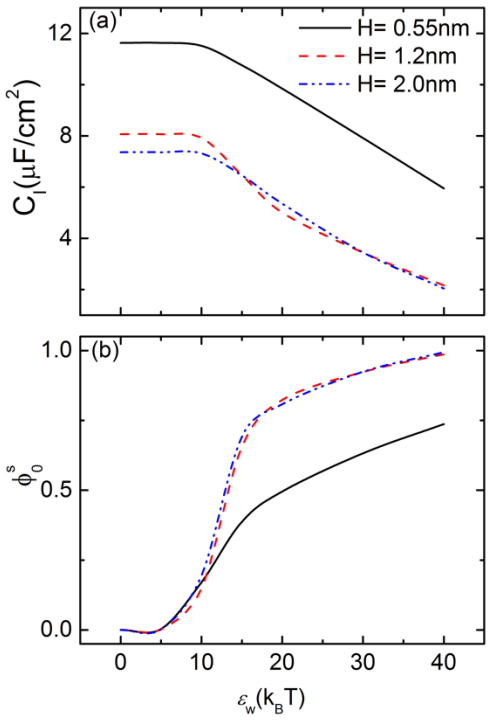

Figure 4.5 The integral capacitance (a) and the mole fraction of the impurity in the contact layer (b) versus the surface energy ε_w at ψ_s =1.5 V. The impurity bulk mole fraction is fixed at x_0 =10^{-4}. The different lines correspond to the pore size H = 0.55, 1.2 and 2.0 nm, respectively

A natural question one may ask is whether the capacitance is sensitive to the impurity bulk density, especially for an even smaller amount of the impurity. To address this question, we

investigate the impurity bulk density effect in a 1.2 nm slit pore, which equals to the pore size when the second peak in the capacitance curve appears (see Figure 4.2). In Figure 4.6, one can see that with zero or a very small surface energy, adsorption of the impurity is almost negligible and the impurity is difficult to accumulate on the electrode surface; when the surface energy is as high as $40\,k_BT$, the slit pore is almost saturated with the impurity even at an extreme low impurity bulk concentration (x_0 =10^{-6}), suggesting that the capacitance is relatively insensitive to the impurity bulk concentration. Both the integral capacitance and the contact layer composition show low sensitivity to the bulk density of the impurity for some magnitudes of the surface energy. As different surface energy reflects the different chemical nature of the impurity, Figure 4.6 indicates the importance of electrolyte purification for different types of impurities.

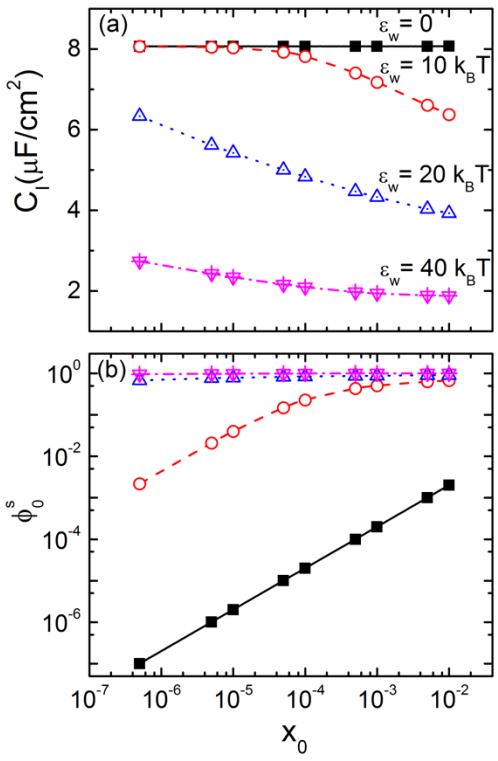

Figure 4.6 The integral capacitance (a) and the mole fraction of impurity in the contact layer (b) versus the impurity bulk mole fraction in a 1.2 nm pore.

4.3.2 Effect of Ion Binding on the Structure and Capacitance of EDLs

For different types of impurity molecules, the impurity can attach not only to the surface but also to the cations or anions in the ionic liquid. As an illustrative example, here we consider an ionic liquid containing impurity that strongly binds with the ionic species. The computational procedure is the same as before. For simplicity, we fixed the intermolecular attraction between the impurity and cations or anion as $\varepsilon_{0,+/-}$ = 40 k_BT while the surface energy acting on the impurity is ε_w =0. The reduced bulk density of the impurity is $\rho_0\sigma_0^3$ = 2.9 × 10^{-5}. We investigate the dependence of capacitance on the pore size and the structure of EDLs in RTIL on a single cathode where the surface voltage is fixed at ψ_s = 1.5V.

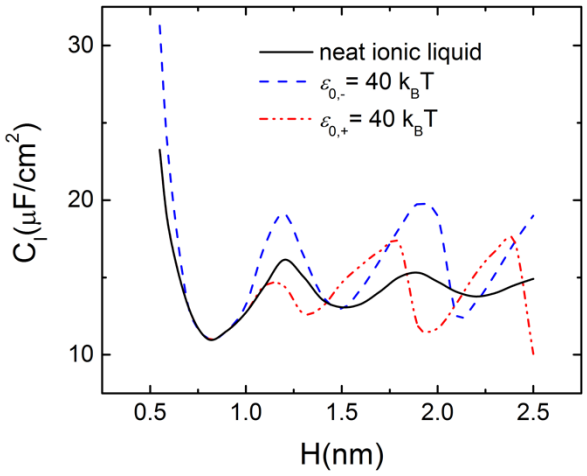

Figure 4.7 The integral capacitance versus the pore size in the presence of an impurity. Here, the voltage is fixed at ψ_s = 1.5 V. The impurity binds strongly with the cation (dashed line) or anions (dash-dotted line). The different lines represent the pure RTIL and mixture, respectively.

Figure 4.7 shows how the capacitance changes with the pore size. The dependence of the capacitance on the pore size of a pure ionic liquid is also shown in this figure as a reference. We find that the magnitude of the capacitance oscillation is enhanced for the two hybrid RTILs and the peaks in the $C_I - H$ curve are shifted in their positions. Compared with that for the pure

RTIL, the integral capacitance does not simply increase or decrease when the impurity molecules strongly bind to the ions. The integral capacitance shows a complex pattern in the pore size range of 1–5 times the ion diameter. In a 0.55 nm pore, the pore size is close to the ion diameter, the capacitance increases only when the impurities are strongly affixed to the counterions. For a pore narrower than 1.4 nm, the integral capacitance of the RTIL with counterion bound impurity shows an increase while that of the RTIL with co-ion bound impurity is reduced. Further increasing the pore size to 1.8 nm, both hybrid RTILs show an increase in the capacitance. When the pore width is larger than 1.8 nm, the size dependence becomes even more complicated.

To understand the change in the $C_I - H$ curve, we present in Figure 4.8 the ionic distributions inside different nanopores. As we discussed before, the constructive or destructive interference between the EDLs stemming from the changes in the layering structure of the ionic liquid, leading to a peak or trough in the capacitance. [47] Both confinement and impurity contribute to the EDL interference. To better illustrate this enhanced oscillation, we have analyzed the EDL structure in the slit pore with various widths. Figure 4.8(a) shows the reduced density profiles of a pure ionic liquid across a 2.5 nm slit pore. We can see the ions form alternating layers inside the pore. The EDL at the interfacial is dominated by counterions. For the RTIL containing counterion-bounded impurity (Figure 4.8(b)), the impurity molecules and the ionic species form more ordered alternating layers compared to that for the pure ionic liquid. In this case, the layering structures become more distinctive. The intensity of the first layer is higher than that of the pure ionic liquid. The strong electrostatic coupling between counter- and co-ions is destroyed by the impurity molecules that distribute around the counterions. For the RTIL containing coion-bounded impurity (Figure 4.8(c)), the impurity has little impact on the EDL structure. However, the presence of impurity alters the counterion density inside the pore. In other

sizes of slit pores, the strongly coupled impurity also shows a significant impact on the ionic distributions (Figure 4.9).

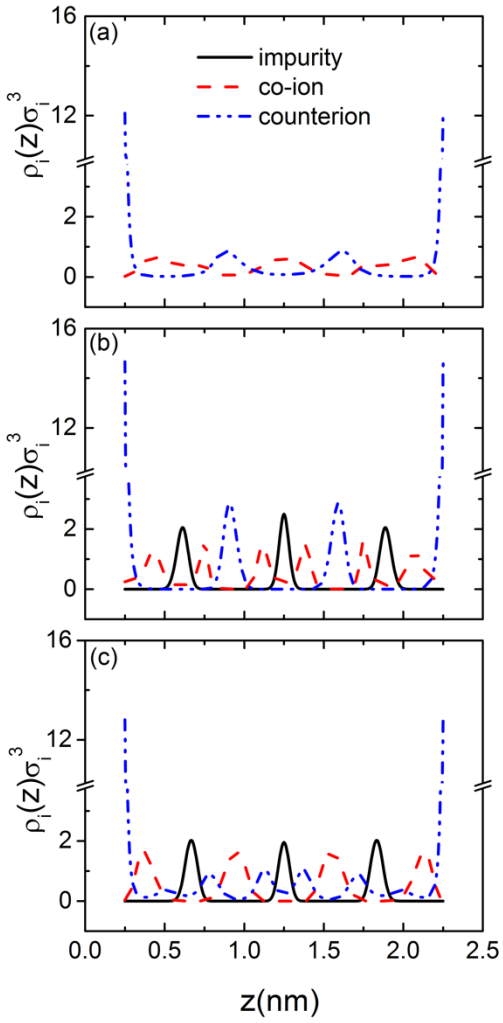

Figure 4.8 The reduced density profiles of the impurity and ions across a 2.5 nm slit pores at ψ_s = 1.5 V (a) a pure RTIL, (b) the RTIL containing an counterion bounded impurity and (c) the ionic liquid containing an co-ion bounded impurity, respectively.

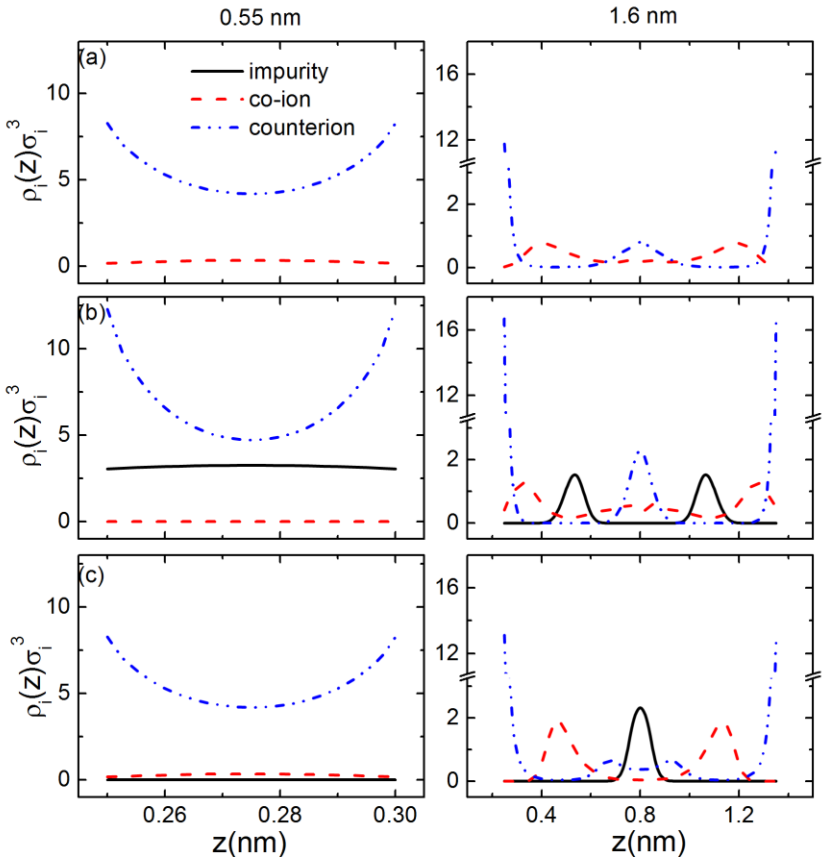

Figure 4.9 The reduced density profiles of the impurity and ions across slit pores with various widths at the positive electrode: (a) a pure RTIL, (b) the RTIL containing counterion bounded impurity and (c) the RTIL containing a co-ion bounded impurity, respectively. The surface electrical potential is fixed at 1.5 V.

It should be noted that strong coupling of the impurity and ionic species results in the formation of clusters rather than dimers. To see the difference between an ionic liquid with strong affinity to impurities and that of an ionic liquid with a neutral segment tethered to ionic species, we investigate a binary ionic liquid in which the coion is the same as that in the above example while each counterion is composed of a monovalent spherical particle. The dumbbell-shaped dimer consists of two tangential tethered hard spheres, one is negative charged and the other is neutral. From the density profiles (Figure 4.10), we found that the ionic distributions for this binary ionic liquid is almost the same as those corresponding to a monomeric ionic liquid with the same ionic density but is quite different from those in the presence of impurity molecules. The

difference in the ionic density profiles suggests that the cooperative coupling is responsible for changing the ionic distributions even at a very low bulk concentration. Such cooperative binding impacts ion packing in the slit pore.

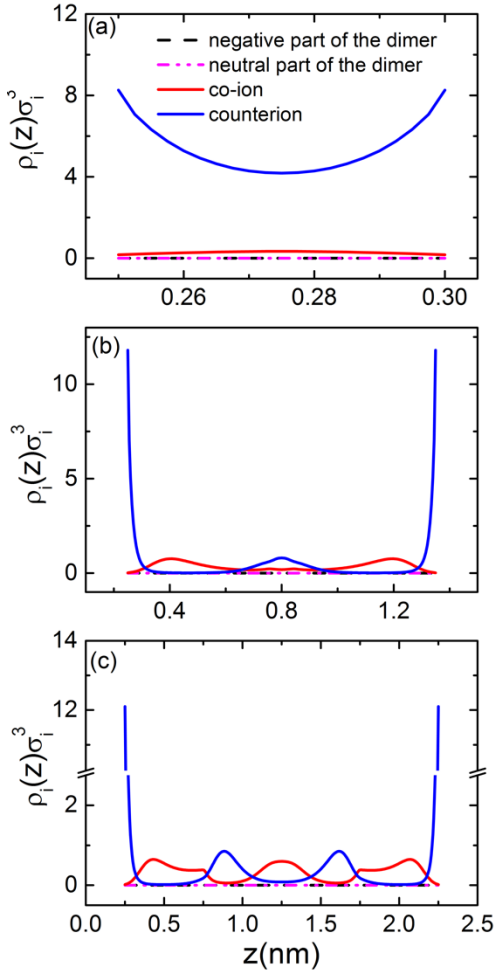

Figure 4.10 The reduced density profiles for a binary mixture of ionic liquids across slit pores with various widths. From the top to bottom, the pore size is 0.55, 1.6 and 2.5 nm respectively. The ratio of the dimer to the monomer co-ion in the ionic mixture is 10^{-4}. The surface voltage is fixed at 1.5 V.

In Figure 4.11, we compare the average ionic density inside the pore for the pure RTIL and for those containing impurities that bind with one of the ionic species. In all cases, the overall number density of the ions in the bulk is 2.32 nm^{-3}. The average number density ρ_i^{ave} inside the pore is defined as

$$\rho_i^{ave} = \frac{1}{H}\int_0^H \rho_i(z)dz. \tag{4.7}$$

We see that the average number density of ions in the hybrid RTIL is higher than that in the pure RTIL. In other words, the impurity would enable a denser packing ionic species in slit pores.

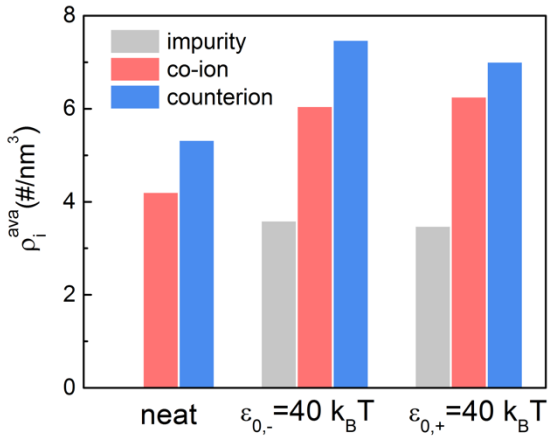

Figure 4.11 The average number density of the impurity and ions inside a 2.5 nm slit pore at ψ_s = 1.5 V.

4.4 Conclusion

In summary, CDFT has been applied to study the interfacial or double layer structure in ionic liquid/impurity mixtures using an explicit model for the ionic liquid and impurity. With a different type of binding energy with the surface or ionic species, the impurity shows a different influence on the EDL microstructures and contributes differently to the integral capacitance. It is noted that the impurity can be considered as either a contaminant or an additive to the ionic

liquid, all depending on the interaction between the impurity and the electrode or ions. Meanwhile, the capacitance strongly oscillates with the variation of the pore size similar to that for the pure ionic liquid electrolyte. With strong binding of impurity to the ionic species, the RTIL/impurity mixture may lead to an enhanced capacitance oscillation. In certain pores, a significant increase in the capacitance can be obtained. The theoretical results provide useful insights for further investigation of supercapacitors aiming at rational design of porous electrode materials and charge carriers.

Bibliography

[1] M. C. Buzzeo, R. G. Evans, and R. G. Compton, "Non-haloaluminate room-temperature ionic liquids in electrochemistry--a review," *Chemphyschem,* vol. 5, no. 8, pp. 1106-20, Aug 20 2004.

[2] A. K. Burrell, R. E. D. Sesto, S. N. Baker, T. M. McCleskey, and G. A. Baker, "The large scale synthesis of pure imidazolium and pyrrolidinium ionic liquids," *Green Chemistry,* vol. 9, no. 5, p. 449, 2007.

[3] G. Feng, X. Jiang, R. Qiao, and A. A. Kornyshev, "Water in ionic liquids at electrified interfaces: the anatomy of electrosorption," *ACS Nano,* vol. 8, no. 11, pp. 11685-94, Nov 25 2014.

[4] F. Endres, N. Borisenko, S. Z. El Abedin, R. Hayes, and R. Atkin, "The interface ionic liquid(s)/electrode(s): In situSTM and AFM measurements," *Faraday Discuss.,* vol. 154, pp. 221-233, 2012.

[5] K. R. Seddon, A. Stark, and M.-J. Torres, "Influence of chloride, water, and organic solvents on the physical properties of ionic liquids," *Pure and Applied Chemistry,* vol. 72, no. 12, pp. 2275-2287, 2000.

[6] B. R. Clare, P. M. Bayley, A. S. Best, M. Forsyth, and D. R. MacFarlane, "Purification or contamination? The effect of sorbents on ionic liquids," *Chem Commun (Camb),* no. 23, pp. 2689-91, Jun 21 2008.

[7] S. Cuadrado-Prado *et al.,* "Experimental measurement of the hygroscopic grade on eight imidazolium based ionic liquids," *Fluid Phase Equilibria,* vol. 278, no. 1-2, pp. 36-40, 2009.

[8] P. Azaïs *et al.,* "Causes of supercapacitors ageing in organic electrolyte," *Journal of Power Sources,* vol. 171, no. 2, pp. 1046-1053, 2007.

[9] M. Zhu *et al.,* "Chemical and electrochemical ageing of carbon materials used in supercapacitor electrodes," *Carbon,* vol. 46, no. 14, pp. 1829-1840, 2008.

[10] D. Cericola, P. W. Ruch, A. Foelske-Schmitz, D. Weingarth, and R. Kötz, "Effect of water on the aging of activated carbon based electrochemical double layer capacitors during constant voltage load tests," *Int. J. Electrochem. Sci,* vol. 6, no. 4, pp. 988-996, 2011.

[11] A. A. Kornyshev, "Double-layer in ionic liquids: paradigm change?," *J Phys Chem B,* vol. 111, no. 20, pp. 5545-57, May 24 2007.

[12] C. M. Yang *et al.,* "Nanowindow-regulated specific capacitance of supercapacitor electrodes of single-wall carbon nanohorns," *J Am Chem Soc,* vol. 129, no. 1, pp. 20-1, Jan 10 2007.

[13] G. Feng, J. S. Zhang, and R. Qiao, "Microstructure and Capacitance of the Electrical Double Layers at the Interface of Ionic Liquids and Planar Electrodes," *The Journal of Physical Chemistry C*, vol. 113, no. 11, pp. 4549-4559, 2009.

[14] A. Uysal *et al.*, "Interfacial ionic 'liquids': connecting static and dynamic structures," *J Phys Condens Matter*, vol. 27, no. 3, p. 032101, Jan 28 2015.

[15] C. C. Rochester, S. Kondrat, G. Pruessner, and A. A. Kornyshev, "Charging Ultrananoporous Electrodes with Size-Asymmetric Ions Assisted by Apolar Solvent," *The Journal of Physical Chemistry C*, vol. 120, no. 29, pp. 16042-16050, 2016.

[16] Y. A. Budkov, A. L. Kolesnikov, and M. G. Kiselev, "On the theory of electric double layer with explicit account of a polarizable co-solvent," *J Chem Phys*, vol. 144, no. 18, p. 184703, May 14 2016.

[17] Y. Lauw, M. D. Horne, T. Rodopoulos, N. A. Webster, B. Minofar, and A. Nelson, "X-ray reflectometry studies on the effect of water on the surface structure of [C4mpyr][NTf2] ionic liquid," *Phys Chem Chem Phys*, vol. 11, no. 48, pp. 11507-14, Dec 28 2009.

[18] R. Hayes, N. Borisenko, B. Corr, G. B. Webber, F. Endres, and R. Atkin, "Effect of dissolved LiCl on the ionic liquid-Au(111) electrical double layer structure," *Chem Commun (Camb)*, vol. 48, no. 82, pp. 10246-8, Oct 21 2012.

[19] K. Tamura and Y. Nishihata, "Study on the Behavior of Halide Ions on the Au(111) Electrode Surface in Ionic Liquids Using Surface X-ray Scattering," *The Journal of Physical Chemistry C*, vol. 120, no. 29, pp. 15691-15697, 2016.

[20] G. Feng, J. Huang, B. G. Sumpter, V. Meunier, and R. Qiao, "Structure and dynamics of electrical double layers in organic electrolytes," *Phys Chem Chem Phys*, vol. 12, no. 20, pp. 5468-79, 2010.

[21] B. Jamnik and V. Vlachy, "Monte Carlo and Poisson-Boltzmann study of electrolyte exclusion from charged cylindrical micropores," *Journal of the American Chemical Society*, vol. 115, no. 2, pp. 660-666, 1993.

[22] R. Lynden-Bell and J. C. Rasaiah, "Mobility and solvation of ions in channels," *The Journal of chemical physics*, vol. 105, no. 20, pp. 9266-9280, 1996.

[23] D. Goulding, J. P. Hansen, and S. Melchionna, "Size selectivity of narrow pores," *Phys Rev Lett*, vol. 85, no. 5, pp. 1132-5, Jul 31 2000.

[24] B. Peng and Y. X. Yu, "Ion distributions, exclusion coefficients, and separation factors of electrolytes in a charged cylindrical nanopore: a partially perturbative density functional theory study," *J Chem Phys*, vol. 131, no. 13, p. 134703, Oct 7 2009.

[25] A. Oleksy and J.-P. Hansen, "Towards a microscopic theory of wetting by ionic solutions. I. Surface properties of the semi-primitive model," *Molecular Physics*, vol. 104, no. 18, pp. 2871-2883, 2006.

[26] A. Oleksy and J.-P. Hansen, "Microscopic density functional theory of wetting and drying of a solid substrate by an explicit solvent model of ionic solutions," *Molecular Physics*, vol. 107, no. 23-24, pp. 2609-2624, 2009.

[27] A. Oleksy and J. P. Hansen, "Wetting of a solid substrate by a "civilized" model of ionic solutions," *J Chem Phys*, vol. 132, no. 20, p. 204702, May 28 2010.

[28] A. Oleksy and J.-P. Hansen, "Wetting and drying scenarios of ionic solutions," *Molecular Physics*, vol. 109, no. 7-10, pp. 1275-1288, 2011.

[29] D.-e. Jiang, D. Meng, and J. Wu, "Density functional theory for differential capacitance of planar electric double layers in ionic liquids," *Chemical Physics Letters*, vol. 504, no. 4-6, pp. 153-158, 2011.

[30] J. Wu, T. Jiang, D.-e. Jiang, Z. Jin, and D. Henderson, "A classical density functional theory for interfacial layering of ionic liquids," *Soft Matter*, vol. 7, no. 23, p. 11222, 2011.

[31] D. E. Jiang, Z. Jin, and J. Wu, "Oscillation of capacitance inside nanopores," *Nano Lett*, vol. 11, no. 12, pp. 5373-7, Dec 14 2011.

[32] D. E. Jiang, Z. Jin, D. Henderson, and J. Wu, "Solvent Effect on the Pore-Size Dependence of an Organic Electrolyte Supercapacitor," *J Phys Chem Lett*, vol. 3, no. 13, pp. 1727-31, Jul 5 2012.

[33] J. Chmiola, G. Yushin, Y. Gogotsi, C. Portet, P. Simon, and P. L. Taberna, "Anomalous increase in carbon capacitance at pore sizes less than 1 nanometer," *Science*, vol. 313, no. 5794, pp. 1760-3, Sep 22 2006.

[34] H. Zhang, G. Cao, Y. Yang, and Z. Gu, "Capacitive performance of an ultralong aligned carbon nanotube electrode in an ionic liquid at 60°C," *Carbon*, vol. 46, no. 1, pp. 30-34, 2008.

[35] T. A. Centeno, O. Sereda, and F. Stoeckli, "Capacitance in carbon pores of 0.7 to 15 nm: a regular pattern," *Phys Chem Chem Phys*, vol. 13, no. 27, pp. 12403-6, Jul 21 2011.

[36] L. B. Bhuiyan, S. Lamperski, J. Wu, and D. Henderson, "Monte Carlo simulation for the double layer structure of an ionic liquid using a dimer model: a comparison with the density functional theory," *J Phys Chem B*, vol. 116, no. 34, pp. 10364-70, Aug 30 2012.

[37] D. E. Jiang and J. Wu, "Microscopic Insights into the Electrochemical Behavior of Nonaqueous Electrolytes in Electric Double-Layer Capacitors," *J Phys Chem Lett*, vol. 4, no. 8, pp. 1260-7, Apr 18 2013.

[38] S. Kondrat and A. Kornyshev, "Corrigendum: Superionic state in double-layer capacitors with nanoporous electrodes," *Journal of Physics: Condensed Matter,* vol. 25, no. 11, p. 119501, 2013.

[39] S. Kondrat, N. Georgi, M. V. Fedorov, and A. A. Kornyshev, "A superionic state in nano-porous double-layer capacitors: insights from Monte Carlo simulations," *Phys Chem Chem Phys,* vol. 13, no. 23, pp. 11359-66, Jun 21 2011.

[40] N. Mehio, S. Dai, J. Wu, and D.-e. Jiang, "Theoretic Insights into Porous Carbon-Based Supercapacitors," *Nanocarbons for Advanced Energy Storage,* vol. 1, pp. 361-378, 2015.

[41] C. C. Rochester, A. A. Lee, G. Pruessner, and A. A. Kornyshev, "Interionic interactions in conducting nanoconfinement," *Chemphyschem,* vol. 14, no. 18, pp. 4121-5, Dec 16 2013.

[42] R. Wang and Z. G. Wang, "On the theoretical description of weakly charged surfaces," *J Chem Phys,* vol. 142, no. 10, p. 104705, Mar 14 2015.

[43] Z. X. Luo, Y. Z. Xing, Y. C. Ling, A. Kleinhammes, and Y. Wu, "Electroneutrality breakdown and specific ion effects in nanoconfined aqueous electrolytes observed by NMR," *Nat Commun,* vol. 6, p. 6358, Feb 20 2015.

[44] T. Colla, M. Girotto, A. P. Dos Santos, and Y. Levin, "Charge neutrality breakdown in confined aqueous electrolytes: Theory and simulation," *J Chem Phys,* vol. 145, no. 9, p. 094704, Sep 7 2016.

[45] G. Feng and P. T. Cummings, "Supercapacitor Capacitance Exhibits Oscillatory Behavior as a Function of Nanopore Size," *The Journal of Physical Chemistry Letters,* vol. 2, no. 22, pp. 2859-2864, 2011.

[46] N. Jäckel *et al.*, "Anomalous or regular capacitance? The influence of pore size dispersity on double-layer formation," *Journal of Power Sources,* vol. 326, pp. 660-671, 2016.

[47] G. Feng, R. Qiao, J. Huang, S. Dai, B. G. Sumpter, and V. Meunier, "The importance of ion size and electrode curvature on electrical double layers in ionic liquids," *Phys Chem Chem Phys,* vol. 13, no. 3, pp. 1152-61, Jan 21 2011.

Chapter 5. Impurity Effects on Charging Mechanism and Energy Storage of Nanoporous Supercapacitors

Room-temperature ionic liquids (RTILs) have been widely used as electrolytes to enhance the capacitive performance of electrochemical capacitors also known as supercapacitors. Whereas impurities are ubiquitous in RTILs (e.g., water, alkali salts, and organic solvents), little is known about their influences on the electrochemical behavior of electrochemical devices. In this chapter, we investigate different impurities in RTILs within the micropores of carbon electrodes via the classical density functional theory (CDFT). We find that under certain conditions impurities can significantly change the charging behavior of electric double layers and the shape of differential capacitance curves even at very low concentrations. More interestingly, an impurity with a strong affinity to the nanopore can increase the energy density beyond a critical charging potential. Our theoretical predictions provide further understanding of how impurity in RTILs affects the performance of supercapacitors.

5.1 Introduction

A wide variety of carbon-based materials with tunable pore size, morphology, architecture, and functionality have been proposed to improve the capacitive performance of electrical double layer capacitors (EDLCs). The effects of the pore size on the electric double layer (EDL) structure, capacitance, and ion transport have been studied in great details both experimentally and theoretically.[1-9] The EDLC capacitance shows an anomalous increase as the pore size becomes comparable to the dimensionality of the ionic species, suggesting that electrodes with sub-nano pores are a better choice than those with larger pores. However, the anomalous increase in pores below 1 nm was not observed in few other experiments, [10] and some theoretical work showed the anomalous increase may be diminished by a pore-width dependent permittivity.[11] The supercapacitor performance depends not only on the electrical

potential and the geometric compatibilities of the electrode pores and ionic species but also on the surface properties of the electrode materials and impurities in the electrolytes.[12-18] Existing theoretical reports are mostly devoted to analyzing electrostatic interactions and confinement effects. Despite the omnipresence of impurities in room temperature ionic liquids (RTILs), relatively little is known on how a small amount of chemicals in the ionic liquid may influence the EDLC performance.[19, 20]Recent experiments and molecular dynamics simulations have shown that the presence of impurities may lead to EDL charging drastically different from that for neat RTILs.[21, 22] It has been shown that EDL charging in RTILs almost always involves ion exchange (swapping of co-ions for counterions) and rarely occurs by counterion adsorption alone.[9] Ionophobic nanopores are able to enhance the energy storage capacity because the surface properties can drastically change the charging mechanism.[23] A new solvent-facilitated charging mechanism has been identified to enhance the electrical energy stored in nanopores.[24] It was found that the use of "pore-philic" solvents will create effectively "ionophobic" pores, which have clear advantage for charge storage and potentially charging dynamics as well.

One of the key difficulties in studying the impurity effect is that impurity species are present at extremely dilute bulk concentrations. Experimental tools such as atomic force microscopy (AFM) and X-ray reflectometry were applied to study the structural properties of EDLs in a hybrid RTIL containing impurity species at the electrode surface.[25, 26]Computational methods, such as molecular dynamics (MD) simulations, were also used to investigate the distribution of impurities near electrified interfaces.[27]It was found that a small amount of polar additives can boost the performance of ionic-liquid-based supercapacitors.[28] Due to the importance of impurity on the EDLC performance, more effort should be devoted to understanding the charging mechanism and capacitive behavior in RTILs containing impurities.

In this work, we discuss the impurity effect on the charging and capacitive behaviors based on the classical density functional theory (CDFT). CDFT had been successfully used in studying the EDL structure and the capacitance of ionic liquids and organic electrolytes systems.[29-31] It has been shown that the CDFT predictions are able to capture the essential results from earlier experimental and simulation studies and provides microscopic insights into the electrochemical behavior of ionic liquids as the working electrolytes for supercapacitors. [32-34] Specifically, we are interested in the dependence of the capacitance and the mechanism of EDL charging on different impurity types in RTILs.

This chapter is structured as follows. First, we describe our coarse-grained models of RTILs and porous materials and provide a brief introduction to the classical DFT method. Next, we discuss the impurity effect on the EDL charging mechanism and the capacitive performance of EDLCs. Finally, we summarize the main results and possible impacts on future experimental work.

5.2 Model and Methods

We consider a generic model for EDL capacitors consisting of porous carbons and RTILs. Figure 5.1 presents a schematic setup for RTILs in the micropores of electrodes. Following the standard model for the pore size distributions of porous materials characterized by gas adsorption,[35] we use slit pores to represent the geometry of porous carbons. The confined RTILs are at equilibrium with a bulk ionic liquid with impurities represented by a coarse-grained model. We consider three types of impurities: (1) Impurity molecules accumulate inside the pore due to strong surface affinity (Figure 5.1a). (2) Both ions and impurity molecules can enter the pore at low electrical potential (Figure 5.1b). (3) No impurity molecule can enter the pore due to surface repulsion (Figure 5.1c). In the coarse-grained model of the ionic liquid, both cations and anions are represented as charged hard spheres, and the neutral sphere represents impurity molecules. We

assume further that all particles have the same size and that impurities molecules bear no net charge. Whereas the coarse-grained model ignores chemical details, it accounts for electrostatic correlations and ionic excluded volume effects important for EDLC performance but neglected in conventional EDL theories. Approximately, the ionic model parameters are selected to match those corresponding to 1-ethyl-3-methylimidazolium bis- (trifluoromethylsulfonyl)imide (EMI-TFSI), a commercial ionic liquid widely used in electrochemical devices. The number density of cations and anions is 2.32nm^{-3}, and that of impurity molecule is 1% of total number density.

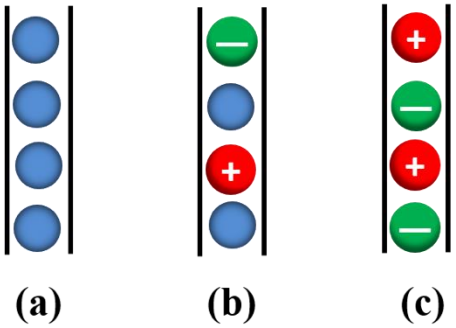

Figure 5.1 Schematic representations of three scenarios considered in this work on the effects of impurities in the room temperature ionic liquids on supercapacitor performance.

The nonelectrostatic component of the external potential, or surface energy, acting on the impurity particles is represented by

$$V_i(z)=\begin{cases}\infty, & z<\sigma_i/2 \text{ or } z>H-\sigma_i/2\\ \omega, & \text{otherwise}\end{cases} \tag{5.1}$$

where ω represents the transfer energy, H is the surface-to-surface separation (or pore width), and z is the perpendicular distance from the surface. The competition of pore adsorption between ions and impurity molecules is controlled by transfer energy ω, which is equivalent to the resolvation energy introduced by Kondrat and Kornyshev to account for the energy cost to transfer an impurity molecule from the bulk to the slit pore.[23, 24] A positive transfer energy means that the nanopore disfavors the adsorption of the impurity molecules compared to that of

cations or anions, while a negative ω means that the pore favors impurity molecules. Because the residual dielectric constant is not much different from the dielectric constant for the carbon electrode, we assume that the image-charge effects are relatively unimportant for determining ionic distributions. Even when the surface potential is fixed, a discontinuity in the dielectric constant at the electrode− electrolyte interface leads to image forces because charge fluctuation near the electrode is correlated with atomic polarization inside the electrode.

Classical density functional theory (CDFT) is used to calculate the ion distributions and subsequently the capacitance of EDLCs. At a given temperature T and a set of ion concentration in the bulk, ρ_i^0 , CDFT predicts the ion distributions inside the pore as

$$\rho_i(z) = \rho_i^0 \exp\left[-\beta V_i(z) - \beta Z_i e\psi(z) - \beta\Delta\mu_i^{ex}(z)\right], \tag{5.2}$$

where $\beta = 1/(k_B T)$, k_B is the Boltzmann constant, and $\Delta\mu_i^{ex}$ accounts for electrostatic correlations and ionic excluded volume effects. The theoretical details of the excess chemical potential and the numerical method can be found in Chapter 2.

5.3 Results and Discussions

For all systems considered in this work, the thermodynamic conditions of the bulk ionic liquid are located in the one-phase region of the phase diagram for the restricted primitive model of electrolytes.[36] Here the concentration of the RTIL is fixed at 3.8 M, the mole fraction of impurity at the bulk is 0.01, and the pore width is H = 0.6 nm. We fix the impurity concentration at 1% mole fraction because it is not a controllable parameter in most experiments. We expect that the main conclusions will be the same if the impurity concentration is slightly changed (as long as it remains small).

Figure 5.2 shows the DFT predictions for the surface charge density versus the surface energy ω for impurities molecules. The interaction between the impurity and the nanopore is

reflected in the surface energy ω, which amounts to the impurity transfer energy from the bulk reservoir into the nanopore. A positive surface energy ω means that the nanopore disfavors the adsorption of the impurity molecules, while a negative ω means that the pore favors impurity adsorption. Because both cations and anions considered in this work have the same size and absolute valence, these plots are symmetric if they are extended to the negative side of the surface electrical potential. Figure 5.2 indicates that regardless of the sign of the surface binding energy ω the charge density of the electrode increases monotonically with the electrode potential. At large electrical potential, the surface charge density becomes independent of the surface energy because ion adsorption inside the pore is dominated by electrostatic interactions. The magnitude of the surface charge density, on the order of $\sim$0.1 C/m^2, is comparable to those observed in molecular dynamics simulation for carbon-based nonaqueous supercapacitors.[37, 38]While the binding energy does not alter the range of the surface charge density, the charging curves are noticeably different for nanopores with different surface energies. If the impurity molecules are strongly favored inside the pores (e.g., $\omega = -20k_BT$), then their presence largely reduces the surface charge density at low potential and thus significantly changes the shape of the $Q-\psi$ curve. For a pore that repels impurity molecules, surface charge density Q increases monotonically with the surface potential ψ , resembling the shape of a Langmuir adsorption isotherm.

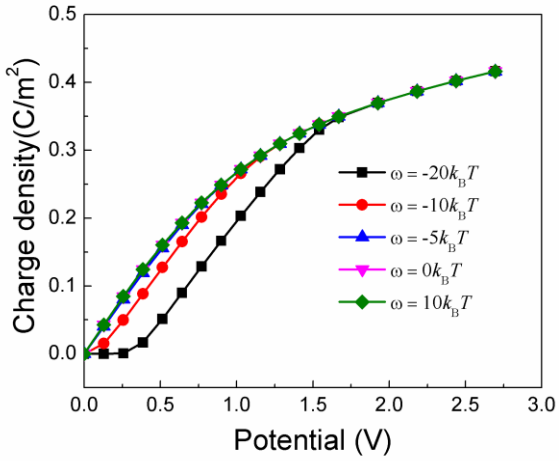

Figure 5.2 Theoretical predictions for the surface charge density versus the electrical potential at different transfer energies of the impurity molecules.

We may attain an understanding of the charging curves by considering the average number density of individual species inside the nanopores during the charging process. Figure 5.3a presents variations of the particle densities versus the surface electrical potential for the case with an impurity binding energy $\omega = -10k_BT$. The number densities of ionic species and impurity molecules in the pore are determined not only by their bulk densities but also by the surface attraction energies, and the latter is responsible for the large surface densities shown in Figure 5.3a. Here the surface charge density can even exceed the maximum packing fraction of uniform hard spheres because the pore width (0.6 nm) is slightly larger than the hard-sphere diameter (0.5 nm). As the surface potential increases, the pore gains electrical charge mainly by exchanging impurity for counterions (anions) from the bulk. When the charging potential larger than 1 V, virtually all impurity molecules have been depleted from the pore, and the charging process is dominated by counterion insertion. For a slit pore with weak attraction ($\omega = -5k_BT$) to the impurity molecules (Figure 5.3b), the EDL charging reflects a combination of impurity-counterion exchange and co-ion−counterion exchange at low surface potential, and a counterion

insertion at high surface potential. For a pore that disfavors impurity adsorption ($\omega \geq 0$) in Figure 5.3c, the charging process consists of both co-ion− counterion exchange and counterion insertion. For all cases, the surface charge density remains the same at high surface potential because at such conditions only counterions are adsorbed inside the nanopores. Because cations and anions have the same size but opposite charge, the surface charge becomes negative but retains the same absolute values if the electrode potential is switched to negative.

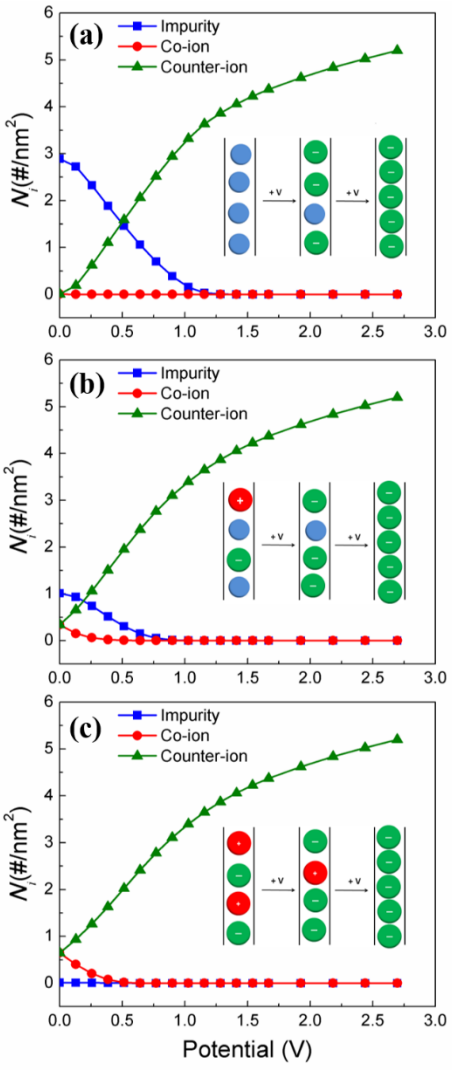

Figure 5.3 Number densities of ions and impurity molecules inside a nanopore of width $H = 0.6$nm with different transfer energies for the impurity molecules: (a) $\omega = -10k_BT$; (b) $\omega = -5k_BT$; (c) $\omega = 0k_BT$.

Three types of charging mechanisms have been identified for neat ionic liquids: [39-41] (i) co-ion−counterion exchange, (ii) counterion insertion, and (iii) desorption of co-ions. When the ionic liquid is diluted with a solvent, two additional charging mechanisms had been proposed:[24] (iv) solvent swapping with co-ions, which themselves are forced out of the pore at higher voltages and replaced with counterions, and (v) direct swapping of solvent with counterions without the inclusion of co-ions in the pore at any voltage. Similar to the solvent effect on the charging mechanisms, we may identify two distinctive charging behaviors in the presence of impurity molecules: (vi) impurity− counterion exchange similar to the solvent effect as shown in (v) and (vii) impurity−counterion exchange concomitant with co-ion−counterion exchange, a combination of charging mechanisms (v) and (i). Like the solvent effect on the charging behavior, the transfer energy (surface energy ω) determines which charging mechanism takes place.

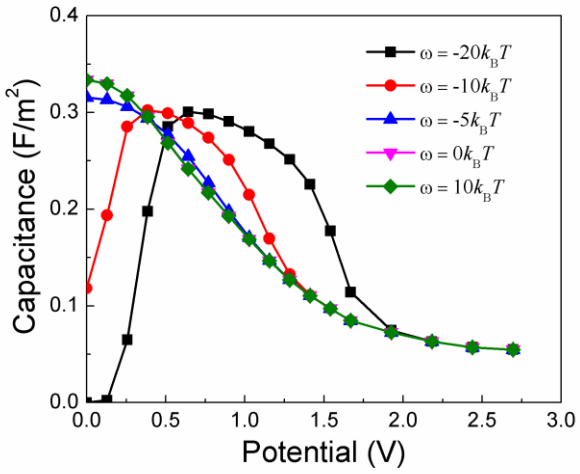

Figure 5.4 Differential capacitance as a function of applied potential shows a transition from a Bactrian camel shape to bell shape as the surface energy of the impurity molecules from attraction to repulsion. For impurity-disfavored nanopores ($\omega \geq 0$), the two $C_d - \psi_0$ curves are almost identical because the impurity molecules do not enter the pore.

The performance of EDLCs can be measured in terms of differential capacitance C_d, which is defined as a derivative of the surface charge density with respect to the electrode potential:

$$C_d = \frac{\partial Q}{\partial \psi} \tag{5.3}$$

Figure 5.4 shows the dependence of the differential capacitance on the electrode potential ($C_d - \psi_0$ curves) at conditions the same as those in Figure 5.2 As discussed above, the impurities have little effect on EDL charging when $\omega \geq 0$. Similar to results for pure ionic liquids studied in our previous work,[42] the $C_d - \psi_0$ curves exhibit an symmetric "bell shape". At low electrode potential (here below 0.5 V), the near-symmetric variations of cation and anion densities suggest that the dominant charging mechanism is the exchange of co-ions (cations) in the pore with the counterions (anions) from the bulk (Figure 5.3c). In this case, the differential capacitance decreases sharply because ion adsorption becomes quickly saturated at small electrical potential. At high electrode potential (here above 0.5 V), co-ions are totally depleted from the pore as indicated by the number density shown in Figure 5.3c. In the latter case, the charging process is dominated by counterion insertion, which leads to a slower decline of the differential capacitance.

When the transfer energy is elevated to $\omega = -20k_BT$ and $-10k_BT$, both counterions and co-ions are excluded from the nanopore at a low charging potential. In this case, the impurities are exchanged by counterions from the bulk only if the electrode potential is sufficiently large to overcome the surface energy ω. The differential capacitance increases to a maximum with the surface potential. A further increase of the electrode potential leads to the saturation of counterions inside the nanopore and thus a decline of the differential capacitance. In other words, the $C_d - \psi$ curves exhibit a Bactrian camel shape. At large surface potential, the differential

capacitance ($\sim 7\mu$F/cm^2) is comparable to those from previous theoretical and experimental investigations for a wide range of nonaqueous supercapacitors with carbon electrodes.[43]For pores with minimal impurity effects, the bell-shaped charging curves are also in good agreement with previous publications.[44]Although our model was not intended to capture the chemical details or the quantitative performance of any specific systems, the maximum differential capacitance ($\sim 30\mu$F/cm^2) at the zero voltage is similar to that for 1-propyl-3-methylimidazolium tetrafluoroborate ($PMIBF_4$) ionic liquid at Hg electrode ($\sim 28\mu$F/cm^2).[45]The maximum differential capacitance shown in Figure 5.4 is slightly larger than those reported in a previous work ($\sim 20\mu$F/cm^2)[46] because of different theoretical models and experimental systems were considered.

Figure 5.4 indicates that the peak capacitance shifts to a higher potential as the surface becomes more attractive (viz., surface energy changes from $\omega = -5k_BT$ to $\omega = -20k_BT$). A bell shape changes to the two-hump camel shape with different impurities in the differential capacitance-charging potential curves, and this indicates that impurities may lead to different charging mechanisms.

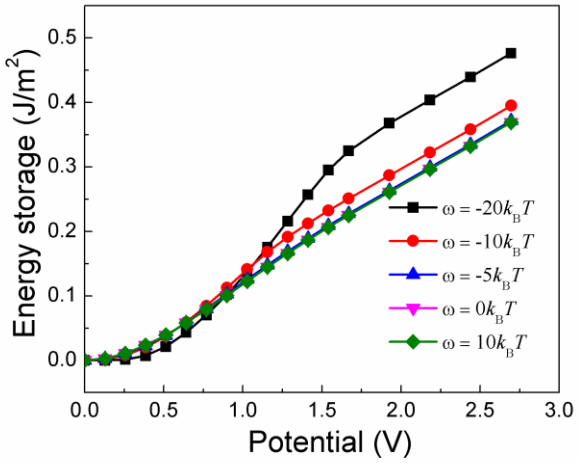

Figure 5.5 Energy per surface area as a function of the applied surface potential with different impurities. While an impurity with strong surface affinity may block a neutral pore thus reduces the energy density at low voltage, they can significantly increase the energy density at high voltage.

The energy density in a nanopore could be obtained by

$$E = \int_0^{\psi_0} C_d V dV \tag{5.4}$$

where C_d is the differential capacitance and ψ_0 corresponds to one-half of the operation potential window (OPW). Figure 5.5 shows the energy density in the nanopore with different types of impurity. At low charging potentials, an impurity repelled from the nanopore yields the energy density higher than that corresponding to an impurity with a strong surface affinity. However, the trend is reversed at high charging potentials. In the former case ($\omega \geq 0$), the impurity molecules hardly enter the nanopore and thus have negligible effects on the energy density. If the impurity has a strong affinity with the pore surface ($\omega < 0$), then the peak position of the differential capacitance shifts to higher potential as indicated in Figure 5.4. In that case, we can obtain a higher differential capacitance at larger charging potentials. According to Eq.(5.4), charging at large capacitance and potential yield a higher energy density.

5.4 Conclusion

The impurity effect on capacitance was examined in our previous work using a similar theoretical model. While the previous work focused on the capacitance as a function of the pore size at a fixed charge potential (+1.5 V), this work investigates the influence of impurity on the charging mechanism and the energy density of electrical double layer (EDL) capacitors in terms of its affinity with the electrode walls. We demonstrate that under conditions favoring impurity accumulation in the nanopores of the electrode impurity can change the EDL charging mechanism even at low bulk densities. As the transfer energy of impurity molecules increases, the capacitance−potential curves can change from the bell shape to the two-hump camel shape, with the peak shifting toward a higher charging potential. The impurity effect on the charging behavior is similar to the solvent effect as studied by Rochester and co-workers.[24]The main difference is that the amount of impurity and solvent in the bulk is very different. As an ionophobic pore could be beneficiary for improving charge storage and charging dynamics, introduction of impurity molecules inside the pore makes it essentially more ionophobic and thus enhances the energy storage. Our theoretical results suggest that special attention should be given to the nature of impurity and operation voltages when the surface properties nanoporous electrodes are modified to enhance the performance of EDLCs. It is worth noting that association between ions and impurity molecules, which might happen for impurity molecules with large polarity, may give rise to different pictures of the charging behavior. For impurity molecules without affinity to ionic species, their accumulation inside the pore will increase the charge storage and capacitance as shown in Figure 5.3, regardless of the polarity. The effects of ion binding with impurity molecules on the charging mechanism and energy density will be investigated in the future work. From a practical prospective, the impurity can be considered as either a contaminant or an additive to ionic liquids. On the basis of this study and our previous work, we suggest new

experimental strategies to introduce additives into ionic liquids with specific surface binding affinity to the porous electrodes (e.g., by surface modifications). While significant efforts have been devoted to formulation of ionic liquid mixtures and selection of solvents,[34]much less is known about how supercapacitor performance may be influenced by potent additives at a low concentration. We hope that this work would inspire future experimental and computational efforts toward these directions.

Bibliography

[1] C. Largeot, C. Portet, J. Chmiola, P. L. Taberna, Y. Gogotsi, and P. Simon, "Relation between the ion size and pore size for an electric double-layer capacitor," *J Am Chem Soc,* vol. 130, no. 9, pp. 2730-1, Mar 5 2008.

[2] D. E. Jiang and J. Wu, "Microscopic Insights into the Electrochemical Behavior of Nonaqueous Electrolytes in Electric Double-Layer Capacitors," *J Phys Chem Lett,* vol. 4, no. 8, pp. 1260-7, Apr 18 2013.

[3] G. Feng, J. S. Zhang, and R. Qiao, "Microstructure and Capacitance of the Electrical Double Layers at the Interface of Ionic Liquids and Planar Electrodes," *The Journal of Physical Chemistry C,* vol. 113, no. 11, pp. 4549-4559, 2009.

[4] P. Wu, J. Huang, V. Meunier, B. G. Sumpter, and R. Qiao, "Complex capacitance scaling in ionic liquids-filled nanopores," *ACS Nano,* vol. 5, no. 11, pp. 9044-51, Nov 22 2011.

[5] S. Kondrat, N. Georgi, M. V. Fedorov, and A. A. Kornyshev, "A superionic state in nano-porous double-layer capacitors: insights from Monte Carlo simulations," *Phys Chem Chem Phys,* vol. 13, no. 23, pp. 11359-66, Jun 21 2011.

[6] S. Kondrat and A. Kornyshev, "Corrigendum: Superionic state in double-layer capacitors with nanoporous electrodes," *Journal of Physics: Condensed Matter,* vol. 25, no. 11, p. 119501, 2013.

[7] C. Merlet *et al.*, "On the molecular origin of supercapacitance in nanoporous carbon electrodes," *Nat Mater,* vol. 11, no. 4, pp. 306-10, Mar 4 2012.

[8] L. Xing, J. Vatamanu, O. Borodin, and D. Bedrov, "On the Atomistic Nature of Capacitance Enhancement Generated by Ionic Liquid Electrolyte Confined in Subnanometer Pores," *J Phys Chem Lett,* vol. 4, no. 1, pp. 132-40, Jan 3 2013.

[9] C. Merlet *et al.*, "Highly confined ions store charge more efficiently in supercapacitors," *Nat Commun,* vol. 4, p. 2701, 2013.

[10] T. A. Centeno, O. Sereda, and F. Stoeckli, "Capacitance in carbon pores of 0.7 to 15 nm: a regular pattern," *Phys Chem Chem Phys,* vol. 13, no. 27, pp. 12403-6, Jul 21 2011.

[11] S. Kondrat, A. Kornyshev, F. Stoeckli, and T. A. Centeno, "The effect of dielectric permittivity on the capacitance of nanoporous electrodes," *Electrochemistry Communications,* vol. 34, pp. 348-350, 2013.

[12] M. Mezger *et al.*, "Molecular layering of fluorinated ionic liquids at a charged sapphire (0001) surface," *Science,* vol. 322, no. 5900, pp. 424-8, Oct 17 2008.

[13] W. Jin, X. Liu, Y. Han, S. Li, and T. Yan, "Effects of repulsive interaction on the electric double layer of an imidazolium-based ionic liquid by molecular dynamics simulation," *Phys Chem Chem Phys,* vol. 17, no. 4, pp. 2628-33, Jan 28 2015.

[14] G. Feng, J. Huang, B. G. Sumpter, V. Meunier, and R. Qiao, "Structure and dynamics of electrical double layers in organic electrolytes," *Phys Chem Chem Phys,* vol. 12, no. 20, pp. 5468-79, 2010.

[15] G. Feng, D. E. Jiang, and P. T. Cummings, "Curvature Effect on the Capacitance of Electric Double Layers at Ionic Liquid/Onion-Like Carbon Interfaces," *J Chem Theory Comput,* vol. 8, no. 3, pp. 1058-63, Mar 13 2012.

[16] J. Vatamanu, M. Vatamanu, and D. Bedrov, "Non-Faradaic Energy Storage by Room Temperature Ionic Liquids in Nanoporous Electrodes," *ACS Nano,* vol. 9, no. 6, pp. 5999-6017, Jun 23 2015.

[17] V. Khomenko, E. Raymundo-Piñero, and F. Béguin, "A new type of high energy asymmetric capacitor with nanoporous carbon electrodes in aqueous electrolyte," *Journal of Power Sources,* vol. 195, no. 13, pp. 4234-4241, 2010.

[18] J. Song *et al.*, "Nitrogen-Doped Mesoporous Carbon Promoted Chemical Adsorption of Sulfur and Fabrication of High-Areal-Capacity Sulfur Cathode with Exceptional Cycling Stability for Lithium-Sulfur Batteries," *Advanced Functional Materials,* vol. 24, no. 9, pp. 1243-1250, 2014.

[19] G. Feng, X. Jiang, R. Qiao, and A. A. Kornyshev, "Water in ionic liquids at electrified interfaces: the anatomy of electrosorption," *ACS Nano,* vol. 8, no. 11, pp. 11685-94, Nov 25 2014.

[20] K. Tamura and Y. Nishihata, "Study on the Behavior of Halide Ions on the Au(111) Electrode Surface in Ionic Liquids Using Surface X-ray Scattering," *The Journal of Physical Chemistry C,* vol. 120, no. 29, pp. 15691-15697, 2016.

[21] V. V. Chaban and O. V. Prezhdo, "Nanoscale carbon greatly enhances mobility of a highly viscous ionic liquid," *ACS Nano,* vol. 8, no. 8, pp. 8190-7, Aug 26 2014.

[22] P. J. F. Harris, "Fullerene-like models for microporous carbon," *Journal of Materials Science,* vol. 48, no. 2, pp. 565-577, 2012.

[23] S. Kondrat and A. A. Kornyshev, "Pressing a spring: what does it take to maximize the energy storage in nanoporous supercapacitors?," *Nanoscale Horizons,* vol. 1, no. 1, pp. 45-52, 2016.

[24] C. C. Rochester, S. Kondrat, G. Pruessner, and A. A. Kornyshev, "Charging Ultrananoporous Electrodes with Size-Asymmetric Ions Assisted by Apolar Solvent," *The Journal of Physical Chemistry C,* vol. 120, no. 29, pp. 16042-16050, 2016.

[25] Y. Lauw, M. D. Horne, T. Rodopoulos, N. A. Webster, B. Minofar, and A. Nelson, "X-ray reflectometry studies on the effect of water on the surface structure of [C4mpyr][NTf2] ionic liquid," *Phys Chem Chem Phys,* vol. 11, no. 48, pp. 11507-14, Dec 28 2009.

[26] R. Hayes, N. Borisenko, B. Corr, G. B. Webber, F. Endres, and R. Atkin, "Effect of dissolved LiCl on the ionic liquid-Au(111) electrical double layer structure," *Chem Commun (Camb)*, vol. 48, no. 82, pp. 10246-8, Oct 21 2012.

[27] A. R. Porter, S. Y. Liem, and P. L. Popelier, "Room temperature ionic liquids containing low water concentrations-a molecular dynamics study," *Phys Chem Chem Phys*, vol. 10, no. 29, pp. 4240-8, Aug 7 2008.

[28] K. Liu and J. Wu, "Boosting the Performance of Ionic-Liquid-Based Supercapacitors with Polar Additives," *The Journal of Physical Chemistry C*, vol. 120, no. 42, pp. 24041-24047, 2016.

[29] D. E. Jiang, Z. Jin, and J. Wu, "Oscillation of capacitance inside nanopores," *Nano Lett*, vol. 11, no. 12, pp. 5373-7, Dec 14 2011.

[30] C. Lian, D.-e. Jiang, H. Liu, and J. Wu, "A Generic Model for Electric Double Layers in Porous Electrodes," *The Journal of Physical Chemistry C*, vol. 120, no. 16, pp. 8704-8710, 2016.

[31] D. E. Jiang and J. Wu, "Unusual effects of solvent polarity on capacitance for organic electrolytes in a nanoporous electrode," *Nanoscale*, vol. 6, no. 10, pp. 5545-50, May 21 2014.

[32] D.-e. Jiang, Z. Jin, D. Henderson, and J. Wu, "Solvent effect on the pore-size dependence of an organic electrolyte supercapacitor," *The journal of physical chemistry letters*, vol. 3, no. 13, pp. 1727-1731, 2012.

[33] J. Wu, T. Jiang, D.-e. Jiang, Z. Jin, and D. Henderson, "A classical density functional theory for interfacial layering of ionic liquids," *Soft Matter*, vol. 7, no. 23, p. 11222, 2011.

[34] C. Lian *et al.*, "Enhancing the Capacitive Performance of Electric Double-Layer Capacitors with Ionic Liquid Mixtures," *ACS Energy Letters*, vol. 1, no. 1, pp. 21-26, 2016.

[35] P. I. Ravikovitch, A. Vishnyakov, R. Russo, and A. V. Neimark, "Unified Approach to Pore Size Characterization of Microporous Carbonaceous Materials from N2, Ar, and CO2Adsorption Isotherms†," *Langmuir*, vol. 16, no. 5, pp. 2311-2320, 2000.

[36] G. Orkoulas and A. Z. Panagiotopoulos, "Phase behavior of the restricted primitive model and square-well fluids from Monte Carlo simulations in the grand canonical ensemble," *The Journal of Chemical Physics*, vol. 110, no. 3, pp. 1581-1590, 1999.

[37] Y. Shim, H. J. Kim, and Y. Jung, "Graphene-based supercapacitors in the parallel-plate electrode configuration: Ionic liquidsversus organic electrolytes," *Faraday Discuss.*, vol. 154, pp. 249-263, 2012.

[38] Y. He *et al.*, "Importance of Ion Packing on the Dynamics of Ionic Liquids during Micropore Charging," *J Phys Chem Lett,* vol. 7, no. 1, pp. 36-42, Jan 7 2016.

[39] C. Lian, H. Liu, D. Henderson, and J. Wu, "Can ionophobic nanopores enhance the energy storage capacity of electric-double-layer capacitors containing nonaqueous electrolytes?," *J Phys Condens Matter,* vol. 28, no. 41, p. 414005, Oct 19 2016.

[40] A. A. Lee, D. Vella, A. Goriely, and S. Kondrat, "Capacitance-Power-Hysteresis Trilemma in Nanoporous Supercapacitors," *Physical Review X,* vol. 6, no. 2, 2016.

[41] A. C. Forse, C. Merlet, J. M. Griffin, and C. P. Grey, "New Perspectives on the Charging Mechanisms of Supercapacitors," *J Am Chem Soc,* vol. 138, no. 18, pp. 5731-44, May 11 2016.

[42] D.-e. Jiang, D. Meng, and J. Wu, "Density functional theory for differential capacitance of planar electric double layers in ionic liquids," *Chemical Physics Letters,* vol. 504, no. 4-6, pp. 153-158, 2011.

[43] N. Jäckel, P. Simon, Y. Gogotsi, and V. Presser, "Increase in Capacitance by Subnanometer Pores in Carbon," *ACS Energy Letters,* vol. 1, no. 6, pp. 1262-1265, 2016.

[44] D. Henderson, S. Lamperski, L. Bari Bhuiyan, and J. Wu, "The tail effect on the shape of an electrical double layer differential capacitance curve," *J Chem Phys,* vol. 138, no. 14, p. 144704, Apr 14 2013.

[45] M. T. Alam, M. Mominul Islam, T. Okajima, and T. Ohsaka, "Measurements of differential capacitance in room temperature ionic liquid at mercury, glassy carbon and gold electrode interfaces," *Electrochemistry Communications,* vol. 9, no. 9, pp. 2370-2374, 2007.

[46] M. V. Fedorov, N. Georgi, and A. A. Kornyshev, "Double layer in ionic liquids: The nature of the camel shape of capacitance," *Electrochemistry Communications,* vol. 12, no. 2, pp. 296-299, 2010.

Chapter 6. Wettability of Ultra-small Pores of Carbon Electrodes by Non-aqueous Electrolytes

Porous carbons have been widely utilized as electrode materials for capacitive energy storage. Whereas the importance of pore size and geometry on the device performance has been well recognized, little guidance is available for identification of carbon materials with ideal porous structures. In this chapter, we study the phase behavior of ionic fluids in slit pores using the classical density functional theory. Within the framework of the restricted primitive model for nonaqueous electrolytes, we demonstrate that the accessibility of micropores depends not only on the ionic diameters (or desolvation) but also on their wetting behavior intrinsically related to the vapor-liquid or liquid-liquid phase separation of the bulk ionic systems. Narrowing the pore size from several tens of nanometers to subnanometers may lead to a drastic reduction in the capacitance due to capillary evaporation. The wettability of micropores deteriorates as the pore size is reduced but can be noticeably improved by raising the surface electrical potential. The theoretical results provide fresh insights into the properties of confined ionic systems beyond electric double layer models commonly employed for rational design/selection of electrolytes and electrode materials.

6.1 Introduction

Capacitive energy storage hinges on electrochemical adsorption/desorption of ionic species at the surface of porous electrodes that are typically made of various forms of activated carbons.[1, 2] The energy storage capacity can be improved by increasing the electric double layer (EDL) capacitance, which is linearly proportional to the surface area, and/or by using nonaqueous electrolytes (viz., organic electrolytes or room-temperature ionic liquids) with wide operating potential windows (OPW). The importance of pore size and shape on capacitive energy storage has been well documented.[3, 4] The customary opinion is that mesoporous carbons, with

the average pore size larger than 2 nm, are ideally suited for the electrode material, while micropores make no significant contributions to energy storage because they are not easily accessible to solvated ions and the ionic motions in such pores may be severely compromised.[5] Recently, a number of experimental and theoretical studies indicate that an anomalous increase in the EDL capacitance can be achieved by matching the pore size with the diameters of ionic species[6] and that ion diffusion in micropores can be an order of magnitude faster than that in the bulk.[7] However, it has been shown by Monte Carlo (MC) simulation that a first-order phase transition may occur in porous electrodes when the pore size is comparable to the ion size.[8-10] Recent molecular dynamics (MD) simulation also indicates that capillary evaporation may take place in 1-ethyl-3-methylimidazolium tetrafluoroborate ([EMIM][BF4]) confined between solvophobic sheets.[11]

Experimental verification of the pore-size effects on EDL capacitance has been elusive because activated carbons typically do not have a well-defined pore structure. The problem is further complicated by the imprecise characterization of porous materials in terms of the surface areas and the pore size distributions. For example, the Brunauer-Emmett-Teller (BET) adsorption isotherms are routinely used to determine the specific surface areas of porous material, but it only works for adsorbents with large pores because it assumes uniform adsorption of gas molecules on a flat surface without lateral interactions. For micropores (pore size < 2 nm), the BET analysis describes only an apparent surface area instead of a true geometrically accessible area. The BET and geometrical surface areas may differ by orders of magnitude.[12] It has been shown that the capacitance per unit area is virtually independent of the average pore size for an organic electrolyte, $(C_2H_5)_4NBF_4$/acetonitrile, in electrodes made of carbon monoliths with narrow pore size distributions.[13] Furthermore, carbon electrodes exhibiting a large area-specific capacitance are not necessarily correlated with those with a high gravimetric capacitance.[14] Nevertheless, a

number of theoretical investigations of ionic liquids in idealized pores unequivocally predict a maximized capacitance when the pore size is comparable to the ion diameters, albeit the oscillatory dependence of the capacitance on the pore size has been subjected to rather different interpretations.[15-18] While various effects may contribute to the oscillatory variation of the capacitance as a function of the pore size, the discrepancy between theory and the experiment may also arise from the accessibility of micropores to ionic species. To our knowledge, none of previous investigations of EDL capacitance account for the accessibility or the phase behavior of ionic liquids in small pores at conditions pertinent to energy storage.

Conventionally the accessibility of ionic fluids to the micropores of a carbon electrode is often loosely defined in terms of the pore geometry; viz., a pore is accessible to solvated or bare ions if its size is larger than the ion diameter. While the geometric constraint for the accessibility of individual ions is rather intuitive, such a definition of pore accessibility can easily be misleading because it assumes molecules as rigid bodies and ignores multi-body correlations or collective effects. Micropores larger than the ionic diameters may not make a significant contribution to energy storage if the ion density inside the pore is exceedingly low. Boukhalfa et al. used in situ small angle neutron scattering (SANS) to study the electroadsorption of organic ions in carbon pores of different sizes. They observed incomplete wetting of the smallest carbon pores by deuterated acetonitrile and enhanced ion sorption in subnanometer pores under the applied potential. This behavior may explain the characteristic butterfly wing shape of the cyclic voltammetry curve of specific capacitance in electrical double layer capacitors.[19] The low-density state may be introduced by either vapor-liquid or liquid-liquid separation of the ionic fluid inside the pore. Unlike the size effects, phase transitions are collective phenomena depending not only on the interactions of ionic species with the pore surface and with themselves but also on the thermodynamic conditions.[20] Although the wettability of micropores has been routinely

discussed in the literature and, clearly, it plays an important role in commercial applications of porous electrodes, substantially less attention has been given to the phase behavior of ionic liquids and organic electrolytes under confinement. Previous studies on the pore-size effects on electrode performance are mostly focused on the EDL capacitances and the ionic distributions without an explicit consideration of possible phase transitions.[3]

Phase transitions in inhomogeneous simple fluids have been reasonably well understood.[21]However, much less is known about how the phase behavior of ionic systems is influenced by confinement, especially under conditions whereby ionic fluids in micropores are subject to an external electrical potential. The long-range Coulomb interactions make the critical behavior and phase transitions in ionic fluids substantially more complicated than those corresponding to neutral systems.[22] In comparison to the bulk systems, theoretical studies of the phase behavior of ionic liquids under confinement are necessarily even more difficult because they must account for the density inhomogeneity and be consistent with the existing results in the bulk limit.

Previous studies on the phase behavior of ionic liquids in the bulk are largely based on the restricted primitive model (RPM), in which ions are described as charged hard spheres of the same size and absolute valence.[23] RPM has been widely used to represent the properties of both aqueous and organic electrolyte solutions, molten salts, as well as room-temperature ionic liquids.[24] Although the model is much oversimplified to quantitatively reproduce the thermodynamic properties of any specific electrolyte, it incorporates key features of ion-ion interactions, namely, the excluded volume effects and the Coulomb potential, which are essential to describe the unique properties of ionic systems. As a result, RPM is routinely used to study the phase behavior of ionic systems including liquid-liquid equilibrium in organic electrolytes [25, 26] and wetting transitions of ionic liquids.[27, 28]

Classical density functional theory (DFT) represents one of the most efficient theoretical tools to study phase transitions in confined fluids.[29, 30]Previously, different versions of DFT had been applied to describe the vapor-liquid coexistence of ionic fluids confined in slit pores.[31, 32] Within the framework of RPM for ionic systems, DFT predicts that confinement leads to a narrowed vapor-liquid coexistence region and reduces both the critical temperature and the critical density as the pore width decreases. It was found that an explicit consideration of association between oppositely charged ions reduces the critical temperature but does not change the qualitative behavior of the vapor-liquid-like phase diagram of confined ionic fluids. Similar predictions were made for the same ionic model in a cylindrical pore using the field theoretical variational approach[33] and in a disordered porous matrix using the method of collective variables.[34, 35] Consistent with MC simulations,[8, 9, 36] these theoretical methods predict that the vapor-liquid coexistence region gets narrower as the pore width or porosity decreases. However, opposite trends were observed on the dependence of capillary evaporation on the electrostatic potential. While MC simulation shows that an ionic liquid in narrow pores can be stabilized by applying a surface electrical potential, classical DFT predicts destabilizing effects, suggesting that the theoretical results are sensitive to the formulation of the free-energy functional.

In this chapter, we study the wettability of nonaqueous electrolytes in the slit pores of carbon electrodes using a new version of classical DFT. RPM is used as a unified model to represent both vapor-liquid and liquid-liquid phase separations in ionic liquids and in organic electrolytes, respectively. Special attention is given to the effects of pore size and surface electrical potential on capillary evaporation and its implications to the properties of ionic fluids in the micropores of activated carbons important for capacitive energy storage. We find that capillary evaporation becomes more likely to occur as the pore width decreases and that the

critical surface electrical potential exhibits a non-monatomic dependence on the pore size. The theoretical results offer fresh insights into the accessibility of ionic fluids to the ultrasmall pores of activated carbons important for the rational design and optimization of porous structure for energy storage.

6.2 The Ionic Liquid Model and Theory

The restricted primitive model (RPM) assumes that cations and anions have the same diameter ($\sigma_+ = \sigma_- = \sigma$) and valence ($Z_+ = -Z_- = 1$). In dimensionless units, the pair potential between two ionic species is given by

$$\beta u_{ij}(r) = \begin{cases} \infty, & r < \sigma_{ij} \\ Z_i Z_j l_B / r, & r \geq \sigma_{ij} \end{cases}, \tag{6.1}$$

where r is the center-center distance between ions i and j, $\sigma_{ij} = \left(\sigma_i + \sigma_j\right)/2$, $\beta = 1/k_B T$, and $l_B = \beta e^2/\left(4\pi\varepsilon_0\varepsilon_r\right)$ is the Bjerrum length. As usual, k_B is the Boltzmann constant, T is the absolute temperature, e is the unit charge, ε_0 is the vacuum permittivity, and ε_r is the relative permittivity of the dielectric background.

In a slit-like pore of width H, each ion experiences an external energy along the normal direction of the planar walls positioned at $z = 0$ and $z = H$,

$$V_i(z) = V_i^{HW}(z) + V_i^{C}(z), \tag{6.2}$$

where $V_i^{HW}(z)$ represents the hard-wall potential

$$V_i^{HW}(z) = \begin{cases} \infty, & z < \sigma_i/2 \text{ or } z > H - \sigma_i/2 \\ 0, & \text{otherwise} \end{cases}, \tag{6.3}$$

and $V_i^{C}(z)$ is the electrical potential due to the surface charge of the planar walls

$$\beta V_i^{C}(z) = -2\pi l_B Z_i HQ/\mathrm{e}, \tag{6.4}$$

where Q is the surface charge density for *each* wall.

Figure 6.1 shows schematically that an ionic fluid in the bulk may exist either as a liquid or as a vapor (in the context of organic electrolytes, two liquid states of different ion densities) in a slit pore. For an ionic fluid with only one type of cations and one type of anions, the phase behavior in the bulk is described in terms of reduced temperature $T^* = 4\pi\varepsilon_0\varepsilon_r\sigma/\left(\beta e^2\right) = \sigma/l_B$ and reduced overall density $\rho^* = \left(\rho_+ + \rho_-\right)\sigma^3$, where ρ_+ and ρ_- are the number densities of cations and anions. For the ionic fluid in a slit pore, the phase behavior depends on thermodynamic conditions in the bulk as well as on the pore width and the surface charge or the surface electrical potential (i.e., voltage). Throughout this work, the pore width and the distance from a slit surface are denoted as $H^* = H/\sigma$ and $z^* = z/\sigma$, respectively. The dimensionless electric potential is defined as $\psi^* = \beta\psi e$, and the dimensionless charge density at the wall is $Q^* = Q\sigma^2/e$.

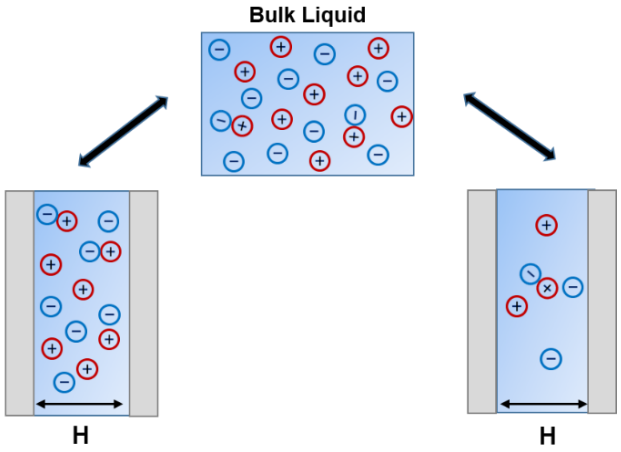

Figure 6.1 Schematic picture of the model ionic liquid in a slit pore. The bulk liquid is in equilibrium with either a liquid-like or a vapor-like phase under confinement.

RPM has been extensively used to represent, among other electrolyte systems, the phase behavior of both room temperature ionic liquids and organic electrolytes. In the former case, the

relative permittivity accounts for polarizability effects and other ionic interactions not included in the charged hard-sphere model. In applications of RPM to organic electrolytes, we assume that the solvent is a dielectric continuum with relative permittivity ε_r . At room temperature, the dielectric constants of bulk ionic liquids are approximately in the range of 5–15,[37] and ε_r =5.5 is chosen in this work to represent a residual relative permittivity for pair interactions between ions. The same dielectric constant is assumed for organic electrolytes or ionic liquids in organic solvents. It should be noted that, for a given ionic system, the relative permittivity is in general not the same as that corresponding to the bulk value; the former accounts for interactions beyond the Coulomb potential between a pair of isolated ions in the medium, while the latter is related to the potential of mean force between ions in a bulk ionic system.

To make RPM relevant to EDL capacitors for energy storage, we take dimensionless temperature $T^* = 0.05$ for most of our discussions on the pore size and the surface voltage effects on wettability. Approximately, the condition corresponds to an ionic liquid or an organic electrolyte of ion diameter $\sigma = 0.5\,\text{nm}$ at temperature $T \approx 300\,\text{K}$(e.g., ionic liquid 1-ethyl-3-methylimidazolium bis(trifluoromethylsulfonyl)imide (EMIM-TFSI) or ionic solutions of C_{18}mim-NTF_2 in decalin). The dimensionless temperature is lower than that corresponding to the critical temperature for the vapor-liquid equilibrium of the bulk ionic system presented by the equation of state used in this work $T_C^* \approx 0.072$.

The basic ideas of classical DFT have been described in detail in Chapter 2. Specifically, in this work, we incorporate the modified fundamental measure theory(MFMT) to account for the ionic excluded volume effects,[38, 39] the reference fluid density (RFD) perturbation for electrostatic correlations, [40]and an extension of MFMT for the association free energy.

[41]Here, we only discuss the explicit expressions for the excess free energy due to ion associations $F_{as}^{ex}\left[\rho_i(z)\right]$.

The Helmholtz energy due to association between oppositely charged ions is formulated at the level of the first-order thermodynamic perturbation (TPT1) theory,[41]

$$\beta F_{as}^{ex}\left[\rho_i(\mathbf{r})\right]=\int d\mathbf{r}\Phi^{as}\left[n_\alpha(\mathbf{r})\right], \tag{6.5}$$

where $\Phi^{as}\left[n_\alpha(\mathbf{r})\right]$ is given by

$$\Phi^{as}\left[n_\alpha(\mathbf{r})\right]=\sum_i n_{0,i}\zeta_i\left[\ln\alpha^{(i)}(\mathbf{r})-\frac{\alpha^{(i)}(\mathbf{r})}{2}+\frac{1}{2}\right]. \tag{6.6}$$

Similar to that for association in uniform systems, $\alpha^{(i)}(\mathbf{r})$ is the degree of dissociation of species *i* at position **r**, and it is obtained from

$$\alpha^{(i)}(\mathbf{r})=\frac{1}{1+n_{0,j}\zeta_j\alpha^{(j)}(\mathbf{r})\Delta^{ij}(\mathbf{r})}, \tag{6.7}$$

where Δ^{ij} is the association constant between cations and anions, $\Delta^{ij}(\mathbf{r})=K^0K^\gamma$. There is a certain kind of arbitrariness in defining the ion pair and hence the association constant K^0. Among several definitions of the ion-association constant, the one introduced by Ebling yields the correct second ionic-virial coefficient.[42] However, this approach does not produce good values for the critical temperature and the critical density of the RPM. As discussed in Ref. 47, we choose K^0 in the form proposed by Olaussen and Stell,[43]

$$K^0\approx 96\pi\sigma^3\sum_{m=2}^{\infty}\frac{\left(T^*\right)^{-2m}}{(2m)!(2m-3)}. \tag{6.8}$$

K^γ is calculated from the simple interpolation scheme

$$K^\gamma=y_{+-}(\sigma), \tag{6.9}$$

where $y_{+-}(\sigma)$ is the contact anion-cation cavity correlation function evaluated at α = 1, the reference ionic fluid without association. The expression for $y_{+-}(\sigma)$ is also discussed in details in Chapter 2.

The functional derivative of excess Helmholtz free energy due to the ion association yields the excess chemical potential $\mu_{as}^{ex}(\mathbf{r})$ given by

$$\beta\mu_{as,i}^{ex}(\mathbf{r}) = \frac{\delta\beta F_{as}^{ex}}{\delta\rho_i(\mathbf{r})} = \sum_{\alpha} d\mathbf{r}' \frac{\partial\Phi_{as}^{ex}}{\partial n_\alpha(\mathbf{r}')}\omega^{(\alpha)}(\mathbf{r}-\mathbf{r}'). \tag{6.10}$$

6.3 Results and Discussions

6.3.1 Phase Diagram of Confined Ionic Fluids

We consider first the phase diagram for the model ionic system in slit pores with uncharged walls. Because of the symmetry for cations and anions, the local electric potential, as well as the local charge density, is everywhere zero, i.e., $\psi^* = 0$ and $Q^* = 0$. In construction of the phase diagram, we calculate the vapor-like and the liquid-like density profiles at different chemical potentials of the ionic species at each temperature. Subsequently, we obtain two curves for the dependence of the grand potential versus the chemical potential, and the crossing point corresponds to the condition of phase coexistence inside the pore.

Figure 6.2(a) illustrates the dependence of the reduced grand potential, $\beta\Omega$, on the reduced chemical potential of the ionic species, $\beta\mu$, in a $H^* = 5.0$ pore at two representative temperatures, $T^* = 0.050$ and 0.0525. At each temperature, the two curves provide the thermodynamic relations for the dilute and the concentrated-branches of the confined ionic system, and their intersection corresponds to the condition of phase equilibrium, i.e., two ionic density profiles for the coexisting vapor-like and liquid-like phases (or dilute and concentrated electrolytes) inside the pore. By applying the same procedure to different temperatures, we can

construct a phase diagram in terms of the reduced temperature and the average reduced ion density similar to that for the bulk system.

Figure 6.2(b) shows the vapor-liquid-like coexistence curves for the model ionic system in slit pores of different pore widths. The solid line corresponds to the coexistence curve in the bulk. Consistent with earlier theoretical investigations,[32, 44] confinement narrows the phase coexistence envelope. While the dilute branch is weakly dependent on the slit pore width, the concentrated branch considerably shifts leftwards as the pore width decreases. Two effects might be responsible for the shift of the binodal curve. First, inhomogeneous screening of electrostatic interactions results in a correlation effect responsible for ion depletion near the surface:[45]an ion interacts more favorably with its full ionic atmosphere far away from the surface than that in the vicinity of the surface. Second, the leftward shift may also be attributed to the inclusion of association between oppositely charged ions. Pizo and Sokołowski[32] compared the phase diagram of the ionic system with and without ion associations. They found that formation of pairs between oppositely charged ions alters the effective interactions between all particles. The ion pairing results in a weaker effective attraction between structural entities and thus lowers the critical temperature of the phase transition. In Figure 6.2(b), we did not include the critical points for the confined ionic systems due to numerical issues. Nevertheless, it is clear that confinement reduces the critical temperature and the critical density as predicted before.[31] As the pore width decreases, the entire coexistence curve is shifted toward lower temperatures and lower densities in comparison to the bulk phase diagram.

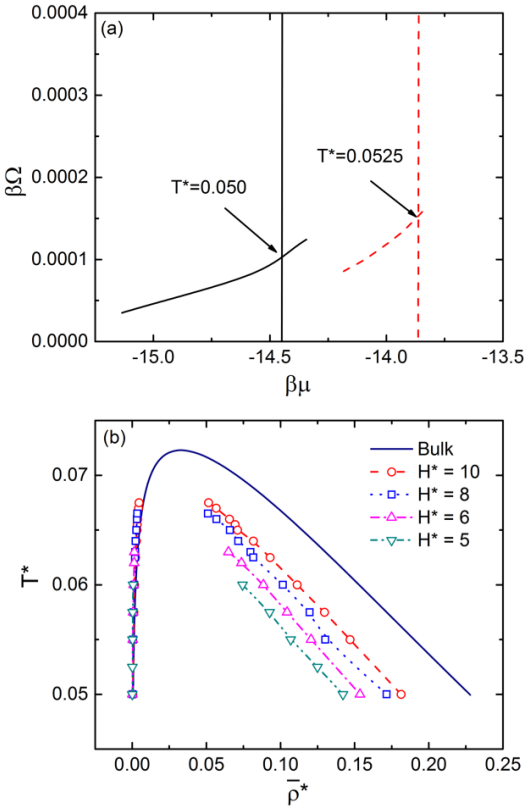

Figure 6.2 (a) The reduced grand potential versus the reduced chemical potential of ionic species in a $H^* = 5.0$ slit pore; (b) Phase diagram for the ionic fluid in the bulk (solid line) and in different neutral slit pores.

As shown in Figure 6.3, the depletion effect near a neutral wall is evident from the ionic density profiles. For the model ionic system in a neutral slit pore, the density profiles of the cations and anions are identical due to the system symmetry. In a dilute phase, the average ion density is small such that the correlation effect is relatively insignificant. As the ionic density increases, electrostatic correlation becomes more important and ion depletion from the surface is more magnified. Similar to the bulk phase diagram, the average coexisting density of the liquid-like phase falls as temperature increases, while the trend is opposite for the vapor-like phase.

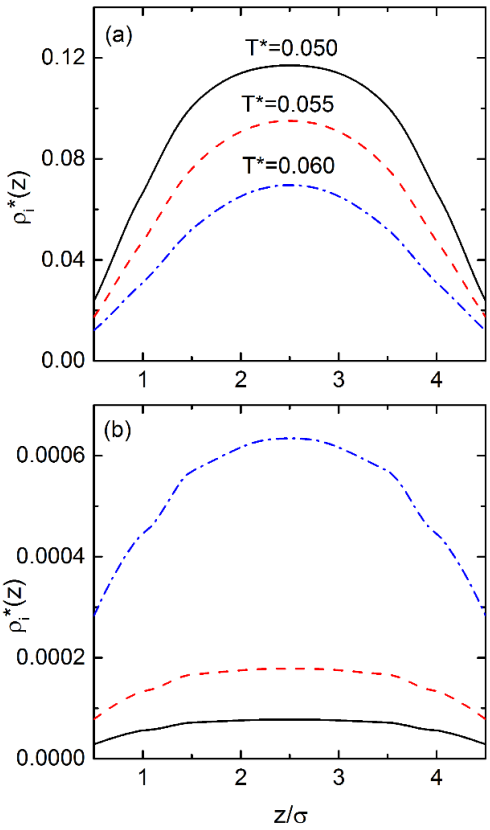

Figure 6.3 The density profiles of the liquid-like (a) and vapor-like (b) phases at coexistence for the model ionic system in a neutral slit pore of width $H^* = 5.0$ at $T^* =$ 0.050 (solid line), 0.055 (dashed line), and 0.060 (dotted-dashed line). Because of the symmetry, the density profiles for the cations and anions are identical.

6.3.2 Capillary Evaporation

At a given temperature, an ionic fluid in a slit pore may exist either as a liquid-like or as a vapor-like phase depending on the pore size, surface electrical potential, as well as temperature and the chemical potential of the ionic species in the bulk. In this work, capillary evaporation is referred to as the phase transition of the confined fluid from a liquid-like to a vapor like phase in response to changes in the external potential or thermodynamic conditions.

Figure 6.4 shows the chemical potential of ionic species in a neutral slit pore and that in the bulk at the condition of vapor liquid-like coexistence. The two curves allow us to predict the

wettability of the slit pore in contact with a bulk ionic system at the same temperature and chemical potential. Wetting transition occurs when the chemical potential of the confined fluid is lower than that in the bulk. As a result, Figure 6.4 predicts that a neutral pore promotes capillary evaporation, i.e., the ionic fluid may exist as a stable liquid in the bulk but a vapor-like phase inside the pore.

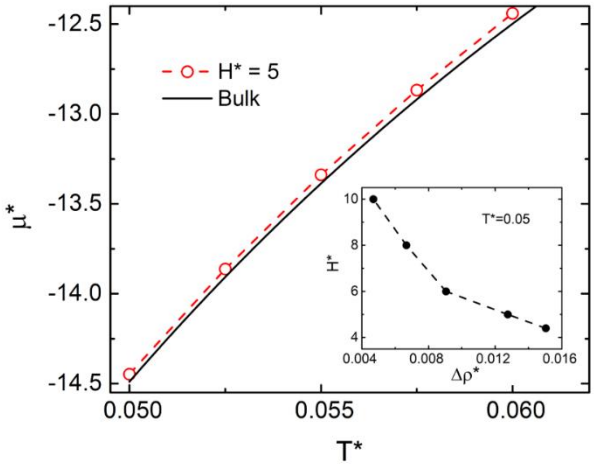

Figure 6.4 The $\mu^* - T^*$ phase diagram for the model ionic system in the bulk and in a $5.0\,\sigma$ slit pore. The inset shows the degree of supersaturation versus the pore width at $T^* = 0.05$. In all cases, the pore surface is uncharged.

The inset of Figure 6.4 shows the dependence of the pore width on the "degree of supersaturation" defined as $\Delta\rho^* = \rho^*_{b,co}(H^*) - \rho^*_b$, where ρ^*_b is the density of the bulk liquid at saturation and $\rho^*_{b,co}(H^*)$ is the density of a bulk liquid that has a chemical potential the same as that of the saturated liquid inside a pore of width H^*. The $\rho^*_{b,co}(H^*)$ can be obtained from the phase diagram shown in Figure 6.2. Figure 6.4 suggests that, to make the liquid state stable inside the pore or to make the pore wet, the corresponding ionic system in the bulk should be "supersaturated," i.e., the ionic density should be larger than that of a saturated liquid at the same temperature. Otherwise, capillary evaporation (or dewetting) takes place inside the pore. For example, for a given ionic liquid with $\Delta\rho^* \approx 0.009$, the coexistence of the liquid-like and vapor-

like phases occurs near $H_C^* \approx 6.0$. In a larger pore, such as $H^* = 10.0$, only the liquid like state is stable; below H_C^* the liquid-like state becomes metastable in comparison with the vapor-like phase, and the phase transition becomes unavoidable.

Capillary evaporation of ionic liquids in porous carbons has been observed in both experimental and simulation studies. For example, Gogotsi *et al.[46]* showed that 1-ethyl-3-methylimidazolium bis(trifluoromethylsulfonyl) imide ([EMIM][TFSI]) cannot wet micropores smaller than 0.75 nm at zero applied potential. Shrivastav and co-workers found from MD simulations a critical pore width, $d_C \approx 1.2\,\text{nm}$, for [EMIM][$BF_4$] in contact with neutral pores.[11] While a quantitative comparison of the theoretical predictions with the experimental or simulation results has not been attempted in this study, it is clear that small pores may not be accessible to an ionic fluid due to dewetting or capillary evaporation.

6.3.3 Electrowetting and Differential Capacitance

Now we proceed to investigate the wettability of the model ionic system in charged pores. Figure 6.5(a) shows the surface charge density as a function of the applied voltage for a slit pore of width $H = 3.5\sigma$ in contact with a bulk ionic fluid at three representative densities. Because of the symmetry of the ionic system, the dependence of the surface charge density on the surface voltage is equally applicable to conditions when both quantities are negative. As the surface voltage of the slit pore increases, the surface charge increases smoothly from zero at high ionic densities (i.e., ρ_b^* = 0.4 and 0.6). In this case, the slit pore is always filled with a liquid-like ionic fluid because the density is remote from that near the vapor-liquid-like coexistence. At a lower density (ρ_b^* = 0.228), however, the surface charge density is virtually zero for a slit pore with a small surface potential; it increases discontinuously to a finite value when the surface potential is above around $\psi^* \approx 4.1$, signaling a first-order phase transition inside the pore.

Qualitatively, the discontinuous variation of the surface charge density in the $\psi^* - Q^*$ phase diagram is consistent with that predicted by Kiyohara and co-workers using Monte Carlo simulation.[8] The phase transition can be understood as a manifestation of the balance between the electrostatic correlations and the volume exclusion interactions. While the electrostatic correlations lead to depletion of the ionic fluid from a neutral surface, application of a surface potential results in electrowetting because of the accumulation of counterions.

A key quantity of practical interest for energy storage is the differential capacitance, which is defined as

$$C_d^* = \partial Q^* / \partial \psi^* . \tag{6.11}$$

Without an explicit consideration of phase transitions, the differential capacitance is always a smooth function of the surface voltage as predicted by typical EDL models.

Figure 6.5(b) shows how the differential capacitance varies with the applied surface voltage for the ionic systems described above. At high ionic density (e.g., ρ_b^* = 0.4), the $\psi^* - C_d^*$ curve exhibits a camel-shape, showing a minimum at zero surface voltage and a maximum at a higher surface voltage. Increasing the density from ρ_b^* = 0.4 to 0.6, the $\psi^* - C_d^*$ curve still shows a camel-shape, while the differential capacitance at zero voltage increases. As discussed in previous studies,[47-49] a further increase in the bulk density induces the change of the $\psi^* - C_d^*$ curve from the camel-shape to a bell-shape. For the model ionic liquid at a lower density, ρ_b^* = 0.228, the $\psi^* - C_d^*$ curve shows a discontinuity around $\psi^* \approx 4.1$, at which condition the first-order phase transition is observed.

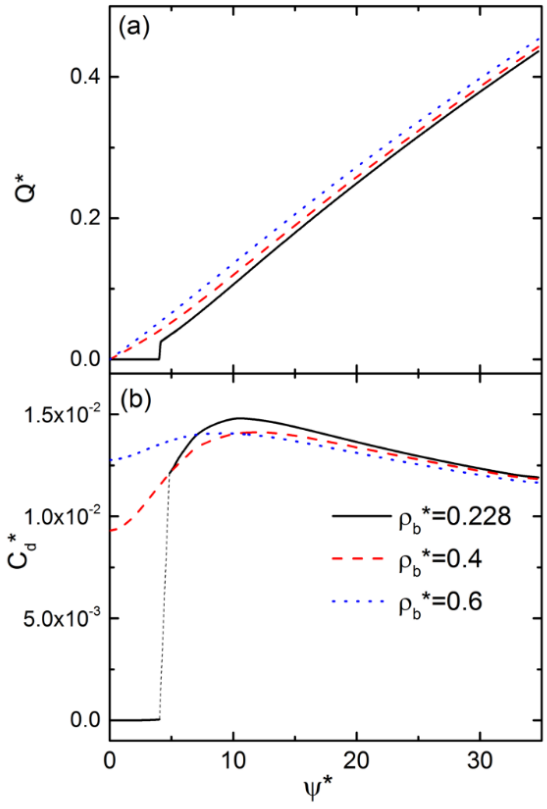

Figure 6.5 The dependence of surface charge density Q^* (a) and the differential capacitance C_d^* (b) on the applied voltage. The calculations are for different bulk densities given in (b). In all cases, the pore width is H^* = 3.5, and the reduced temperature is T^* = 0.05. The reduced voltage and charge density are $\psi^* = \beta\psi e$ and $Q^* = Q\sigma^2 / e$, respectively.

Figure 6.6 presents the density profiles of ions inside the pore at surface potentials slightly below and above that corresponding to the jump in the surface charge density. At $\psi^* = 4.2$, the ionic fluid is in a liquid-like state inside the pore. Although counterions are accumulated near the surface, the local density inside the pore is uniformly lower than that in the bulk due to the depletion of the coions. At the pore center, the coion concentration is slightly larger than the counterion concentration, which can be attributed to the local charge inversion, i.e., the local electrical potential has a sign opposite to that of the surface charge. At a slightly lower surface potential, $\psi^* = 4.0$, the pore is filled with an ionic fluid at a much lower density. In

this case, the density profiles show depletion of both coions and counterions because of long-range electrostatic correlations. As expected, C_d^* is virtually negligible if the micropore is filled with a low density ionic fluid. A drastic increase in the capacitance occurs when the slit pore is wetted by the ionic fluid, i.e., when the ionic fluid inside the pore exists in a liquid-like state (see Figure 6.5(b)).

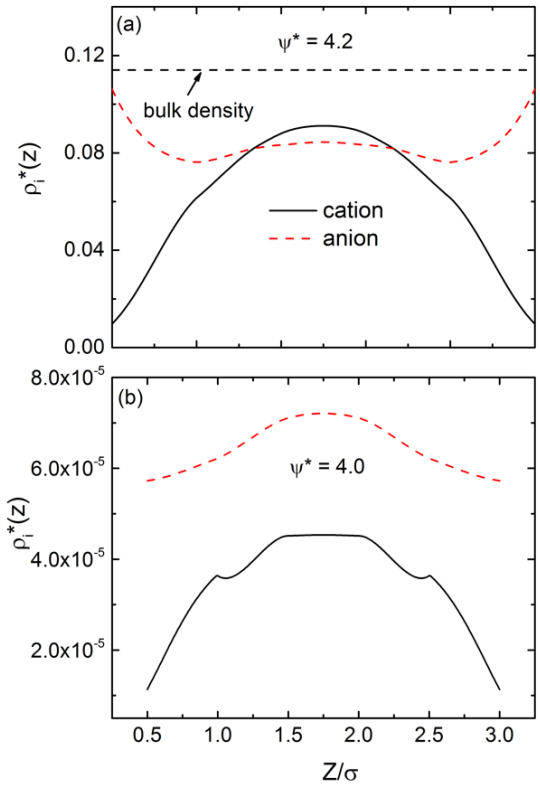

Figure 6.6 Density profiles of cations and anions in a slit pore of H =3.5σ at T^* = 0.05 and reduced surface potential (a) ψ^* = 4.2 and (b) ψ^* = 4.0. The reduced density for the bulk ionic liquid is ρ_b^* = 0.228.

Figure 6.7(a) shows the surface charge density as a function of the voltage for different pore sizes, H^* = 1.6, 2.0, 2.4, 3.2, and 4.8. In small pores (e.g., H^* < 4.8), the surface charge density is virtually zero until the voltage is larger than a certain value, $\psi^* \approx 4.0$. Beyond that voltage, the surface charge density jumps to a finite value and rises continuously as the voltage is

further increased. In a large pore (viz., H^* = 4.8), the surface charge density increases smoothly with the surface potential over the entire range of the voltage. Qualitatively, the response of the surface charge density to the surface potential is similar to the MC results reported by Kiyohara[8] but contradicts to that from earlier classical DFT predictions.[31] Although MSA was used in both versions of classical DFT, the results are qualitatively different because we formulated the free-energy functional in terms of the non-local reference fluid theory and the thermodynamic perturbation theory rather than the weighted density approximations. Apparently, the subtle difference leads to opposite predictions of the phase behavior of the confined ionic fluids.

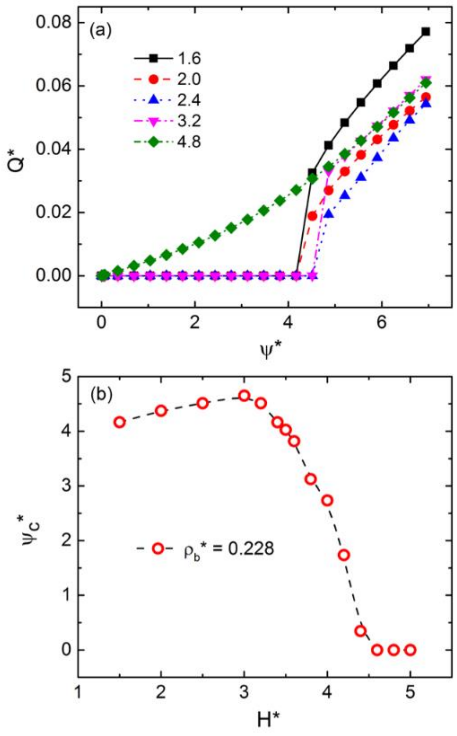

Figure 6.7 (a) The surface charge density as a function of the voltage in slit pores of different reduced pore width $H^* = H/\sigma$. (b) The critical surface potential as a function of the reduced pore width. Here the density for the bulk ionic liquid is $\rho_b^* = 0.228$.

The surface voltage at which the discontinuity of differential capacitance occurs can be regarded as the "critical" voltage, ψ_C^*. Beyond this voltage, the slit pore is filled with an ionic fluid in the liquid-like state. Figure 6.7(b) shows the dependence of the critical voltage as a function of the pore size when the ion density is approaching that for the saturated liquid in the bulk. ψ_C^* disappears for $H^* > 4.5$, suggesting that the first-order phase transition occurs only in small pores. Interestingly, the critical voltage first increases slightly with the pore size and falls abruptly beyond a certain pore width. The non-monotonic behavior reflects not only a competition of electrostatic correlations and excluded-volume interactions but also the confinement effects on the vapor-liquid-like transitions.

6.4 Conclusions

To conclude, we have investigated the phase behavior of ionic fluids in the micropores of carbon electrodes using the restricted primitive model (RPM). By constructing a new version of the classical density functional theory (DFT) that accounts for electrostatic correlations and associating between oppositely charged ions, we demonstrate that capillary evaporation may take place in the micropores of carbon when the pore size is comparable to the ion diameter of nonaqueous electrolytes and that application of a surface electrical potential promotes wetting transition. In the latter case, the theoretical results contradict earlier DFT predictions but are consistent with recent Monte Carlo simulation, suggesting that the DFT performance is sensitive to the formulation of the free-energy functional, in particular, for phase-equilibrium calculations.

In stark contrast to conventional understandings of the accessibility of micropores to ionic fluids, capillary evaporation is determined by the pore geometry as well as ion-ion and ion-surface interactions underlying the phase behavior of the entire ionic system. Because capillary evaporation may result in a drastic reduction in the capacitance, the pore size effects on the performance of carbon electrodes depend on the temperature, the ionic density, as well as the

surface electrical potential. According to our theoretical calculations, wetting transition is most likely due to the liquid-liquid phase separation of an organic electrolyte in small pores. Vapor-liquid-like coexistence is less likely for room temperature ionic liquids because the liquid density is typically remote from that corresponding to the coexistence point. The sharp difference may help explain discrepancies observed in experiments on the pore effects on the performance of various carbon electrodes for capacitive energy storage.

RPM is clearly oversimplified to quantitatively represent the properties of real ionic liquids or organic electrolytes. Nevertheless, it is our hope that this work would usher in a new direction of theoretical investigation of electrolytes in a porous electrode beyond electric double layer models that have been of central interest in electrochemistry for centuries. To highlight the essential features of the capillary evaporation induced by ion-ion correlation and confinement, we have implicitly assumed in this work that the dielectric constant of the electrode is the same as that of the electrolyte solution. In experiment, the dielectric constant of the electrode and that of the solution are generally different and this dielectric discontinuity may also play a significant role in determining the surface structure, as suggested by recent theoretical and simulation work.[18, 45, 50, 51]A systematic study on all of these effects, however, is still lacking and can be pursued in future work.

Bibliography

[1] C. Liu, X. Yan, F. Hu, G. Gao, G. Wu, and X. Yang, "Toward Superior Capacitive Energy Storage: Recent Advances in Pore Engineering for Dense Electrodes," *Adv Mater*, vol. 30, no. 17, p. e1705713, Apr 2018.

[2] C. Zhan *et al.*, "Computational Insights into Materials and Interfaces for Capacitive Energy Storage," *Adv Sci (Weinh)*, vol. 4, no. 7, p. 1700059, Jul 2017.

[3] M. V. Fedorov and A. A. Kornyshev, "Ionic liquids at electrified interfaces," *Chem Rev*, vol. 114, no. 5, pp. 2978-3036, Mar 12 2014.

[4] D. E. Jiang and J. Wu, "Microscopic Insights into the Electrochemical Behavior of Nonaqueous Electrolytes in Electric Double-Layer Capacitors," *J Phys Chem Lett*, vol. 4, no. 8, pp. 1260-7, Apr 18 2013.

[5] A. B. Fuertes, G. Lota, T. A. Centeno, and E. Frackowiak, "Templated mesoporous carbons for supercapacitor application," *Electrochimica Acta*, vol. 50, no. 14, pp. 2799-2805, 2005.

[6] N. Jäckel, P. Simon, Y. Gogotsi, and V. Presser, "Increase in Capacitance by Subnanometer Pores in Carbon," *ACS Energy Letters*, vol. 1, no. 6, pp. 1262-1265, 2016.

[7] S. Kondrat, P. Wu, R. Qiao, and A. A. Kornyshev, "Accelerating charging dynamics in subnanometre pores," *Nat Mater*, vol. 13, no. 4, pp. 387-93, Apr 2014.

[8] K. Kiyohara, T. Sugino, and K. Asaka, "Phase transition in porous electrodes," *J Chem Phys*, vol. 134, no. 15, p. 154710, Apr 21 2011.

[9] K. Kiyohara, H. Shioyama, T. Sugino, and K. Asaka, "Phase transition in porous electrodes. II. Effect of asymmetry in the ion size," *J Chem Phys*, vol. 136, no. 9, p. 094701, Mar 7 2012.

[10] F. J. Montes Ruiz-Cabello, P. Maroni, and M. Borkovec, "Direct measurements of forces between different charged colloidal particles and their prediction by the theory of Derjaguin, Landau, Verwey, and Overbeek (DLVO)," *J Chem Phys*, vol. 138, no. 23, p. 234705, Jun 21 2013.

[11] G. Shrivastav, R. C. Remsing, and H. K. Kashyap, "Capillary evaporation of the ionic liquid [EMIM][BF4] in nanoscale solvophobic confinement," *The Journal of Chemical Physics*, vol. 148, no. 19, p. 193810, 2018.

[12] Y. Tian and J. Wu, "A comprehensive analysis of the BET area for nanoporous materials," *AIChE Journal*, vol. 64, no. 1, pp. 286-293, 2018.

[13] A. Garcia-Gomez, G. Moreno-Fernandez, B. Lobato, and T. A. Centeno, "Constant capacitance in nanopores of carbon monoliths," *Phys Chem Chem Phys*, vol. 17, no. 24, pp. 15687-90, Jun 28 2015.

[14] K. Urita, C. Urita, K. Fujita, K. Horio, M. Yoshida, and I. Moriguchi, "The ideal porous structure of EDLC carbon electrodes with extremely high capacitance," *Nanoscale,* vol. 9, no. 40, pp. 15643-15649, Oct 19 2017.

[15] D. E. Jiang, Z. Jin, and J. Wu, "Oscillation of capacitance inside nanopores," *Nano Lett,* vol. 11, no. 12, pp. 5373-7, Dec 14 2011.

[16] P. Wu, J. Huang, V. Meunier, B. G. Sumpter, and R. Qiao, "Complex capacitance scaling in ionic liquids-filled nanopores," *ACS Nano,* vol. 5, no. 11, pp. 9044-51, Nov 22 2011.

[17] G. Feng and P. T. Cummings, "Supercapacitor Capacitance Exhibits Oscillatory Behavior as a Function of Nanopore Size," *The Journal of Physical Chemistry Letters,* vol. 2, no. 22, pp. 2859-2864, 2011.

[18] S. Kondrat and A. Kornyshev, "Corrigendum: Superionic state in double-layer capacitors with nanoporous electrodes," *Journal of Physics: Condensed Matter,* vol. 25, no. 11, p. 119501, 2013.

[19] S. Boukhalfa *et al.*, "In situ small angle neutron scattering revealing ion sorption in microporous carbon electrical double layer capacitors," *ACS Nano,* vol. 8, no. 3, pp. 2495-503, Mar 25 2014.

[20] D. Bonn and D. Ross, "Wetting transitions," *Reports on Progress in Physics,* vol. 64, no. 9, pp. 1085-1163, 2001.

[21] L. D. Gelb, K. E. Gubbins, R. Radhakrishnan, and M. Sliwinska-Bartkowiak, "Phase separation in confined systems," *Reports on Progress in Physics,* vol. 62, no. 12, pp. 1573-1659, 1999.

[22] G. Stell, "Criticality and phase transitions in ionic fluids," *Journal of Statistical Physics,* journal article vol. 78, no. 1, pp. 197-238, January 01 1995.

[23] Y. Levin, "Electrostatic correlations: from plasma to biology," *Reports on Progress in Physics,* vol. 65, no. 11, pp. 1577-1632, 2002.

[24] H. Lu, B. Li, S. Nordholm, C. E. Woodward, and J. Forsman, "Ion pairing and phase behaviour of an asymmetric restricted primitive model of ionic liquids," *J Chem Phys,* vol. 145, no. 23, p. 234510, Dec 21 2016.

[25] M. Wagner, O. Stanga, and W. Schröer, "The liquid–liquid coexistence of binary mixtures of the room temperature ionic liquid 1-methyl-3-hexylimidazolium tetrafluoroborate with alcohols," *Phys. Chem. Chem. Phys.*, vol. 6, no. 18, pp. 4421-4431, 2004.

[26] W. Schroer and V. R. Vale, "Liquid-liquid phase separation in solutions of ionic liquids: phase diagrams, corresponding state analysis and comparison with simulations of the primitive model," *J Phys Condens Matter,* vol. 21, no. 42, p. 424119, Oct 21 2009.

[27] R. Szparaga, C. E. Woodward, and J. Forsman, "Capillary Condensation of Ionic Liquid Solutions in Porous Electrodes," *The Journal of Physical Chemistry C,* vol. 117, no. 4, pp. 1728-1734, 2013.

[28] M. Mussotter and M. Bier, "Wedge wetting by electrolyte solutions," *Phys Rev E,* vol. 96, no. 3-1, p. 032605, Sep 2017.

[29] R. Evans, "The nature of the liquid-vapour interface and other topics in the statistical mechanics of non-uniform, classical fluids," *Advances in Physics,* vol. 28, no. 2, pp. 143-200, 1979.

[30] J. Wu and Z. Li, "Density-functional theory for complex fluids," *Annu Rev Phys Chem,* vol. 58, pp. 85-112, 2007.

[31] O. Pizio, A. Patrykiejew, and S. Sokolowski, "Phase behavior of ionic fluids in slitlike pores: a density functional approach for the restricted primitive model," *J Chem Phys,* vol. 121, no. 23, pp. 11957-64, Dec 15 2004.

[32] O. Pizio and S. Sokolowski, "Phase behavior of the restricted primitive model of ionic fluids with association in slitlike pores. Density-functional approach," *J Chem Phys,* vol. 122, no. 14, p. 144707, Apr 8 2005.

[33] B. Loubet, M. Manghi, and J. Palmeri, "A variational approach to the liquid-vapor phase transition for hardcore ions in the bulk and in nanopores," *J Chem Phys,* vol. 145, no. 4, p. 044107, Jul 28 2016.

[34] M. Holovko, O. Patsahan, and T. Patsahan, "Vapour-liquid phase diagram for an ionic fluid in a random porous medium," *Journal of Physics: Condensed Matter,* vol. 28, no. 41, p. 414003, 2016.

[35] M. F. Holovko, T. M. Patsahan, and O. V. Patsahan, "Application of the ionic association concept to the study of the phase behaviour of size-asymmetric ionic fluids in disordered porous media," *Journal of Molecular Liquids,* vol. 235, pp. 53-59, 2017.

[36] K. Kiyohara *et al.*, "Phase transition in porous electrodes. III. For the case of a two component electrolyte," *J Chem Phys,* vol. 138, no. 23, p. 234704, Jun 21 2013.

[37] T. Singh and A. Kumar, "Static dielectric constant of room temperature ionic liquids: internal pressure and cohesive energy density approach," *J Phys Chem B,* vol. 112, no. 41, pp. 12968-72, Oct 16 2008.

[38] Y.-X. Yu and J. Wu, "A fundamental-measure theory for inhomogeneous associating fluids," *The Journal of Chemical Physics,* vol. 116, no. 16, pp. 7094-7103, 2002.

[39] R. Roth, R. Evans, A. Lang, and G. Kahl, "Fundamental measure theory for hard-sphere mixtures revisited: the White Bear version," *Journal of Physics: Condensed Matter,* vol. 14, no. 46, pp. 12063-12078, 2002.

[40] D. Gillespie, W. Nonner, and R. S. Eisenberg, "Coupling Poisson Nernst Planck and density functional theory to calculate ion flux," *Journal of Physics: Condensed Matter,* vol. 14, no. 46, pp. 12129-12145, 2002.

[41] Y.-X. Yu and J. Wu, "Structures of hard-sphere fluids from a modified fundamental-measure theory," *The Journal of Chemical Physics,* vol. 117, no. 22, pp. 10156-10164, 2002.

[42] W. Ebeling and M. Grigo, "Mean spherical approximation-mass action law theory of equilibrium and conductance in ionic solutions," *Journal of Solution Chemistry,* vol. 11, no. 3, pp. 151-167, 1982.

[43] K. Olaussen and G. Stell, "New microscopic approach to the statistical mechanics of chemical association," *Journal of Statistical Physics,* vol. 62, no. 1-2, pp. 221-237, 1991.

[44] M. Holovko, T. Patsahan, and O. Patsahan, "Effects of disordered porous media on the vapour-liquid phase equilibrium in ionic fluids: application of the association concept," *Journal of Molecular Liquids,* vol. 228, pp. 215-223, 2017.

[45] R. Wang and Z. G. Wang, "On the theoretical description of weakly charged surfaces," *J Chem Phys,* vol. 142, no. 10, p. 104705, Mar 14 2015.

[46] J. Vatamanu, Z. Hu, D. Bedrov, C. Perez, and Y. Gogotsi, "Increasing Energy Storage in Electrochemical Capacitors with Ionic Liquid Electrolytes and Nanostructured Carbon Electrodes," *The Journal of Physical Chemistry Letters,* vol. 4, no. 17, pp. 2829-2837, 2013.

[47] A. A. Kornyshev, "Double-layer in ionic liquids: paradigm change?," *J Phys Chem B,* vol. 111, no. 20, pp. 5545-57, May 24 2007.

[48] M. T. Alam, M. Mominul Islam, T. Okajima, and T. Ohsaka, "Measurements of differential capacitance in room temperature ionic liquid at mercury, glassy carbon and gold electrode interfaces," *Electrochemistry Communications,* vol. 9, no. 9, pp. 2370-2374, 2007.

[49] D.-e. Jiang, D. Meng, and J. Wu, "Density functional theory for differential capacitance of planar electric double layers in ionic liquids," *Chemical Physics Letters,* vol. 504, no. 4-6, pp. 153-158, 2011.

[50] A. A. Lee and S. Perkin, "Ion-Image Interactions and Phase Transition at Electrolyte-Metal Interfaces," *J Phys Chem Lett,* vol. 7, no. 14, pp. 2753-7, Jul 21 2016.

[51] M. Girotto, A. P. Dos Santos, and Y. Levin, "Simulations of ionic liquids confined by metal electrodes using periodic Green functions," *J Chem Phys,* vol. 147, no. 7, p. 074109, Aug 21 2017.

Chapter 7. Conclusions and Outlook

In this thesis, Classical Density Functional Theory (CDFT) has been used to provide insights into the mechanisms of charge storage in Electric Double Layer Capacitors (EDLCs). CDFT is a versatile and powerful modeling tool for studying interfacial phenomena including the phase behavior of electrolytes under confinement.

Following the introductory chapters on the background and methodology (Chpaters 1 and 2), Chapter 3 and Chapter 4 investigated how additives/impurities in ionic liquid influence the EDL structure and charge storage in EDLC. The key findings are as follows:

1. Because of the electrostatic attraction from the ionic species and the polarized electrode, the additive molecules of low molecular weight and high polarity will accumulate in the nanopores even at a very low bulk density, i.e. the ratio of additives to ionic liquid is as low as 10^{-4}. The competitive adsorption of counter-ions and additive molecules alters the EDL structure at the vicinity of the electrode surface and the charge storage in the pore, leading to the increase of the integral capacitance compared to that in a pure ionic liquid.

2. Adding highly polar additives to the ionic liquid may inhibit the pore size effect on integral capacitance. The oscillation behavior of the capacitance with pore size is reduced compared to that in pure ionic liquids, without scarifying the performance. It will enable a broader usage of amorphous carbon material, such as low-cost activated carbon.

3. For an arbitrary impurity, tuning its binding energy with the electrode surface will lead to a drastic reduction of the capacitance. With a strong binding energy with the surface, the charge effect would be screened by the impurity and the ions would be repelled from the pore. With a strong binding energy with the ions, an enhanced capacitance oscillation is observed, due to the changings for the ion packing inside the pore.

Chapter 5 examines the idea whether the charge would be stored more efficiently in an "ionophobic" pore. The electrolyte consists of ionic liquid and small amount of impurity, and the transfer energy for the impurities is varied to create an ionophobic or ionophilic environment inside pore. The key findings are as follows:

1. By decreasing the transfer energy of impurity molecules, a micropore can change from ionophilic to ionophobic; the corresponding capacitance-potential curve changes from a bell shape to a camel shape, with the peak shifting toward a higher charging potential.

2. The corresponding calculation of the energy density in different pores shows that the ionophobic pore could store more charge than the ionophilic pore, mainly due to the different charging process. This study demonstrate the hypothesis that ionophobic pore is beneficial for charge storage.

Finally, Chapter 6 explores the accessibility of non-aqueous electrolytes to ultra-small pores. The key findings are:

1. When the pore size is comparable to the ion diameter of the non-aqueous electrolyte, capillary evaporation may take place in such micropores, leading to a drastic reduction of the capacitance.

2. As the bulk density of the non-aqueous electrolyte approaches to the demixing point, there would be no or very few ions in the pore at low voltage. However, the counterions abruptly enter the pore at some critical voltage, indicating a first-order phase transition in response to the surface charge increase.

3. The treatment of solvent as a dielectric media may not be reasonable for the high concentrated electrolyte solutions. The extended work that utilizing a model taking into account the size, shape, or valence effect and explicitly treatment of the solvent molecular should be the focus in the future study.

To sum up, we hope the conclusions and insights from this thesis work would be useful for the rational design of optimal electrolyte/electrode systems for electrical energy storage, for understanding the EDL structures in dense electrolytes, and for exploring the rich wetting scenarios of ionic systems under confinement.